BOREAS An international journal of Quaternary research

Flow-pattern evolution of the Scandinavian Ice Sheet indicated by the subglacial lineation record over Norway, Sweden and Finland

FRANCES E. G. BUTCHER, ANNA L. C. HUGHES, HELEN E. DULFER, CHRISTOPHER D. CLARK, JEREMY C. ELY, EMMA L. M. LEWINGTON, BENJAMIN M. BOYES, ALEX C. SCOFFIELD, STEPHEN HOWCUTT AND CHRISTIAAN R. DIEMONT

BOREAS

Butcher, F. E. G., Hughes, A. L. C., Dulfer, H. E., Clark, C. D., Ely, J. C., Lewington, E. L. M., Boyes, B. M., Scoffield, A. C., Howcutt, S. & Diemont, C. R.: Flow-pattern evolution of the Scandinavian Ice Sheet indicated by the subglacial lineation record over Norway, Sweden and Finland. *Boreas*. https://doi.org/10.1111/bor.70050. ISSN 0300-9483.

Streamlined subglacial bedforms, including drumlins, mega-scale glacial lineations, crag-and-tails and roche moutonnées, provide evidence for the past flow of large mid-latitude ice sheets during the late Quaternary. Empirical reconstructions of palaeo-ice sheet flow, based on such landforms, provide valuable insights into how ice sheets evolve over time and adjust their internal dynamics in response to climate change. We present a new 25-stage reconstruction of changing flow directions of the Scandinavian Ice Sheet (SIS) based on systematic mapping of ~240 000 subglacial bedforms across Norway, Sweden, Finland and parts of NW Russia. Of these, 23 stages depict the ice flow evolution during advance and retreat of the SIS through Marine Isotope Stage (MIS) 2. Two additional stages likely represent flow patterns of an earlier ice sheet (potentially MIS 4 or older). Our reconstruction was enabled by the recent revolution in the availability of high-resolution (1–2 m) digital terrain models. It is based on 611 flowsets, which summarise discrete ice-flow patterns recorded by subglacial lineations and are individually categorised by their glaciodynamic contexts. The reconstruction honours the relative-age chronology of flowsets indicated by cross-cutting relationships of the subglacial lineations. We reconstruct, and provide maps of, changing ice-sheet flow patterns and the migration of ice divides starting with ice-sheet inception, through advance and subsequent deglaciation, and ultimately the fragmentation into independent ice masses. The primary ice divide migrated up to 500 km and developed a branched configuration during deglaciation. The reconstruction of SIS flow patterns we present is the most detailed and comprehensive to date, and the fact that we independently verify many properties of the ice sheet invoked by earlier workers is testament to the quality, rigour and enduring legacies of those studies. We release flowsets, relative chronology and flow-pattern data along with a dataset of ~58 000 lineation linkages which summarise our detailed landform mapping and were invaluable for reconstructing ice-flow patterns at the ice-sheet-scale. In releasing these data, we intend for them to serve as useful inputs or comparative data for future studies in palaeoglaciology. This includes, for example, approaches combining flow pattern information with numerical ice sheet modelling to improve representations of ice sheet behaviour. Such improvements should yield increased robustness of information on time-varying glacio-isostatic loading by the ice sheet, relevant for sea-level forecasting. Our datasets also have wide utility for applications beyond palaeoglaciology, such as for mineral exploration.

Frances E. G. Butcher (f.butcher@sheffield.ac.uk), Helen E. Dulfer, Christopher D. Clark, Jeremy C. Ely, Emma L. M. Lewington, Benjamin M. Boyes**, Alex C. Scoffield***, Stephen Howcutt and Christiaan R. Diemont, School of Geography and Planning, University of Sheffield, Winter Street, Sheffield S3 7ND, UK (*present address: Geography, School of Natural Sciences Trinity College Dublin College Green, Dublin 2, Ireland; **present address: iC3: Centre for Ice, Cryosphere, Carbon and Climate, Department of Geosciences, UiT The Arctic University of Norway, 9037 Tromsø, Norway; ***present address: School of Geography University of Leeds Woodhouse Lane, Leeds LS2 9JT, UK); Anna L. C. Hughes, Department of Geography, School of Environment, Education and Development, University of Manchester, Oxford Road, Manchester M13 9PL, UK;* *received 10th September 2024, accepted 16th December 2025.*

The Scandinavian Ice Sheet (SIS) reached its maximum extent over Fennoscandia and NW Europe ~21 000–20 000 years ago (Fig. 1), forming the largest component of the ~5.5 million km^2 Eurasian Ice Sheet Complex (Svendsen *et al*. 2004; Hughes *et al*. 2016) along with the British-Irish (BIIS; e.g. Clark *et al*. 2022) and Barents-Kara (BKIS; e.g. Ingólfsson & Landvik 2013) ice sheets. The SIS left behind a rich variety of glacial landforms across the former ice sheet bed, which can be used to reconstruct the ice sheet geometry and its evolution over time. Empirical reconstructions of past ice sheets, based on landform records, can provide insight into ice sheet dynamics and their effects on glacio-geomorphic processes (see e.g. Andrews 1982; Kleman & Borgström 1996; Clark 1997, 2022; Kleman *et al*. 1997, 2006; Greenwood & Clark 2009a, b; Hughes *et al*. 2014; Stokes *et al*. 2015; Stroeven *et al*. 2016). They can also be compared to the results of numerical ice sheet models and used to validate model representations of ice sheet dynamics and evolution (e.g. Kleman *et al*. 2002; Näslund *et al*. 2003; Li *et al*. 2007; Napieralski *et al*. 2007; Tarasov *et al*. 2012; Clason *et al*. 2014; Patton *et al*. 2015, 2016, 2017; Petrini *et al*. 2018; Ely *et al*. 2019, 2021, 2024; Gandy *et al*. 2021; Archer *et al*. 2023).

By improving our understanding of the range of ice sheet behaviours evidenced in the palaeo-record of former ice sheet beds, we should be able to better predict the potential responses of contemporary ice sheets to anthropogenic climate change and constrain their likely future contributions to global sea level rise (Stokes *et al*. 2015). The SIS is

DOI 10.1111/bor.70050

Fig. 1. Overview of Fennoscandia and NW Europe showing the non-synchronous (i.e. time-transgressive) maximum extent of the last Scandinavian Ice Sheet (SIS, solid white line) based on Hughes *et al.* (2016). Our core study area—onshore Norway, Sweden and Finland—is outlined in red. Our extended study area in NW Russia covered portions of the ice sheet bed within the latitude range covered by the ArcticDEM (southern boundary indicated by blue line), with the exception of the Kola Peninsula and Russian Lapland (outlined in dark grey) where we used flowsets from the existing stages of regional flow-pattern evolution from Boyes *et al.* (2023) for our ice-sheet-scale flow-pattern reconstruction. Analysis of the portions of the ice sheet bed between our core study area and the maximum SIS limit was the subject of a parallel study by Diemont (2024). Specific locations referred to in the text are labelled. The data products used for mapping are summarised (see Table 1 for full details), and the locations of subsequent figures are indicated. Basemap credit: GEBCO 2024 Grid (GEBCO Compilation Group 2024).

an important palaeo-analogue for contemporary ice sheets; it interacted with diverse topographic and ice-terminal environments similar to those which influence the dynamics and flow of the Greenland and Antarctic ice sheets (Morlighem 2017, 2020). These include (i) marine-terminating settings—on the continental shelf and within deep fjords—which are particularly analogous to margins of the Greenland Ice Sheet (GrIS; Catania *et al.* 2020) and sectors of both the East and West Antarctic ice sheets, and (ii) expansive terrestrial and lake-terminating margins across the lowlands of NW Europe which are analogues for environments that will be encountered during potential future retreat of the GrIS (Carrivick *et al.* 2022). The SIS also had significant

dynamic interactions with the marine-based BKIS to which it was connected to the north, and which is an important palaeo-analogue for the contemporary West Antarctic Ice Sheet (Mercer 1970; Patton *et al.* 2015).

An aspect of ice sheet behaviour that is critical to reconstructing and understanding ice sheet evolution is the pattern of ice flow, its relationship to the centre(s) of mass of the ice sheet (i.e. the ice divides) and changes in these properties over time (Boulton & Clark 1990a, b). It has long been recognised that ice sheet flow patterns are more complex than simple radial flow from a central dome and can vary over time in connection to multiple factors including climate, ice thickness, bed topography, substrate geology and terminus environment (Vorren 1977; Kleman *et al.* 1997; Greenwood & Clark 2009a, b; Joughin *et al.* 2010; Hughes *et al.* 2014; Patton *et al.* 2016, 2017; Putniņš & Henriksen 2017; Margold *et al.* 2018; Clark *et al.* 2022). Streamlined subglacial lineations including drumlins, mega-scale glacial lineations, crag-and-tails and roche moutonnées provide key observational records of ice-flow patterns (Fig. 2), as do smaller (mm–cm) scale glacial striae on bedrock surfaces. There was a time when streamlined subglacial lineations were considered to have formed exclusively at short distances (10s km) behind retreating ice margins and could therefore be used as signals of ice-marginal retreat (e.g. Boulton *et al.* 1985 and references therein). However, subsequent research across Fennoscandia and the Laurentide, Cordilleran and British-Irish ice sheets (Sollid & Sørbel 1994; Dongelmans 1996; Kleman *et al.* 1997, 2010; Clark *et al.* 2000; Greenwood & Clark 2009a, b; Hughes *et al.* 2014) has demonstrated that the subglacial conditions required for the generation of subglacial bedforms span a wide range of ice thicknesses, from thin (~100s m) to thick (order of kilometres), and that preserved subglacial lineation records may include signals of ice sheet flow patterns during advance as well as deglaciation.

Cross-cutting and superimposition relationships between subglacial lineations show that ice flow directions can shift over time; in many cases this can be related to shifts in wider ice sheet geometry and the migration of ice divides during ice sheet growth and decay (e.g. Vorren 1977; Dyke & Prest 1987; Boulton & Clark 1990b; Dongelmans 1996; Kleman *et al.* 1997, 2006; Clark *et al.* 2000; Boulton *et al.* 2001; Greenwood & Clark 2009a, b; Winsborrow *et al.* 2010; Hughes *et al.* 2014). Glacial striae also record cross-cutting ice-flow patterns (e.g. Glückert 1974; Mangerud *et al.* 2019), though in many locations these records often relate to local-scale (sub-metre) flow variability which must be filtered out to extract signals of ice-sheet-scale (and longer term) flow evolution (e.g. Kleman 1990). Here we analyse the record of SIS ice flow pattern evolution, including changes in ice divide positions and ice sheet geometry recorded by subglacial lineations across Norway, Finland, Sweden and parts of NW Russia.

There is an extensive body of research analysing the glacial landform record of the SIS, including signatures of ice flow. The vast majority has been undertaken at local (e.g. Kjær *et al.* 2003; Follestad & Fredin 2007; Putniņš & Henriksen 2017; Mangerud *et al.* 2019) and regional-to-national scales (e.g. Vorren 1977; Salonen 1986; Nordkalott Project 1986a, b; Hirvas *et al.* 1988; Heikkinen & Tikkanen 1989; Putkinen *et al.* 2017; Boyes *et al.* 2021; Greenwood *et al.* 2023), and is extremely valuable for understanding landform genesis and the behaviour of ice-sheet sectors in high levels of detail. Both onshore and offshore records have been interrogated (e.g. Ottesen *et al.* 2005, 2022; Winsborrow *et al.* 2010; Greenwood *et al.* 2015, 2017, 2023), incorporating a variety of field (e.g. Anundsen 1990; Putniņš & Henriksen 2017) and remote-sensing techniques (e.g. Punkari 1994; Putkinen *et al.* 2017; Sarala & Räisänen 2017). In contrast, relatively few studies have performed landform-driven reconstructions of ice flow at the ice-sheet scale; that is, to resolve ice-flow patterns holistically across the ice sheet and reconcile evidence from different ice-sheet sectors. Recent studies have used empirical evidence (including landforms and dating) to reconstruct the spatial extent of the SIS and its pattern of retreat (e.g. Hughes *et al.* 2016; Stroeven *et al.* 2016), but do not include new information about internal ice-flow patterns and their evolution. Those ice-sheet-scale reconstructions of flow-pattern evolution that do exist (e.g. Lundqvist 1986; Dongelmans 1996; Kleman *et al.* 1997; Boulton *et al.* 2001), such as that shown in Fig. 3, have become broadly accepted frameworks for the flow evolution of the SIS; however, they necessarily relied upon the decametre-scale remote-sensing datasets that were available, primarily aerial and satellite images (alongside extensive field-scale observations such as striations and till fabrics). Since the 2010s, there has been a revolution in the availability, coverage, continuity and resolution of remote sensing data over the interior regions of the SIS (e.g. Dowling *et al.* 2013; Johnson *et al.* 2015). At the time this study was undertaken, Finland and Sweden had complete digital terrain model (DTM) coverage at 2 m pixel^{-1} derived from LiDAR surveys. Similarly, Norway had national DTM coverage at 1 m pixel^{-1} derived from LiDAR surveys and supplemental stereo photogrammetry in the most mountainous regions (Norwegian Mapping Authority, Kartverket 2023). When combined, these DTMs provide coverage of extensive regions of the ice sheet interior above contemporary sea level and, importantly, reveal the morphology of the land surface beneath dense forests which previously obscured many details of the landform record (Dowling *et al.* 2013; Johnson *et al.* 2015) for both remote and field mapping approaches. Several studies have used the new DTMs to generate detailed maps of glacial landforms for some portions of the SIS domain and to explore SIS dynamics and flow patterns in specific regions (e.g.

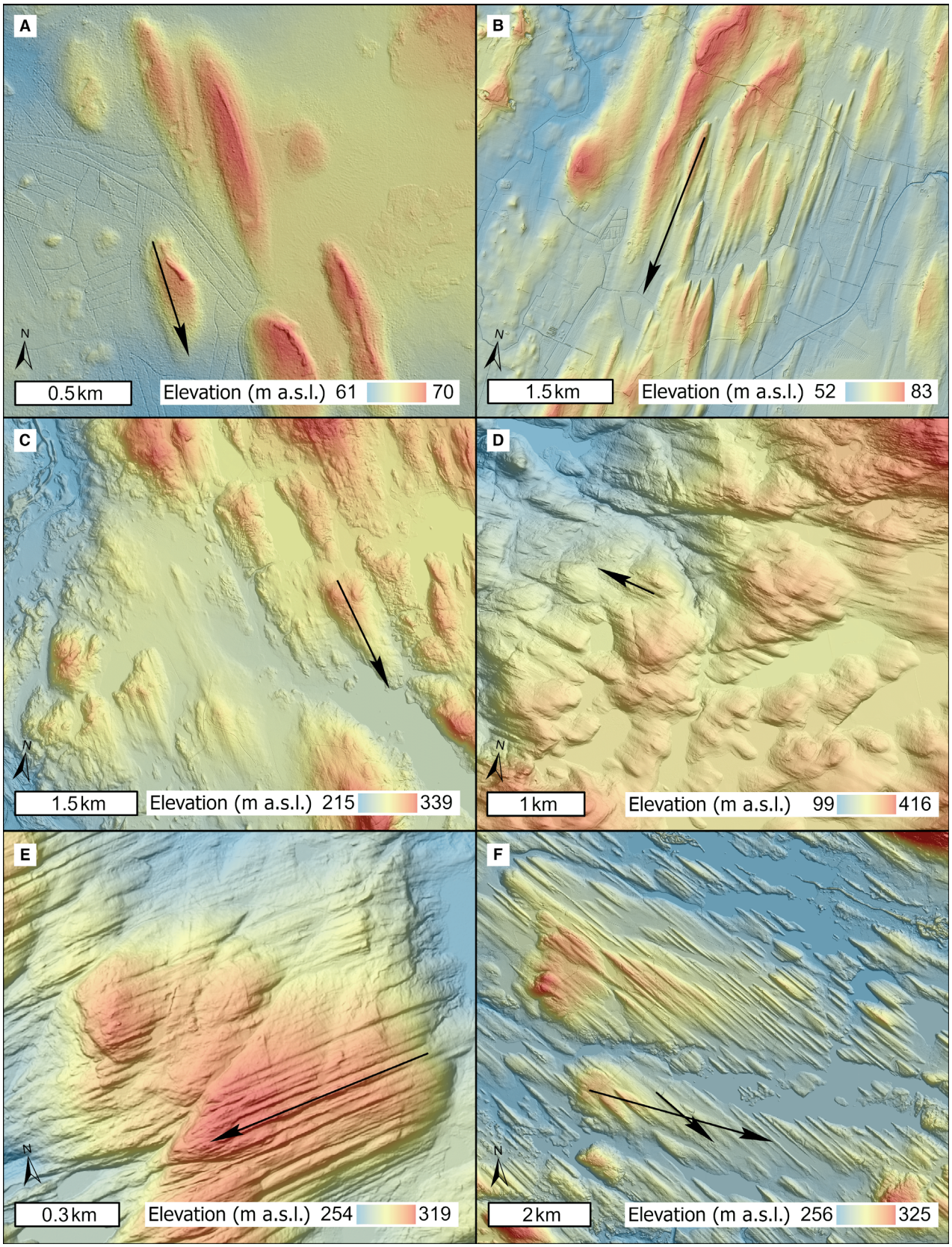

Fig. 2. Examples of streamlined subglacial bedforms in Fennoscandia, which record past ice-flow directions (black arrows), visualised in shaded-relief maps. These examples illustrate the richness and quality of glacial landform information provided by new metre-scale bare-earth digital terrain models over Fennoscandia. A. Drumlins in N Finland (25.07°E, 65.78°N). B. Mega-scale glacial lineations in central Sweden (14.92°E, 59.13°N). C. Crag-and-tails in N Sweden (16.52°E, 63.81°N). D. Moulded bedrock forms in N Norway (24.79°E, 70.76°N). E. Small bedforms in N Norway, here expressed in bedrock (24.63°E, 70.75°N). F. Cross-cutting subglacial lineation patterns in central Finland (29.62°E, 65.74°N). The location of each panel is shown in Fig. 1. Data sources: A and F, National Land Survey of Finland Elevation model 2 m; B and C, GSD-Höjddata, grid 2+ © Lantmäteriet; D and E, National Detailed Height Model (NHM) Kartverket (Norwegian Mapping Authority) resampled to 2 m (Kartverket 2023).

Dowling *et al.* 2015, 2016; Möller & Dowling 2016; Nikarmaa *et al.* 2017; Peterson *et al.* 2017; Putkinen *et al.* 2017; Putniņš & Henriksen 2017; Sarala & Räisänen 2017; Goodship & Alexanderson 2020; Öhrling *et al.* 2020; Lunkka *et al.* 2021; Peterson Becher *et al.* 2024; Ploeg & Stroeven 2025).

The seminal flow reconstructions of the SIS by Kleman *et al.* (1997; Fig. 3) and Boulton *et al.* (2001, which builds on Dongelmans 1996) preceded widespread digital map publication and open-access data conventions, such that the underlying data are effectively inaccessible for direct reuse or reanalysis. There is a growing demand for openly accessible datasets in palaeoglaciology, for example for numerical modelling approaches which combine empirical data and model reconstructions to improve model representations of past ice sheet configurations and behaviour (e.g. Kleman *et al.* 2002; Napieralski *et al.* 2007; Stokes *et al.* 2015; Patton *et al.* 2017; Ely *et al.* 2021, 2024; Archer *et al.* 2023). This requirement will likely grow as empirical datasets become more detailed, and hence manual extraction of data from published maps (e.g. Li *et al.* 2007; Napieralski *et al.* 2007; Patton *et al.* 2017) becomes increasingly impractical.

Several recent studies have released useful digital datasets pertaining to SIS extent and retreat pattern (Hughes *et al.* 2016; Stroeven *et al.* 2016; Batchelor *et al.* 2019), but these do not contain new information on ice-flow patterns. Some recent studies have released digital datasets associated with detailed local-to-national scale maps of the glacial landform record of the SIS, which include subglacial lineations (e.g. Peterson *et al.* 2017; Putkinen *et al.* 2017; Boyes *et al.* 2021; Leigh *et al.* 2021; Ploeg & Stroeven 2025). However, this is not the case for the majority of glacial landform maps in the literature, nor the majority of the SIS domain. Further, to facilitate data-model comparisons, there is a need for datasets which attempt to separate out complex, overprinted landform signals of time-varying glacial processes (such as cross-cutting subglacial lineations; e.g. Fig. 2F) and overcome scale discrepancies between individual landforms (typically 100s m) and ice-sheet-scale models (with grid sizes of 10s km).

We seek to fulfil the requirement for spatially extensive, spatially consistent, accessible and reusable information on the patterns and evolution of SIS ice flow, derived from subglacial lineations across the entire onshore areas of Norway, Sweden and Finland and parts of NW Russia. In doing so, we also exploit the opportunities provided by the recent revolution in the coverage and availability of high-resolution DTMs to reveal new details of ice flow-pattern evolution in the glacial landform record of the SIS. We present a new 25-stage reconstruction of SIS ice-flow pattern evolution, including changes in ice flow directions, ice divide positions, and ice sheet geometry. This includes 23 stages of flow-pattern evolution as the SIS grew and decayed over the last glacial period (Marine Isotope Stages, MIS 3–2) and into the Early Holocene (MIS 1), and two stages of ice flow which may relate to an older (MIS 4 or earlier) ice sheet.

Aims, key outputs and scope

Aims

We have three primary aims: to (i) ascertain former ice-flow directions recorded by macro-scale subglacial lineations such as drumlins, mega-scale glacial lineations, crag-and-tails and roche moutonées across the interior of the SIS, including details revealed by new high-resolution DTMs; (ii) develop a new reconstruction of the flow-pattern evolution of the SIS, based on patterns of subglacial lineations across the ice sheet interior, which deciphers the relative timings of major shifts in ice flow geometry and ice divide positions, and provides more detailed insights into ice flow-pattern evolution than previous ice-sheet-scale reconstructions; and (iii) provide useful, accessible datasets which communicate interpretations of time-varying ice-flow patterns in the palimpsest subglacial lineation record and can be incorporated into a range of contemporary approaches to studying past ice sheets. For the latter, our primary focus is to provide outputs that can be used for numerical ice-sheet modelling approaches which incorporate or compare to empirical data (e.g. Patton *et al.* 2017; Ely *et al.* 2021; Archer *et al.* 2023).

Our flow-pattern reconstruction derives from original mapping of subglacial bedforms (Fig. 2) interpreted as having formed parallel to former ice flow directions and mapped using a sampling approach designed to enable robust and spatially consistent flow-pattern reconstruction at the ice-sheet scale. Our reconstruction covers the entirety of the contemporary onshore areas of Norway, Sweden and Finland, and additionally incorporates areas of NW Russia where landform patterns indicate direct extensions of ice flow from Finland and

Fig. 3. Reconstruction of ice sheet flow patterns over Fennoscandia by Kleman *et al.* (1997), and examples of the key datasets that contributed to it. A. Map of subglacial lineations expressed in glacial sediments (till) over Fennoscandia, reproduced and modified from Kleman *et al.* (1997: fig. 3). The mapping includes data compiled from Sollid & Torp (1984), Lidmar-Bergström *et al.* (1991), Kleman (1992), Punkari (1984), Niemelä *et al.* (1993), the Nordkalott Project (1986b, c), a previously unpublished glacial geomorphological map by C. Hättestrand and original mapping by Kleman *et al.* (1997) from stereoscopic satellite images. B. Flow-trace fans generated by Kleman *et al.* (1997), which incorporate information from subglacial lineations expressed in glacial till (see panel A), glacial striae, clast fabrics and meltwater landforms. The map includes 56 fans with interpretations of relative chronology (older and younger), classified into three interpreted glaciodynamic categories. Reproduced and modified from Kleman *et al.* (1997: fig. 4). C. Six time slices of ice sheet evolution over Fennoscandia generated by Kleman *et al.* (1997) based on the flow trace fans in panel B, with interpreted connections to timings of ice sheet evolution. The time slices include interpreted ice flow vectors (arrows), locations of ice dispersal centres (i.e. zones containing the interpreted ice divide, denoted by D symbols) and approximate ice-sheet outlines. Reproduced and modified from Kleman *et al.* (1997: fig. 11).

Norway (Fig. 1). With the exception of NW Russia, this study area corresponds to a contiguous region above contemporary sea level that is covered by high-quality and high-resolution (1–2 m pixel^{-1}) bare-earth DTMs (from which vegetation and cultural objects have been removed) across which we could deploy a consistent approach to mapping and analysis (Table 1). We integrate our interpretations with the recent regional-scale reconstruction of SIS ice flow evolution over the Kola Peninsula and Russian Lapland by Boyes *et al.* (2023).

An alternative approach that we chose not to take could have been to compile existing published mapping from numerous local, regional and national-scale studies and to fill in any remaining gaps with original mapping. While such a compilation would be valuable, there are several challenges, which led us away from this approach. First, while the availability of digital mapping files associated with published studies within our study domain is improving (e.g. Peterson *et al.* 2017; Putkinen *et al.* 2017; Leigh *et al.* 2021; Ploeg & Stroeven 2025), the underlying data for the majority of published studies are not readily available for reuse, necessitating significant time investment in obtaining, georeferencing and digitising published maps. Digital datasets of glacial landforms are not publicly available for most of our study domain. Secondly, differences in aims, data sources, methods, mapping scales, interpretative approaches and uses of nomenclature present challenges for reconciling interpretations between different study regions to build an internally consistent reconstruction at the ice-sheet scale. This applies even to those studies for which underlying data are available in digital formats. Thirdly, even detailed, high-resolution, high-quality maps of glacial landforms may not capture some key landform relationships such that relevant evidence may be missed or inconsistently treated across the ice sheet domain when relying on compilations of previously published maps. Particularly relevant for this study, for example, are cross-cutting and superposition relationships between individual subglacial lineations, which may not be captured nor consistently represented by maps for which cross-cut identification was not a primary objective. Hence, even where detailed mapping exists, it remains important to directly scrutinise the landscape to address the specific aims of a new scientific study. Fourthly, even after compiling and reconciling published mapping, significant spatial gaps in mapping often remain (as illustrated for the NW Laurentide Ice Sheet in Stoker *et al.* 2025: fig. 1B), necessitating additional original mapping to achieve complete coverage.

It is therefore common practice among flow-pattern reconstructions of ice sheets and major ice-sheet sectors to base analyses on dedicated, spatially extensive and spatially consistent mapping efforts (e.g. Dongel-

Table 1. Basemap data products and sources. (1) https://tiedostopalvelu.maanmittauslaitos.fi/tp/kartta, (2) https://www.lantmateriet.se/sv/ (1 m pixel^{-1} data have superseded 2 m pixel^{-1} data since our study), (3) https://hoydedata.no/LaserInnsyn (now available from: https://hoydedata.no/LaserInnsyn2), (4) https://doi.org/10.7910/DVN/3VDC4W, (5) https://services.arcgisonline.com/ArcGIS/rest/services/World_Imagery/MapServer (Credit: ESRI, Maxar, Earthstar Geographics, and the GIS User Community), (6) https://doi.org/10.5270/ESA-c5d3d65.

Country	Data type	Bare Earth?	Source	URL	Last accessed
Finland	2 m pixel^{-1} DTM	Yes	National Land Service of Finland (n.d.)	(1)	07/11/2019
Sweden	2 m pixel^{-1} DTM	Yes	Swedish Ordnance Survey (Lantmäteriet) (n.d.)	(2)	30/09/2019
Norway	2 m pixel^{-1} DTM (downsampled from 1 m pixel^{-1})	Yes	Norwegian Mapping Authority (Kartverket)	(3)	16/04/2021
NW Russia, >60°N	2 m pixel^{-1} ArcticDEM v3 mosaic	No	Porter *et al.* (2018), via ESRI ArcGIS Online	(4)	16/01/2024
NW Russia, >60°N	0.6–1.2 m pixel^{-1} ESRI ArcGIS World Imagery layer	No	ESRI ArcGIS Online	(5)	16/01/2024
NW Russia >60°N	30 m pixel^{-1} Copernicus GLO-30 DSM (COP-DEM_GLO-30-DGED)	No	European Space Agency (n.d.)	(6)	28/02/2021

mans 1996; Boulton *et al.* 2001; Greenwood & Clark 2008, 2009a, b; Hughes *et al.* 2010, 2014; Kleman *et al.* 2010; Kalm 2012; Principato *et al.* 2016; Boyes *et al.* 2021, 2023; Dulfer & Margold 2021; Szuman *et al.* 2021, 2024; Benediktsson *et al.* 2022; Dulfer *et al.* 2022; Greenwood *et al.* 2023; Stoker *et al.* 2025). Even ice sheet-scale reconstruction studies, which do incorporate flow-pattern data from numerous previous studies are typically underpinned by a significant component of new coordinated mapping effort (see e.g. Kleman *et al.* 1997; Clark *et al.* 2022, and references therein). In the case of the reconstruction of the BIIS by Clark *et al.* (2022), the initial landform mapping compilation work alone took more than a decade to complete, for a significantly smaller ice sheet than the SIS (Clark *et al.* 2004, 2018).

Key outputs

In order to interpret the history of ice flow recorded by subglacial lineations across Norway, Sweden and Finland, we first generated a map of ~240 000 subglacial lineations and lineation fields. It is not intended for this landform-scale mapping to supersede other high-quality landform maps generated by previous workers in some areas of our study domain (e.g. Peterson *et al.* 2017; Putkinen *et al.* 2017; Leigh *et al.* 2021; Ploeg & Stroeven 2025). Instead, our mapping approach, which involved systematic sampling of subglacial lineations at two different scales rather than nominally 'complete' mapping of all lineations (see 'Data and methods'), was specifically conceived to facilitate interpretation of ice flow-pattern evolution over a large study domain. Our focus is on four new analytical products, which build from landform-scale mapping:

- A map of lineation linkages, which summarise ice flow orientations indicated by subglacial lineations.
- Flowsets, which compartmentalise discrete packages of ice flow according to the spatial extents of their landform imprints, and are classified according to their interpreted glaciodynamic contexts and the influence of bed topography upon their internal ice flow vectors.
- Relative chronology information for flowsets based on cross-cutting relationships between subglacial lineations.
- Reconstructions of 25 stages of ice-sheet flow geometry evolution over Fennoscandia, including former ice divide positions and broad ice flow directions. This includes 23 stages which we attribute to the advance and retreat of the last SIS, and two stages of ice flow that appear to precede these.

Taken in sequence, these products represent progressive levels of interpretation and abstraction, derived from mapping of individual landforms, towards interpretations of ice flow-pattern geometry and changes thereof at the scale of the ice sheet (Fig. 4).

Study scope

Our focus is onshore Norway, Sweden and Finland and part of NW Russia (Fig. 1). The terrestrial glacial land-

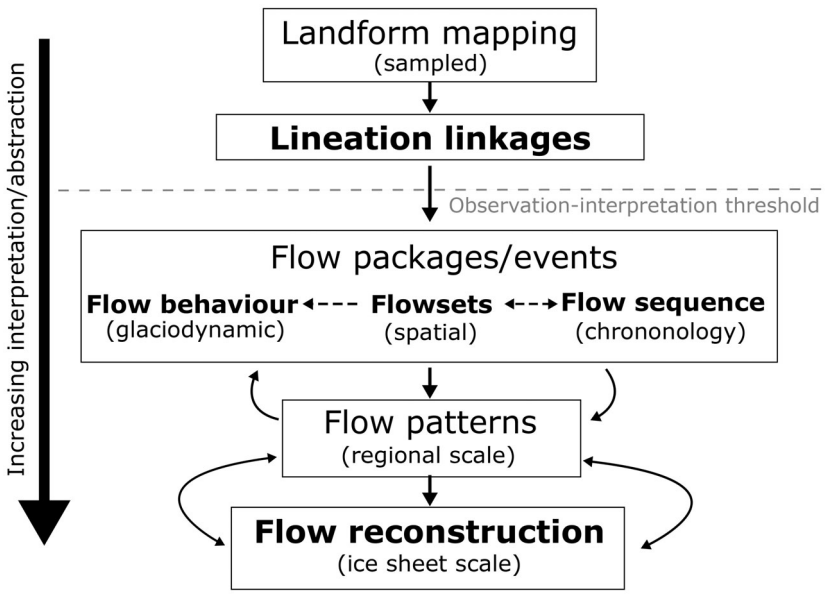

Fig. 4. Flowchart outlining the glacial geomorphological inversion approach used here, and the increasing levels of interpretation of—and abstraction from—the glacial landform record through the process. Curved arrows indicate iteration loops. Data products included in Data S1 are shown in bold. Adapted from Greenwood & Clark (2009a).

form record around the ice sheet periphery, south and east of the Baltic Sea (e.g. van der Wateren 1995; Perry 1998; Boulton *et al*. 2001; Kalm 2012; Astakhov *et al*. 2016; Larsen *et al*. 2016; Szuman *et al*. 2021) generally records spatially variable, time-transgressive ice margins and local ice-flow patterns. A new and detailed scrutiny of the evolution of the SIS periphery is the subject of a coordinated parallel study (Diemont 2024). Here, we use flow patterns identified in our core study domain to make generalised inferences about the dispersal of ice into these peripheral areas.

There are other forms of evidence for palaeo-ice flow direction, aside from subglacial lineations, which are not included in this reconstruction. This includes the orientations of small-scale (cm-mm) glacial striae on bedrock surfaces, clast fabrics in till and erratic dispersal pathways (e.g. Glückert 1974; Vorren 1977, 1979; Anundsen 1990; Kleman 1990; Mattsson 1997; Kjær *et al*. 2003; Smith *et al*. 2008; Smith & Knight 2011; Mangerud *et al*. 2019), all of which are derived from field-based observations. Additional landforms observable in metre-scale DTMs, aside from subglacial lineations, can also provide indirect evidence of ice flow directions. For example, eskers and ice-marginal landforms provide evidence for the local ice-flow orientation and surface slope close to the ice margin. The reconstruction by Kleman *et al*. (1997) combines evidence from subglacial lineations, glacial striae, till fabrics and other landforms, including eskers and ice-marginal landforms. In this study, we purposefully keep our flow-pattern reconstruction independent from these additional lines of evidence for several key reasons:

- Of the available lines of evidence, subglacial lineations have the most direct connection to ice-sheet-scale flow patterns. Glacial striae can contain useful information on regional-scale ice flow, but are also sensitive to local deviations in ice flow around metre- and decametre-scale bed topography (Kleman 1990). To extract patterns relevant to ice-sheet-scale flow from striae—a worthy task that we would like to see achieved by future studies—signals of local-scale fluctuations need to be carefully filtered out. Such a task requires significant, dedicated time investment and would be greatly enhanced by additional field campaigns across many parts of the SIS domain. Additionally, at the time that this study was undertaken, detailed national-scale striae maps were not consistently available from all of the relevant geological surveys. Those that did exist were not publicly available in downloadable Geographic Information System (GIS) formats (with the exception of Finland, for which a national striae dataset can be downloaded from the Geological Survey of Finland, GTK) required for detailed data analysis, filtering, and visualisation against high-resolution DTMs and other geospatial datasets.
- In any given location, where two or more lines of empirical evidence indicate the same ice flow direction, this does not necessarily mean that they reflect the same ice-flow phase (or event). Our approach acknowledges that different types of evidence for ice flow could conceivably develop in the same region, with coherent spatial relationships, during different phases of ice-sheet evolution. For example, macro-scale subglacial lineations have higher preservation potential than mm-scale glacial striae, and likely provide a longer record of ice sheet flow history; striae are more likely to reflect only the latter stages of glaciation and/or local-scale patterns (Kleman 1990). Similarly, most eskers are thought to reflect subglacial drainage near to retreating ice margins during deglaciation (e.g. Kleman & Borgström 1996; Hewitt & Creyts 2019); in contrast, there is abundant evidence that subglacial lineations form at various stages during glacial cycles and can form relatively far from the ice margin (e.g. Boulton & Clark 1990a; Kleman & Borgström 1996; Clark 1999; Ely *et al*. 2023). Subglacial meltwater features formed beneath retreating ice margins are often superposed upon subglacial lineations with which they broadly co-align. Hence subglacial lineations, glacial striae and eskers while often spatially contiguous can form at different stages of ice flow evolution.
- We aim to provide a thoroughly documented and reproducible interpretation of ice sheet flow-pattern evolution based on the subglacial lineation record, which can be used to independently verify and test interpretations arising from other techniques, such as ice-flow modelling, and revisited as new evidence arises and knowledge of glacial processes evolves. Critical to this goal is documenting decision-making for traceability of interpretations and therefore reproducibility. This is inherently more difficult for approaches which compound multiple lines of qualitative evidence—each with their own nuances—in a single interpretative scheme. This challenge becomes more acute as the level of detail that can be extracted from empirical records (and inevitably therefore the complexity of the evidence base) increases, as has occurred since the seminal ice-sheet-scale SIS reconstructions of Kleman *et al*. (1997) and Boulton *et al*. (2001). In generating our reconstruction independently of other sources of empirical information, we aim to provide a valuable tool which can now be integrated with and compared against other lines of evidence (see 'Logical next steps').

Data and methods

Data

We constructed 2 m pixel^{-1} DTM mosaics for Norway, Sweden and Finland (see Table 1 for data sources) using

ESRI ArcGIS 10.7. We downsampled 1 m pixel^{-1} DTMs for Norway to 2 m pixel^{-1} to reduce data volume, noting that this downsampling does not appreciably modify features at the scale of subglacial bedforms (typically >100 m long) (Napieralski & Nalepa 2010).

We generated multiple shaded-relief maps from each DTM mosaic, illuminated from solar azimuths of 45° and 315° (to minimise azimuth-bias: Smith & Clark 2005), with the Sun at 60° above the horizon. We also generated shaded-relief maps illuminated from directly overhead (Sun 90° above horizon, e.g. Hughes *et al.* 2010). All shaded-relief maps were generated with three times vertical exaggeration to emphasise terrain features. During mapping and throughout flowset-building, we visualised both the shaded-relief maps and the elevation information from the DTMs.

There are several areas where subglacial bedforms record direct ice flow extensions from Finland and Norway into NW Russia, where the quality and availability of remote sensing data is more limited. In this region, we deployed an adapted approach using the 2 m pixel^{-1} ArcticDEM (Porter *et al.* 2018; strictly a digital surface model, DSM, which retains vegetation and artificial structures). While the ArcticDEM provides 2 m pixel^{-1} DSM coverage at latitudes >60°N, it has significant quality issues in Russia, with numerous data gaps and artefacts, and more limited usefulness for landform mapping in forested regions. To capture direct ice flow connections into NW Russia (south of the area covered by the flow-pattern reconstruction of Boyes *et al.* 2023; Fig. 1), we used a multi-directional shaded-relief map (e.g. Boyes *et al.* 2021) of the 2 m pixel^{-1} ArcticDEM streamed directly into ArcGIS from the ArcGIS Online data-portal, and used the 0.6–1.2 m pixel^{-1} World Imagery layer (also via ArcGIS Online) in any data gaps (Table 1). We then compared this mapping against shaded-relief maps derived from the global 30 m pixel^{-1} Copernicus DSM (Table 1); in some places landform-scale topographic features can appear somewhat clearer in this dataset, despite it having a lower spatial resolution than the ArcticDEM.

Subglacial bedform mapping using a new multi-scale sampling approach

While the abundance of high-resolution remote sensing data brings significant new opportunities for analysing the glacial landform record, it also presents challenges for ice-sheet-scale reconstructions using glacial geomorphological inversion approaches. Mapping and analysis of metre-scale data over large portions of an ice sheet bed is extremely labour intensive. However, it is not necessary to map every individual landform in order to build a picture of the flow evolution of an ice sheet (De Angelis & Kleman 2005).

We developed a manual, multi-scale sampling approach to map streamlined subglacial lineations. This approach (illustrated in Fig. 5) reduces labour intensity, while still capturing new details of ice sheet flow. Our approach comprised two initial mapping steps with different degrees of sampling (mapping of a sample of individual landforms within a sampled hexagonal grid in Step 1, then more generalised mapping of 'grain' with no grid sampling in Step 2), followed by data reduction (Step 3) to produce a map of lineation linkages which summarises all observed flow directions (Fig. 5). In this process, we performed three complete passes over our study domain, at different scales and with different degrees of sampling. We used the reduced data (lineation linkages) to construct flowsets (Step 4) and then referred back to individual landforms (from Step 1) to interpret flowset relative-age chronologies based on cross-cutting and superimposition relationships between their constituent subglacial lineations (Step 5).

A small number of DTM data gaps remained in the interior of Norway at the time of Steps 1 and 2 mapping, predominantly in high-elevation and presently glaciated regions where glacial bedforms are rare. We integrated these areas at Step 3 once DTM coverage became available. The vast majority of mapping for Steps 1 and 2 was undertaken by a core group of four expert mappers. A small number of relatively simple areas were mapped by two additional mapping assistants, under the supervision of the lead author. All mappers undertook preliminary repeat-mapping exercises to ensure consistency of approach and interpretation, and all mapping was reviewed and quality checked by the lead author before integration. We used the Geological Society of Finland's (GTK) glacial landform map (Putkinen *et al.* 2017) to validate early-stage mapping in Finland; this confirmed that our mapping was robust and that our sampling scheme provided a good representation of the range of landform orientations.

We generated two different grids to guide systematic mapping during Steps 1 and 2, comprising hexagonal cells with areas of 25 and 100 km^2, respectively. We

Fig. 5. Schematic illustrating our multi-scale mapping approach to generating flowsets (fs) and interpreting their relative-age sequences indicated by cross-cutting subglacial lineations (cc—yellow stars). Our approach begins with sampled mapping of subglacial lineations at two different scales, followed by a data-reduction step in which summary lines called lineation linkages are generated. These are then used to generate flowsets (see text for method). Critical cross cuts identified for intersecting flowsets allow a relative-age sequence to be tabulated. Our ice-sheet-scale flow-pattern reconstruction must honour the observed superposition relationships and relative age sequencing of flowsets. The guiding principles for reconstructing ice-sheet-scale flow patterns are detailed in the text; they additionally allow those flowsets which do not cross-cut one another to be placed into the flow-pattern sequence.

Step 1: Map sample of subglacial lineation crestlines in a sampled grid of 25 km^2 hexagons (mapping scale 1:24000)

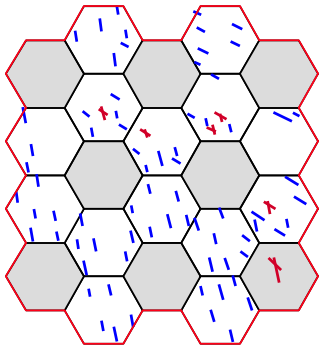

25 km^2

Sampled: Map sample of lineation crestlines within hex to represent all major flow orientations, capturing cross-cutting lineations

25 km^2

Unsampled at this scale, but map cross-cutting lineations if seen.

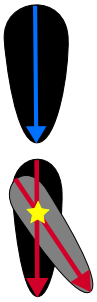

Step 2: Map 'grain' over the entire domain using a grid of 100 km^2 hexagons, without sampling (mapping scale 1:50000)

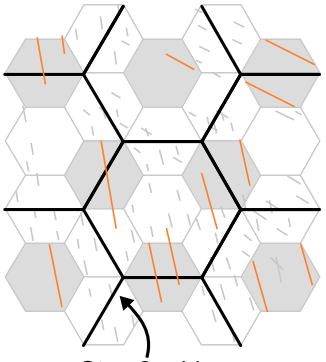

Summarise additional bedform fields (and large bedforms) in gaps left by step 1 sampling and at coarser scale than step 1

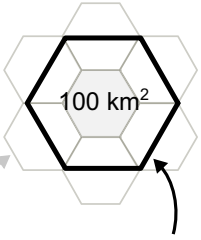

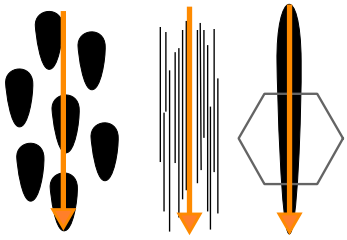

Step 2 grid

Step 1 grid

Step 2 grid

Step 3: Summarise step 1 & 2 mapping with 'lineation linkages' (without extrapolating over large distances)

Step 4: Generate flowsets delimiting discrete flow patterns in the ice sheet.

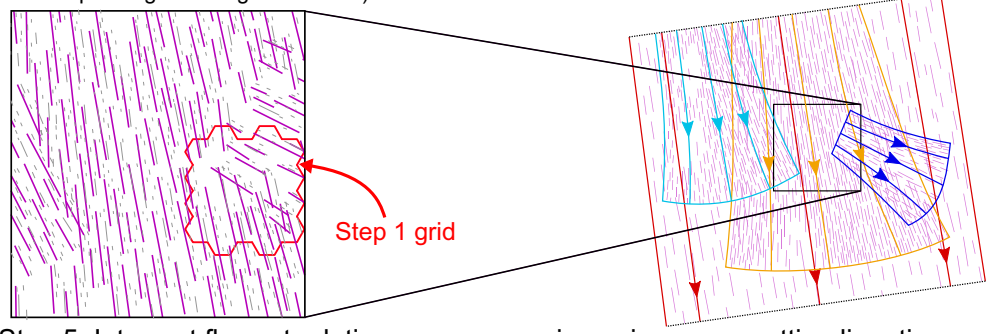

Step 5: Interpret flowset relative-age sequencing using cross-cutting lineations

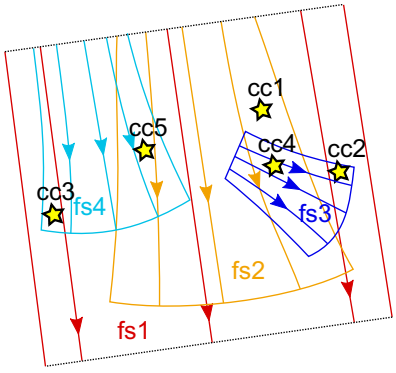

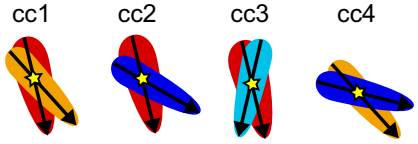

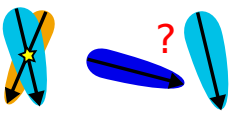

!fs1is older than !fs2
Relative ages of fs3 and fs4 unknown; both are younger than fs1 & fs2

selected a hexagonal grid to minimise directional biases during sampling. Both grid sizes allow clear visualisation of subglacial bedforms and can be viewed on a 27-inch computer screen at scales of 1:24 000 and 1:50 000, respectively, while retaining contextual visualisation of landforms in adjoining hexagons (which also prevents visual and sampling bias towards the centre of the grid cell being mapped). Mappers were encouraged to zoom in further to scrutinise the landforms within a given hexagon during mapping. In step 1, we used the 25 km^2 hexagonal grid with a sampling scheme applied (Fig. 5). In Step 2, we used the 100 km^2 hexagonal grid with no sampling applied; hence, all onshore parts of the ice sheet bed with data coverage were incorporated via our multi-scale approach.

In Step 1, we sampled ~33 250 hexagons over Norway, Sweden and Finland, corresponding to ~67% of hexagons (total ~50 000) in the 25 km^2 grid. Within each sampled hexagon, we mapped a sample of streamlined subglacial lineations (generally ~3–10, where present) representing each flow direction. We took care to capture the spread of landforms representing a given flow direction throughout each sampled hexagon, with a particular emphasis on capturing the distribution along the inferred flow axis, and any cross-cutting (superimposed) lineations. Cross-cutting lineations provide useful information on the sequence of ice flow events that generated the lineations. Mapping of geomorphologically diverse landscapes generated by complex and dynamic processes requires pragmatism; hence, the above scheme was established as the minimum level of mapping, and mappers were encouraged to use their judgement to capture complexities of ice flow. This included an allowance for mapping a larger sample of landforms where necessary to capture flow complexity. We did not map subglacial lineations that were clearly associated with contemporary glaciers in Norway and Sweden. The glacial landform record of the SIS includes a significant component of glacially streamlined bedrock forms (Fig. 2D, E); in places these can be oriented parallel to bedrock strike. To aid our mapping, and to help distinguish glacially streamlined bedrock forms from geological structures in bedrock, we zoomed out frequently to consider the wider context of mapped features, beyond the specific hexagon being mapped.

In Step 2, we used the 100 km^2 hexagonal grid (comprising ~12 500 hexagons, with no sampling applied) to perform a second pass over the entire mapping area. We mapped additional lineation fields as summary lines which we term 'grain' (Fig. 5). This included fields of subglacial lineations (or extensions of them) representing ice flow directions that were not captured by landform and hexagon sampling in step 1, and particularly large landforms which exceeded the scale of the 25 km^2 hexagons. In practice, it was rare that large landforms had not been captured in Step 1, giving us confidence that the grid scales selected were appropriate. We retained all recognisable subglacial lineations in our mapping, regardless of their posited ages in relation to the last glacial period; such interpretations were made later. For example, there are fields of subglacial lineations (along with eskers and ice-marginal landforms) in N Fennoscandia which previous studies have attributed to ice sheets preceding the Last Glacial Maximum (LGM) (e.g. Kleman 1992; Kleman *et al.* 1997; Greenwood & Hughes 2022a).

Steps 1 and 2 provided a comprehensive map of ice flow directions over the onshore portions of the SIS interior (Fig. 6). The map contains 210 909 lineation crestlines and 30 342 grain lines (total 241 251 lines).

In order to interpret flow patterns at the ice-sheet scale, a data reduction step was necessary to improve the clarity of visualisation over length scales relevant to ice-sheet-scale flow dynamics (i.e. up to hundreds of kilometres). In Step 3 (Fig. 5), we passed systematically over the mapping area for a third time, guided by the 100 km^2 hexagon grid, visualising both the mapping and basemap data. We summarised the landform observations from Steps 1 and 2 as lineation linkages (Fig. 5). We also carefully generated linkages to fill in the small mapping gaps in areas of Norway that lacked DTM coverage at the time of mapping Steps 1 and 2 (hashed areas in Fig. 6). Our lineation linkages reduce the landform observations into a map that can be visualised more easily at smaller map scales (Fig. 7; having an average length of 5 km, and a maximum length of 30 km), without extrapolating over large distances between observed landforms. The number of mapped lineations represented varies depending on landform abundance, size, density, topographic context, and the degree of curvature within the landform field. The lengths and densities of lineation linkages are influenced by the scale and complexity of the landforms and landform fields that they summarise. Landform fields with smaller individual landforms or higher levels of complexity required closer scrutiny and a level of representation that prevented them from being lost as 'noise' compared to linkages representing larger or simpler landform fields. The vast majority of lineation linkages were digitised as straight lines unless there was a particularly clear self-explanatory curve (for example where landforms clearly followed a significant topographic feature such as a valley or side of a fjord).

Lineation linkages provide a data product that is interpretable at the ice-sheet scale and yet closely tied to landform observations, without the application of a significant level of interpretation regarding ice flow connections between disparate locales. Whereas Steps 1 and 2 combined mapping by six individuals to ensure internal consistency within the dataset, lineation linkages were generated by a single mapper over Sweden and Finland, and a second mapper over Norway, with those linkages being reviewed by the first mapper. Individual landform mapping (Steps 1 and 2) was quality-checked during this

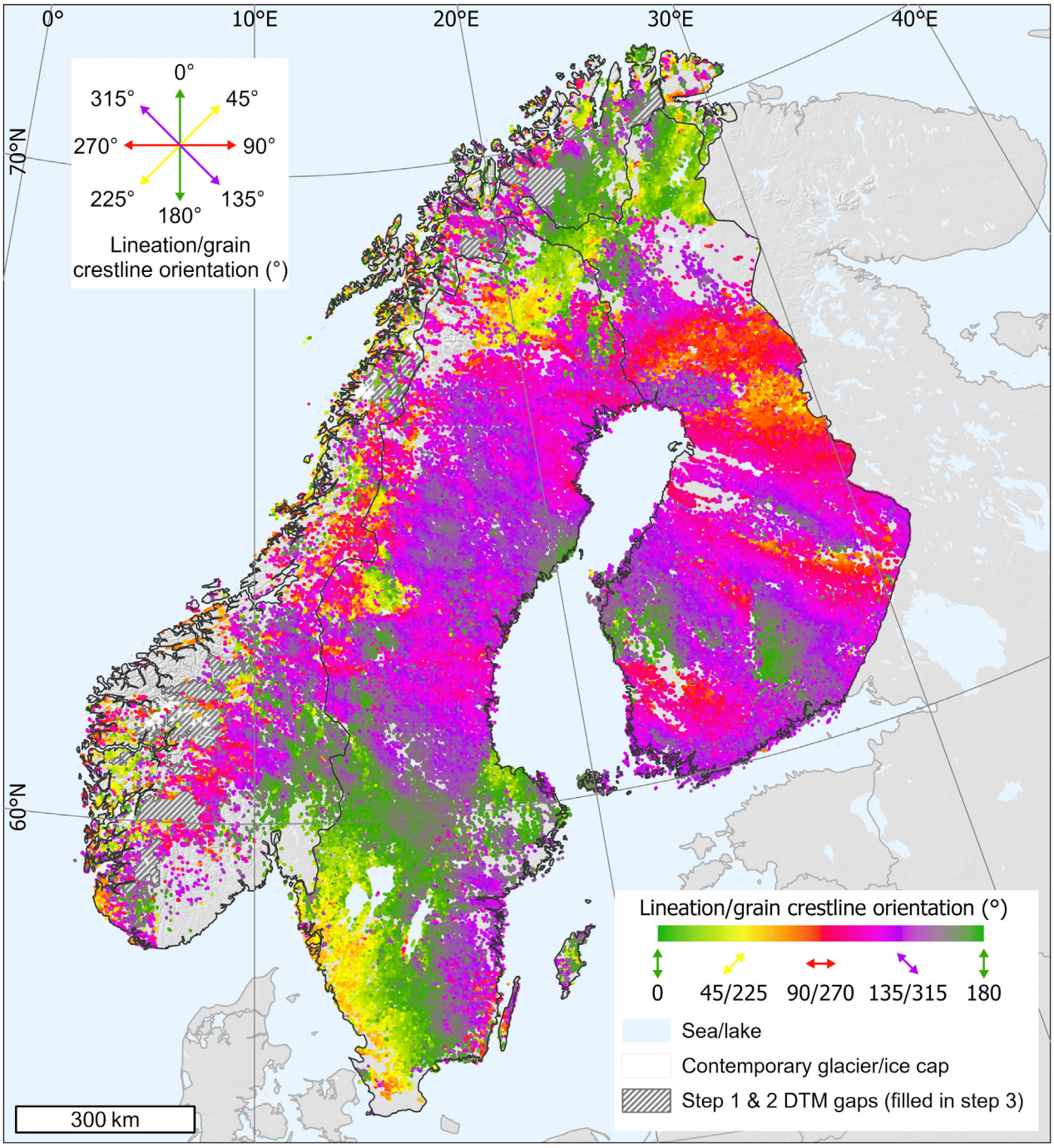

Fig. 6. Orientations of subglacial lineation crestlines (n = 210 909) and grain (n = 30 342) mapped in Steps 1 and 2 of our multi-scale sampled mapping approach. See Fig. S1 for a larger map. Hashed areas show areas where DTMs did not provide coverage at the time of mapping Steps 1 and 2; these were carefully in-filled during Step 3 when DTMs became available—they are largely in high-relief areas where subglacial lineations are sparse. Data credit for shaded-relief basemap: Airbus, USGS, NGA, NASA, CGIAR, NLS, OS, NMA, Geodatastyrelsen, GSA, GSI and the GIS User Community.

process, with the lowest-confidence landform observations filtered out. We applied a three-class confidence scale to lineation linkages: (1) 'high-medium confidence', (2) 'low confidence' and (3) 'very low confidence'. High-medium confidence linkages generally represent clearly streamlined landforms, be they in thick sediments, regions with thin sediment cover or expressed in exposed bedrock. Low-confidence lineation linkages generally represent landforms that likely represent a former ice flow direction but, for example, (i) are less pro-

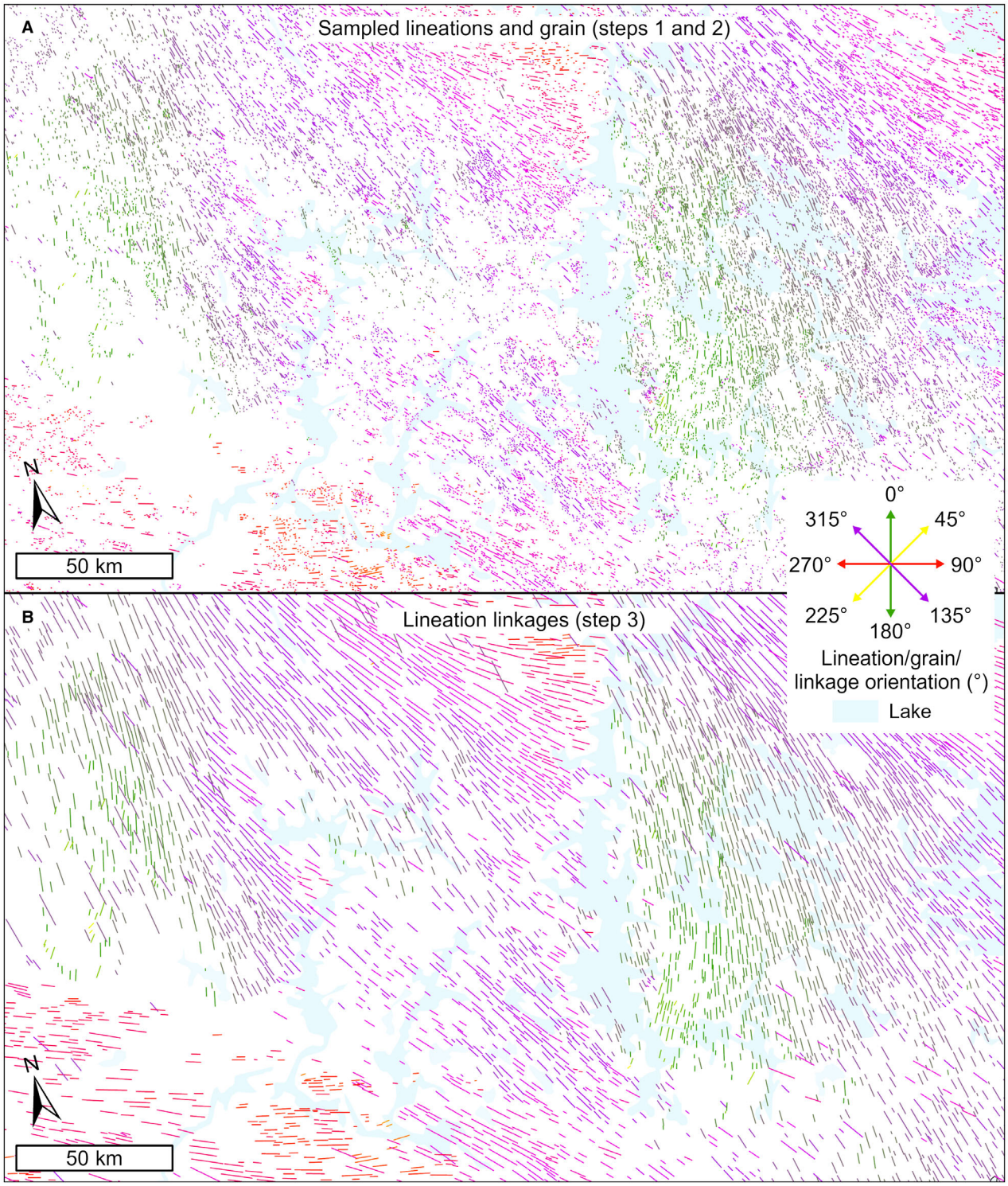

Fig. 7. Comparison of A. lineation crestline and grain mapping, and B. lineation linkage mapping over S Finland, illustrating the greater clarity of flow patterns afforded by lineation linkages when viewing at the scale of ice sheet-scale flow patterns. Ice flow direction is broadly towards the south and east. In general, the longer lines in panel A are Step 2 grain mapping. Panel B reveals several broadly divergent flow patterns representing well-studied ice lobes in Finland: the Näsijärvi Ice Lobe (top left quadrant of panels) and Lake District Ice Lobe (right third of panels) (e.g. Aario 1977; Punkari 1980; Putkinen *et al.* 2017). The W–E trending linkages (reds and oranges) in the bottom left of the panels are part of the Baltic Sea Ice Lobe. Note that unlike traditional maps of glacial lineations, where the mapped line length represents lineation length, the key information here is the orientation of subglacial lineations; line lengths result from how we have summarised this information so that it can be interpreted at the scale of ice sheet flow. Extent shown in Fig. 1.

nounced (often being subtle, low-relief features), (ii) have been significantly modified by later cross-cutting subglacial lineations or (iii) exhibit relatively weak streamlining in an area where bedrock structure is visible in the surface topography, thus reducing confidence that the streamlining is truly glacial in origin. The final confidence category ('very low confidence') represents landforms that we suspect to be best explained as bedrock structure, but for which there are some hints of glacial streamlining. The vast majority of the latter category were not used to generate flowsets, particularly where they were not associated with similarly oriented lineation linkages with higher levels of confidence.

To capture direct extensions of subglacial lineation fields into NW Russia, south of the study area of Boyes *et al.* (2023), we performed reconnaissance-style lineation-linkage mapping over Russian Karelia, using the ArcticDEM and the ArcGIS Online World Imagery layer as a basemap (see Table 1). Due to quality issues and the retention of vegetation and cultural structures in the ArcticDEM, our lineation linkages are less detailed here than those in the core study region and should be considered as a contextual supplement to our core linkage dataset.

Flowset building and glaciodynamic interpretation

We deployed, and built upon, the glacial geomorphological inversion approach established via numerous previous studies (e.g. Boulton & Clark 1990a, b; Kleman & Borgström 1996; Clark 1997, 1999; Clark *et al.* 2000; Kleman *et al.* 2006; Greenwood & Clark 2009a, b). Flowsets derived from the record of subglacial lineations via lineation linkages are the major interpretative tool used in this approach. Flowsets are cartographic representations of discrete packages of ice flow. They illustrate the generalised ice flow directions recorded by groups of subglacial lineations interpreted to have formed under similar glaciodynamic regimes (e.g. Clark 1999) during the same general phase of ice flow evolution. In our approach, the cartographic boundaries of flowsets uniquely delimit areas of subglacial lineations. This differs from the 'fans' generated for the SIS by Kleman *et al.* (1997; Fig. 3B), which compound evidence provided by subglacial lineations, striae, till fabrics, and meltwater landforms into indivisible interpretative units (see Kleman & Borgström 1996). Our approach acknowledges that subglacial lineations, meltwater drainage and ice-marginal landforms could conceivably develop in the same region, with coherent spatial relationships, during different phases of ice sheet evolution. These features can be spatially contiguous but non-synchronous. We constructed flowsets based on the lineation linkages and, given the sampled nature of our mapping approach, visualised the landform record in shaded-relief and DTM basemaps for context throughout this process. The vast majority of lineation linkages are accounted for by the resulting flowsets, with the exception of some isolated or anomalously oriented lineation linkages that did not form sufficiently coherent spatial patterns to be included in a flowset.

We labelled those flowsets in which a significant number of constituent subglacial lineations appear to comprise a component of bedrock. Bedrock that is exposed or near to the surface often creates distinctive textures and morphologies in shaded relief maps (e.g. Fig. 2D, E). We also labelled those flowsets in which subglacial lineations align with linear-to-curvilinear bedrock structures. This information is included in the flowset shapefile (Data S1).

Several flowset classification schemes have been established by previous studies to describe the glaciodynamic context under which their associated subglacial lineations formed (e.g. Clark 1990, 1997, 1999; Kleman 1992, 1994; Kleman & Borgström 1996; Clark *et al.* 2000; Kleman *et al.* 2006; Greenwood & Clark 2009a; Hughes *et al.* 2014). We adapt previous flowset classification schemes and use these to infer the glaciodynamic context of each of our SIS flowsets (Fig. 8, Table 2). Two top-level categories are 'isochronous' and 'time-transgressive' flowsets. Isochronous flowsets represent relatively stable ice flow conditions; subglacial lineations within such flowsets typically exhibit high levels of parallel conformity, with any variations in lineation orientations exhibiting gradual spatial trends that do not produce cross-cutting of lineations within the flowset. In contrast, time-transgressive flowsets exhibit more internal complexity, reflecting dynamic ice flow conditions which cannot be satisfactorily subdivided into coherent, discrete imprints of isochronous ice flow (Kleman & Borgström 1996; Clark 1997, 1999; Clark *et al.* 2000; Greenwood & Clark 2009a). This classification thus allows us to identify flowsets that indicate minor changes in ice flow conditions, such as ice thinning, thickening, retreat or migration of the flowline axis due to a shifting ice divide and/or margin geometry (Fig. 8).

The specific inferred glaciodynamic context for each flowset is influenced by the degree to which internal flow vectors (i.e. constituent lineation linkages) follow, sense or ignore bed topography (Table 2). The probable ice thickness and proximity to the ice margin that can be inferred is dependent upon the ratio of ice thickness to the magnitude of the local topographic relief. In high-relief areas, a greater thickness of ice is likely required than in flatter areas for ice flow direction to become insensitive to bed topography. Hence, topographically influenced flowsets in areas such as the Scandinavian mountains and the Norwegian fjords could represent the flow of relatively thick ice further from the ice margin compared to those in relatively low-relief regions of Sweden and Finland.

Isochronous flowsets may reflect spatially continuous areas of consistent, sub-parallel ice flow vectors (sheet flow), which may exhibit minimal or minor influence

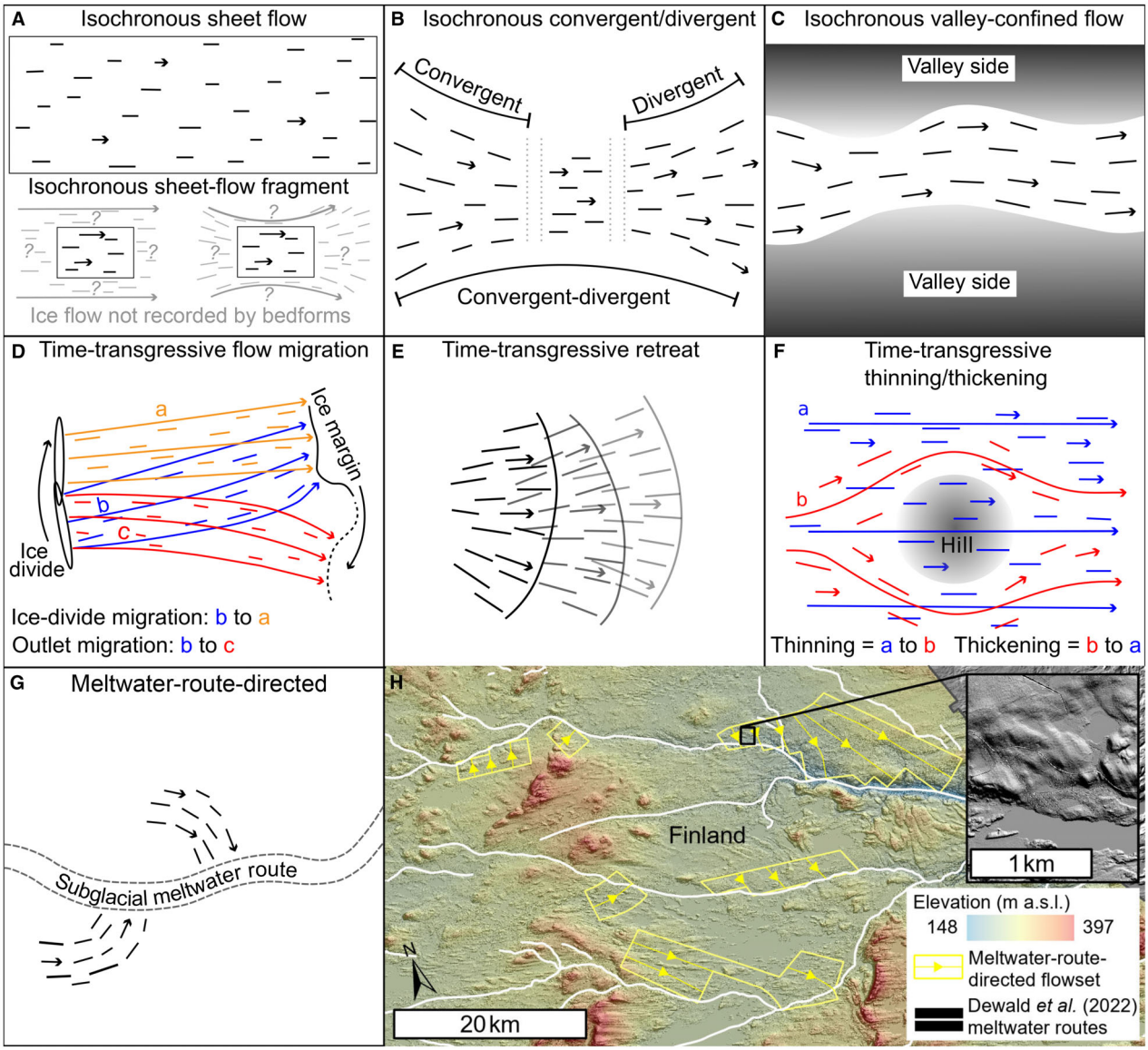

Fig. 8. Schematic representations of flowset glaciodynamic classifications based on their landform imprints, and examples of a new meltwater route-directed flowset classification. A. Isochronous sheet-flow and isochronous sheet-flow fragments; sheet-flow flowsets comprise lineation imprints of spatially extensive flow, whereas sheet-flow fragments are relatively small such that the spatial extent of linear flow they represent is unknown; they could be linear segments of more spatially extensive linear or curving flow vectors. B. Isochronous convergent and/or divergent flow. Some flowsets are only convergent or only divergent, while others exhibit a continuation from convergent to divergent. Note that flow imprints in valleys were not included in this category; rather they are included as a distinct sub-category. C. Isochronous valley-confined flow. Note that cross-cutting or overprinted time-transgressive signatures could also occur in valley-confined settings. D. Time-transgressive flowline migration, which could relate to migration of the ice divide, migration of the outlet due to ice-margin reconfiguration, or a combination of both. E. Time-transgressive retreat, representing complex overprinting of landforms generated behind a retreating ice margin. F. Time-transgressive thinning or thickening represented by cross-cutting of landform imprints with different degrees of topographic influence on ice flow vectors (including hills or valleys), but with no overall change to the general flow direction. The relative ages of cross-cutting landforms inform the interpretation of whether ice was thinning or thickening. G. Meltwater-route-directed flowsets, in which subglacial lineation imprints appear to curve towards, and terminate at, subglacial meltwater routes. H. Examples of meltwater-route-directed flowsets in Finland (29.04°E, 66.34°N—location shown in Fig. 1) on a shaded-relief map, and their relationships to meltwater routes mapped by Dewald *et al.* (2022). Inset shows examples of landforms within meltwater-directed flowset fs59. Panels D–F are adapted and redrawn from Greenwood & Clark (2009a: fig. 10). Basemap data source for panel H: National Land Survey of Finland Elevation model 2 m 11/19.

of underlying topography upon the orientation of constituent lineations, and may have formed either during a short-lived flow event or under stable ice flow conditions over a longer period. In some cases, isochronous subglacial lineations appear to converge and/or diverge at their up and/or down-flow ends while only sensing or ignoring underlying topography. Alternatively, isochronous flowsets may be confined to valleys. We distin-

Table 2. Flowset classification templates used for our SIS flow-pattern reconstruction, adapted from the approaches developed by Boulton & Clark (1990b), Clark (1990, 1997, 1999), Kleman & Borgström (1996), Kleman *et al.* (1997, 2006), Clark *et al.* (2000), Greenwood & Clark (2009a) and Hughes *et al.* (2014).

Flowset classification	Lineation properties	Lineation orientation relationship to topography	Glaciodynamic context
Isochronous—sheet flow (SHEET)	• No cross-cutting. • High parallel conformity. • Spatially extensive. • Spatial variations in lineation orientations are gradual.	Lineations ignore local topography.	• Extensive area of consistent ice flow. Thick ice compared to magnitude of local topographic relief. • In areas of high topographic relief, flow likely in interior zone of ice sheet. • In areas of low topographic relief, could represent flow closer to the ice margin.
		Lineations partially 'sense' local topography (i.e. some deviations with underlying topography, but may not directly follow valley axes).	• Extensive area of consistent ice flow. Ice is not thick enough with respect to the magnitude of local topographic relief for flow to completely ignore topography, but is not thin enough for topography to dominate flow geometry. • Ice margin may be closer than above.
Isochronous sheet—flow fragment (SHEET FRAG)	• As above, but over a smaller area.	Lineations ignore local topography.	• Spatially limited area of consistent ice flow compared to SHEET. Could reflect extent of original bedform formation, or poorer preservation of bedforms. • Thick ice compared to magnitude of local topographic relief. • In areas of high topographic relief, flow could be in interior zone of ice sheet. • In areas of low topographic relief, could represent flow closer to the ice margin.
		Lineations partially sense local topography.	• Spatially limited area of consistent ice flow compared to SHEET. Could reflect extent of original bedform formation, or poorer preservation of bedforms. • Ice is not thick enough with respect to the magnitude of local topographic relief for flow to completely ignore topography, but is not thin enough for topography to dominate flow geometry.
Isochronous convergent/divergent flow (CONV, DIV, or CONV_DIV)	• No cross-cutting • Lineations converge upflow and/or diverge down-flow, forming a splayed pattern. • Spatial variations in lineation orientations are gradual.	Lineations ignore local topography.	• May suggest zone of relatively fast ice flow. • Convergent signatures may represent flow in interior zone of ice sheet, or flow of relatively thick ice towards an embayment at the ice margin. • -Divergent signatures may represent flow of ice nearer to the ice margin that is relatively thick compared to the magnitude of topographic relief.
		Partially sense topographic features such as large valleys or depressions.	• As above, but ice may be thinner relative to magnitude of relief and/or the ice margin may be closer. Though in high-relief areas, ice could still be thick enough to overtop peaks.
		Lineations funnel into valleys from wider headward zone. Funnelling zone may ignore or only partially sense local topography.	• Ice flow sourcing from large area with relatively thick ice. • Candidate for zone of particularly fast ice flow.

(continued)

Table 2. (continued)

Flowset classification	Lineation properties	Lineation orientation relationship to topography	Glaciodynamic context
			• Potential outlet glacier; relatively thin/slow-flowing ice may remain on adjacent high ground.
Isochronous—valley-confined flow (VALLEY)	• No cross-cutting. • High parallel conformity. • Spatial variations in lineation orientation vary along the axes of the host valley(s).	Lineations are constrained by valleys and follow valley axes, but may ignore or only partially sense local-scale topographic features on valley floors.	• Thin ice relative to the magnitude of topographic relief. Ice could be valley-confined, but thin (cold-based?) ice may remain on higher ground. • Flow near to marginal zone. In areas of high topographic relief, ice could be relatively thick and margin could be relatively far away, but likely closer than for topographically unconfined sheet flow.
		Lineations follow topographic features such as valleys, and also deviate around small-scale topographic features on valley floors.	• Thin, valley-confined ice. • Margin likely nearby.
Time-transgressive—flowline migration (FLOW MIGR)	• Lower parallel conformity. • Spatial discontinuities in lineation orientations. • Lineations may cross-cut. • May exhibit overprinted curved patterns.	May ignore, sense or follow topography. The topographic axis followed by lineations may switch.	• Changing flow pattern due to migration of ice divide and/or outlet, or dynamic onset of CONV, DIV, or CONV_DIV flow.
Time-transgressive—behind retreating ice margin (RETREAT)	As FLOW MIGR, plus: • May exhibit overprinted, backstepping curved or splayed patterns. • Flowset planform may have crenulated lateral margins.	May ignore, sense or follow topography.	• Rapid variation in ice flow direction beneath thin ice near a retreating ice margin.
Time-transgressive—thinning/thickening ice (THINNING, THICKENING)	• Low parallel conformity. • Cross-cutting clustered around topographic features.	Evidence for changes in the degree to which lineations follow topography. If changes reflected in lineation cross-cuts: Ignoring to sensing/following topography = thinning Following/sensing to ignoring topography = thickening.	• Changing thickness of ice relative to local topography, that is, thinning or thickening ice. • Ice margin may be retreating towards (thinning) or advancing away (thickening) from area.
Meltwater-route directed[1] (MELT ROUTE)	• High parallel conformity. • Terminate at margins of subglacial meltwater routes (tunnel valleys or eskers), and at an oblique angle to them (up to 90°). • May exhibit abrupt changes in orientation approaching meltwater routes.	Deflection towards meltwater routes dominates lineation orientations.	• Ice flow locally deflected towards subglacial meltwater drainage pathways. • Flow axis and local ice margin could deviate significantly from regional flow/margin configuration[1].
Unknown (UNKNOWN)	• Few lineations, and/or limited spatial distribution.		• Too few lineations for glaciodynamic interpretation.

[1]As a result of our hypothesis that subglacial lineations in meltwater-route-directed flowsets could have orientations which deviate significantly from regional-scale ice flow directions (see text for explanation), these flowsets were not used to reconstruct ice-sheet-scale flow directions.

guish spatially extensive signatures of sheet flow from smaller, topographically unconfined sheet fragments. Caution is required in interpreting the glaciodynamics of such flowsets; given the large spatial scales of ice-flow sectors of the SIS, relatively small patches of highly parallel lineations could form in a range of contexts. They could represent either fragmentary imprints of more spatially extensive, highly parallel sheet flow or linear segments of broadly curving ice flow vectors that have not been preserved in the subglacial lineation record.

Over time, several sub-classifications of time-transgressive flowsets have developed, reflecting differences in the dominant glaciodynamic conditions reflected in the landform imprint (e.g. Kleman 1994; Kleman & Borgström 1996; Clark *et al.* 2000). We include three sub-classifications adapted from Greenwood &

Clark (2009a) and Hughes *et al.* (2014): (i) ice sheet flowline migration in response to ice divide and/or margin migration, (ii) ice sheet retreat and (iii) ice thinning/thickening.

In some cases, we apply multiple classifications to time-transgressive flowsets which we consider to indicate a combination of margin retreat, ice sheet thinning and/or flowline migration. This reflects the fact that any one of these dynamics is often accompanied by one or both of the other processes, particularly during deglaciation. Some small flowsets lacked sufficient lineations to ascribe a confident glaciodynamic classification and were categorised as 'unknown'.

Within our adapted framework, we also establish a new class of flowset which does not have a legacy in published literature on ice sheet flow-pattern reconstruction. We term this class 'meltwater-route-directed' flowsets. These flowsets comprise small fields of subglacial bedforms which occur adjacent to subglacial meltwater routes (including eskers and tunnel valleys; Dewald *et al.* 2022), and host small, highly parallel subglacial lineations which are oriented obliquely to the meltwater route (at angles up to 90° from the meltwater route axis). In some locations, the lineations curve inwards as they approach a meltwater route from a less oblique orientation up-flow. The constituent lineations often cross-cut subglacial bedforms which exhibit more parallel alignment to meltwater routes. We do not ascribe either an isochronous or time-transgressive classification to these flowsets and return to our interpretation of them and their implications for glaciodynamics and ice flow-pattern reconstruction in the results.

Whereas some previous studies identified ice streams —corridors of particularly fast flow which drain large volumes of ice from ice sheets—as a glaciodynamic subcategory of isochronous flowsets (e.g. De Angelis & Kleman 2005; Greenwood & Clark 2009a; Hughes *et al.* 2014; Boyes *et al.* 2023), we opted not to include this category in our classification scheme. This approach acknowledges that the lineation imprints of ice streams may not always be isochronous and could reflect time-transgressive dynamics such as retreat, thinning, and/or flowline migration during ice streaming. Ice streams can host particularly elongate subglacial lineations interpreted as indicators of fast ice flow, but their robust identification requires the application of a set of additional morphological criteria beyond subglacial lineations (e.g. Stokes & Clark 1999, 2001, 2002; Margold *et al.* 2015), which is beyond the scope of this work.

Our flowset classification scheme does not stipulate that certain classes of flowset relate to a specific phase of ice sheet evolution (i.e. ice sheet advance or deglaciation). The top-level classification of isochronous versus time-transgressive flowsets simply pertains to the divisibility of discrete imprints of ice flow in the subglacial lineation record; isochronous flowsets exist where the subglacial lineation imprint is divisible into discrete flow patterns, while time-transgressive flowsets represent compound imprints of time-variable ice flow. While time-transgressive retreat flowsets (as well as meltwater route-directed flowsets) most likely relate to deglaciation, other time-transgressive flowsets could relate to either advance or retreat phases. Time-transgressive thinning/thickening flowsets could reflect wider changes in ice thickness during overall ice sheet retreat/advance, or shorter-term or more localized variations in the height of the ice surface during either of these phases. Isochronous flowsets can relate to ice sheet advance or retreat phases; an isochronous flowset could form beneath ice in the ice-sheet interior, or closer to an advancing or retreating ice margin (Table 2). To begin ascertaining the different stages of ice flow evolution to which individual flowsets likely relate, we next placed them into relative-age sequences indicated by cross-cutting and superimposition relationships.

Flow-pattern evolution

Subglacial lineations provide a fragmentary record of ice flow evolution. This is because subglacial bedforms do not form on every part of the ice sheet bed, and in many areas, are likely to have been either eroded or buried by later processes (cf. Kleman 1994). Hence, our flowsets represent a multi-layered, fragmentary palaeoglaciological 'jigsaw puzzle' (see e.g. Kleman & Borgström 1996: fig. 2). In this multi-layered puzzle, individual layers contain groups of flowsets that represent a coherent, glaciologically plausible spatial pattern of ice flow during a broad stage of ice sheet evolution. Different layers represent distinct stages of ice sheet evolution. Between these stages, the size and shape, ice divide position (i.e. centre-of-mass) and/or flow patterns of the ice sheet (or major ice-sheet sectors) may have changed. Thus, the sequencing of the stages should capture the overall evolution of the ice sheet flow geometry through time.

To begin separating plausible stages of ice sheet flow geometry, and to place them in temporal order, we identified locations where two or more flowsets intersect. Often, subglacial lineations that belong to distinct intersecting flowsets exhibit superimposition (i.e. cross-cutting) relationships, which provide direct evidence for the relative-age sequence of the ice flow events that formed them (Figs 2F, 5). We used these landform cross-cuts to establish the relative-age sequence of flowsets and narrow down the range of possible stages they could belong to. We identified a 'critical cross-cut' for each flowset intersection where cross-cutting subglacial lineations were observed and marked their locations in a dedicated GIS layer (points shapefile—Data S1) containing the relative-age information. We also mapped the crestlines of the critical cross-cuts in another layer (polyline shapefile—Data S1), which records the orientations of the constituent subglacial lineations.

We synthesised the critical cross-cut information into a table (Table S1), which represents the relative-age sequences observed. Figure 5 illustrates this process, with horizontal bars representing observed cross-cutting relationships. 44% of our flowsets are 'floating' (Table S1); that is, they either lack distinct cross-cutting relationships with intersecting flowset(s) or are spatially separated from other flowsets. Floating flowsets thus have unconstrained relative ages based on subglacial lineation cross-cuts alone, and could fit into any layer of our figurative jigsaw puzzle. Similarly, cross-cutting rarely generates contiguous relative-age sequences across large sectors of the ice sheet (e.g. Greenwood & Clark 2009a; Kleman *et al.* 2010; Hughes *et al.* 2014). Hence, groups of cross-cutting flowsets often have unconstrained relative ages to flowsets in neighbouring areas, and could slide up or down the sequence relative to them (represented by vertical bars in Table S1).

Each layer of our SIS jigsaw puzzle should contain flowset groupings that represent a glaciologically coherent spatial pattern consistent with a broad stage of ice sheet flow evolution. Thus, we applied two further, more interpretative steps, first at the regional scale, then at the ice-sheet scale (Fig. 4), with iteration between the two. We divided the ice sheet into 14 'working regions', defining region boundaries where cross-cutting between flowsets in adjacent regions was minimal, and flagging 'connector flowsets' which did cross-cut in (and thus could be used to link) multiple regions. We used the critical cross-cuts to generate 120 initial interpretative 'flowset pattern groups', which represent groups of flowsets with coherent spatial patterns which could have formed under similar regional-scale ice flow configurations and, based on cross-cutting relationships (or a lack thereof), at similar stages of ice flow evolution. We aimed to explain regional flowset patterns with the minimum level of complexity while honouring relative-age information provided by cross-cutting landforms. When ascribing connector flowsets to pattern groups, we considered their patterns and cross-cutting relationships with flowsets in the relevant adjacent region. This process placed many flowsets—including floating flowsets which lacked cross-cutting information—into initial inferred relative-age sequences at the regional scale. Some floating flowsets did not form spatially coherent patterns within their respective regions, and remained unassigned to pattern groups; where possible they were incorporated at the ice-sheet scale later.

We used our first iteration of the pattern groups to identify potential correlations between adjacent working regions, ensuring that cross-cutting information from connector flowsets was honoured. This reduced the pattern groups into a set of initial draft stages of flow-pattern evolution, which we then iterated. Stages do not necessarily represent an exact snapshot in time, rather a broad phase of ice flow at the ice-sheet scale that can be inferred from spatially coherent groups of flowsets preserved across the SIS bed. The formation of subglacial lineations may have been somewhat asynchronous between different flowsets in any given stage. Flowsets assigned to any given stage should also honour a set of basic assumptions of ice sheet behaviour, informed by observations of contemporary ice sheets (e.g. following Clark *et al.* 2006; Greenwood & Clark 2009b; Hughes *et al.* 2014). We used the following guiding principles to iterate upon our initial stage assignations for individual flowsets, and generate a final set of ice sheet stages which represent a glaciologically plausible scenario for the flow-pattern evolution of the SIS:

- Ice sheets tend to initiate in mountainous areas (e.g. Barry *et al.* 1975; Ives *et al.* 1975; Andrews & Barry 1978; Fredin 2002; Oerlemans 2002; Bahadory *et al.* 2021), before flowing out into adjacent lowlands.
- Ice sheet flow radiates from an ice divide. There will always be at least one (primary) ice divide, though subsidiary divides may also occur, either branching from the major divide or being connected to the primary divide across a saddle (a lower-elevation ice divide between thicker ice masses) in the ice sheet surface.
- Contemporary ice sheets in Antarctica and Greenland are broadly symmetrical, with a similar extension in most directions from their primary ice divides. The topography of the former bed of the SIS—with a spine of high-relief mountains only a short distance from the Norwegian continental shelf break to the west, and extensive low-relief regions to the east—likely necessitates more significant asymmetry in ice sheet planform. We therefore allow asymmetry; that is, a greater extension of the ice sheet eastwards from the ice divide.
- Ice can extend beyond the contemporary landmass of Fennoscandia, including across the Gulf of Bothnia and Baltic Sea, into the North Sea, White Sea and Barents Sea and out to the Norwegian continental shelf. Depending on the thickness of ice at any given time, ice flow may have been influenced by topographic depressions offshore, including in the Gulf of Bothnia, the Baltic Sea, the Skagerrak and Kattegat straits, and the White Sea. The SIS is known to have connected with the BKIS to the north and the BIIS to the southwest (Hughes *et al.* 2016 and references therein; Sejrup *et al.* 2022).
- Subglacial lineations are not expected to form directly underneath the ice divide, where ice velocity tends towards zero. Therefore, flowsets must relate to ice flow at some distance from the ice divide. To explain flowsets that are in close proximity to one another but summarise subglacial lineations which indicate opposing flow directions, it is usually necessary to invoke migration of the ice divide (Fig. S2; e.g. Boulton & Clark 1990a, 1990b). Similarly, flowsets do not necessarily extend all the way to the ice margin posi-

tion, which may be a significant distance down-flow from the termination of subglacial lineations.

- Changes in ice flow configuration are required, at least locally, to explain observed superimposition of cross-cutting landforms. Local-scale ice flow fluctuations do not necessarily require major reconfiguration of ice-sheet-scale flow and can be caused by local thinning or thickening, and advance or retreat.
- Major reconfiguration of ice sheet flow can occur asynchronously across different sectors of an ice sheet, for example, due to spatially variable rates of ice advance and/or retreat (e.g. Clark *et al*. 2022: fig. 11).
- Time-transgressive flowsets inherently represent changes in ice flow direction and/or ice divide/margin position that cannot be robustly separated into distinct packages (i.e. two or more isochronous flowsets). Thus, different portions of a time-transgressive flowset may have been 'active' in different stages of ice flow evolution. In these cases, an ice divide or ice margin could be located over portions of time-transgressive flowsets that are interpreted as relating to a different stage of ice sheet flow evolution.
- The state of an ice sheet at any given stage will be influenced by its antecedent state. Hence, a given stage of ice flow evolution may be constructed with 'memory' of preceding stage(s). In using flowset evidence to reconstruct stages of ice-flow evolution, where choices are available, it is preferable to choose that scenario which requires the minimum level of complexity.
- While the glacial landform record is assumed to primarily derive from the most recent ice sheet, it is thought that landforms from earlier glaciations form part of the preserved evidence in Fennoscandia (e.g. Hoppe 1952; Hirvas *et al*. 1988; Lagerbäck 1988; Kleman *et al*. 1997; Alexanderson *et al*. 2022; Greenwood & Hughes 2022a). We therefore do not attempt to explain all of the identified flowsets within a single ice advance and retreat cycle. We take a 'no preconceptions' approach, in which we identify flowsets potentially relating to earlier glacial cycles purely based on flowset pattern and relative age relationships recorded by cross-cutting landforms.

The process of assigning individual flowsets to final ice-sheet-scale stages was necessarily iterative. Flowsets were first considered individually and in the context of regional pattern groups (see above). Considering regional pattern groups at the ice-sheet scale resulted in many flowsets—and particularly 'floating' flowsets with no cross cuts—being detached from their original regional pattern groups and reconciled into different stages of ice flow. During this iterative process, we ensured that the relative-age sequences (Table S1) were honoured. We identify 14 flowsets which represented minor reconfigurations of regional-scale flow that did not warrant a separate stage of flow evolution at the ice-sheet scale (fs610, fs668, fs892, fs257, fs50, fs706, fs29, fs30, fs875, fs971, fs104, fs693, fs695, fs696; see Data S2). We interpret these flowsets as describing intermediate, local-scale flow fluctuations occurring between our reconstructed stages of ice flow; this substage information is recorded in Tables S1 and S2, in Data S2, and in the flowset shapefiles (Data S1). Some flowsets appear in multiple stages (up to three), for example, where we infer stability of a sector of the ice sheet while another sector evolves. We correlated our stages with ice-flow stages and flowset groupings of Boyes *et al*. (2023) over the Kola Peninsula and Russian Lapland (see Table S2).

Final groupings of flowsets into ice-sheet-scale stages differ significantly from the original pattern groupings we generated at regional scales; hence we have not included the initial pattern groupings in our published datasets to minimise confusion for those re-using the data. However, we found that the pattern group approach was an extremely useful—perhaps essential—methodological step to reduce the rich and complex relative age and flow-pattern information into a manageable format upon which we could then iterate.

We used the extent and configuration of flowsets in each stage to infer the position(s) of the ice divide(s) and generalised ice-sheet-scale flow vectors. We also infer an 'ice bounding line' to represent the approximate size and shape of the ice sheet that is required to contain the flow information for each stage. We strongly emphasise that these ice bounding lines do not represent exact ice extents or margin positions, nor do they necessarily represent exactly time-synchronous configurations; rather they are a representation of the approximate ice sheet geometry that would be compatible with the reconstructed ice-flow-pattern configuration. Connecting our flow patterns to specific ice margin positions is beyond the scope of the present study, requiring extensive integration with mapping of ice-marginal landforms across the ice sheet domain and significant additional interpretation to connect them to detailed ice-flow patterns.

As a general rule, while generating our stage reconstructions, we avoided making inferences about their placement in absolute time. The exceptions were stages containing flowsets entirely within, or just beyond, the generally well-established maximum limits achieved during MIS 2 and the Younger Dryas (YD; see Andersen *et al*. 1995a, b; Hughes *et al*. 2016; Stroeven *et al*. 2016; Batchelor *et al*. 2019; Mangerud, Hughes, *et al*. 2023b; Boyes *et al*. 2024). Flowsets ascribed to Stage 17 and subsequent stages were not allowed to extend beyond the outermost YD extent delimited in Hughes *et al*. (2016: fig. 8) and Boyes *et al*. (2024), and the most areally extensive bounding line for all stages could not extend beyond the maximum-achieved extent of the last SIS (based on Hughes *et al*. 2016). Where necessary, we modified the inferred flow vectors, ice divides and outer bounding lines inferred by Boyes *et al*. (2023) over the Kola Penin-

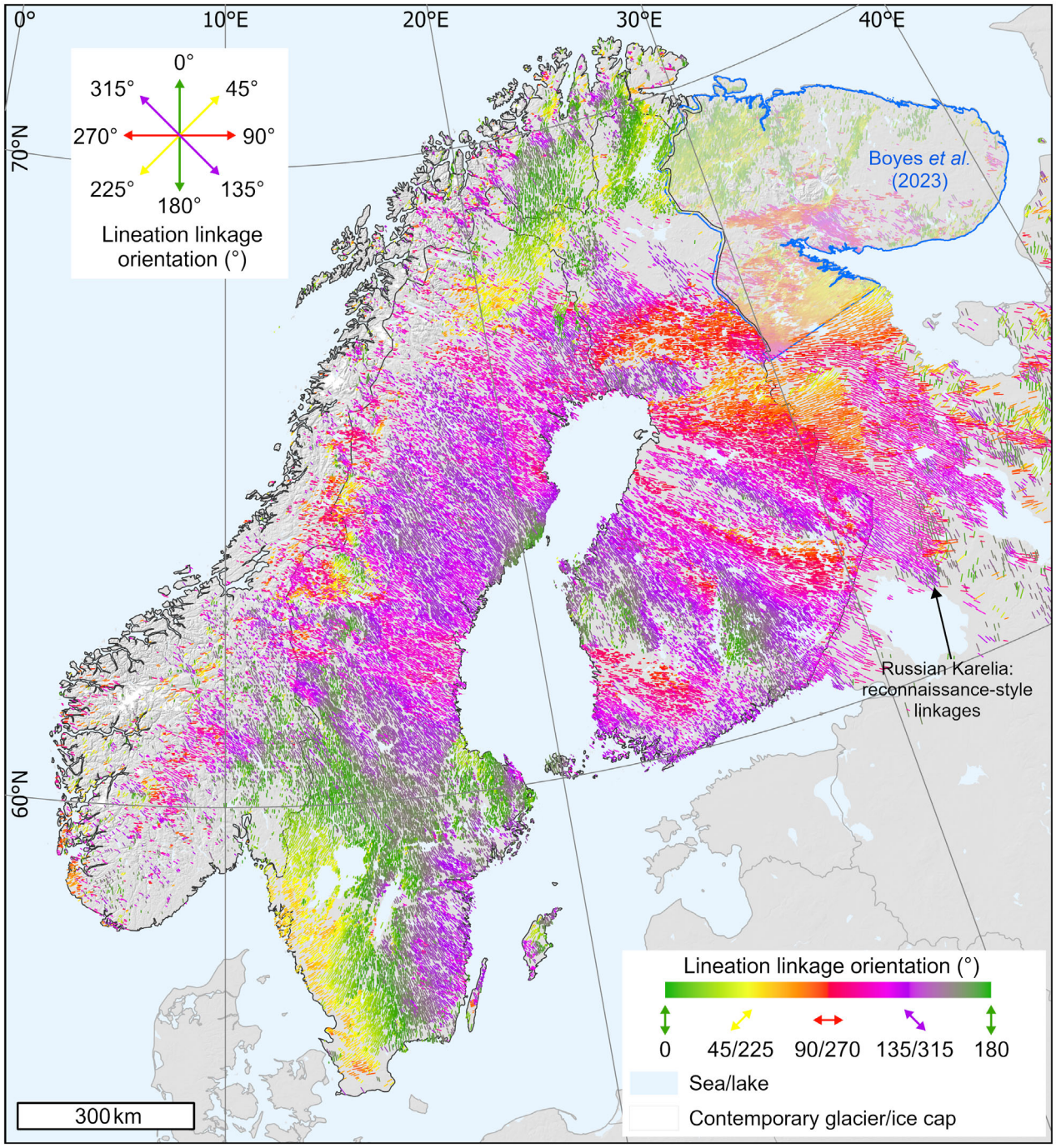

Fig. 9. Lineation linkages over Fennoscandia (n = 53 433) and NW Russia (n = 4355), colourised by orientation. Note that orientation is with respect to the map frame rather than true north. See Fig. S3 for a larger map and Data S1 for the shapefile data. The map includes the following: lineation linkages generated in step 3 of our multi-scale mapping approach over Norway, Sweden and Finland; supplementary reconnaissance-style linkages extending into and beyond Russian Karelia (see Data and methods); and lineation linkages from Boyes *et al.* (2023) over the Kola Peninsula and Russian Lapland. Note, the specific approaches to linkage generation differ somewhat between our study and that of Boyes *et al.* (2023), but they are shown here (with transparency applied) to illustrate the relationship to ice-flow orientations in our mapping area. For visual clarity, orientations are represented on a 0°–180° colour scale, but note that the dataset (Data S1) also includes orientations on a 0°–360° scale. The small DTM gaps that existed in Norway during mapping Steps 1 and 2 (Fig. 5) were carefully filled in during the generation of lineation linkages, as DTM coverage became available. Our linkage dataset extends to the ice sheet's eastern maximum limit; the easternmost linkages (included in the larger map in Fig. S3) are not visualised here to improve clarity over the main study area. See Fig. S4 for lineation linkages colourised by confidence. Data credit for shaded-relief basemap: Airbus, USGS, NGA, NASA, CGIAR, NLS, OS, NMA, Geodatastyrelsen, GSA, GSI and the GIS User Community.

sula and Russian Lapland based on the wider ice sheet context. Given the ice-sheet-wide scale of our flow-pattern reconstruction, this typically resulted in a simplified representation of localised complexities with respect to Boyes *et al*. (2023).

Results

Ice flow directions recorded by subglacial bedforms over the interior of the Scandinavian Ice Sheet

We generated 53 433 lineation linkages over Norway, Sweden and Finland, and a further 4355 supplementary reconnaissance-style lineation linkages (see Data and methods) over NW Russia. Figure 9 (see also Fig. S3) shows a map of our lineation linkages along with those generated over the Kola Peninsula and Russian Lapland by Boyes *et al*. (2023). In both the core mapping area and NW Russia, the proportion of our linkages ranked as medium-to-high confidence exceeds 90%. Low-confidence linkages represent <10% of the population, and very low confidence linkages represent ~1%. Lineation linkages categorised by confidence are shown in Fig. S4.

Flowsets and glaciodynamic interpretations

We generated 611 flowsets over Norway, Sweden, Finland, and extending into Russian Karelia (Figs 10, S5). Our flowsets have a cumulative area of 1.59×10^6 km^2. Of this area, 32% is accounted for by overlaps between flowsets; the total Earth surface area covered by one or multiple flowsets is 1.08×10^6 km^2. Flowsets cover the majority of Sweden and Finland (both 93% coverage), but only 52% of Norway. For the flow-pattern reconstruction, we additionally adopt 171 flowsets of Boyes *et al*. (2023), and the regional flow-pattern stage groupings to which they were assigned in that study. These flowsets were based on landform mapping that extended 5 km into Finland and Norway; they intersect with six of our flowsets, with good flowline agreement in the overlapping areas. The remainder of the Boyes *et al*. (2023) flowsets initiate outside of our mapping area.

Flowset size varies significantly, from 1.14 km^2 (fs820, a valley-confined flowset on a small Norwegian island) to 103 760 km^2 (fs297, a time-transgressive thinning and retreat flowset in S Sweden). Flowset size exhibits a significant positive skew, with a median area of 152 km^2 and a mean area of 2597 km^2; this results from the large numbers of small flowsets that occur within the complex, high-relief terrains of Norway and the Scandinavian mountains. Flowsets in low-relief regions of Finland and Sweden tend to be more spatially extensive.

Of the 611 flowsets generated in this study, 63 (10%) were marked as low confidence, and 5 (1%) as very low confidence. These flowsets tend to be small, accounting for just ~3% of the cumulative flowset area. Flowsets were given these confidence classifications if, for example, they hosted a significant proportion of low or very low confidence lineation linkages, sparse lineation linkages or occurred in areas where bedrock structure made the identification of glacially streamlined features more challenging. The ice flow direction was deemed uncertain for a small number of flowsets (19), accounting for 0.05% of the cumulative flowset area. In these cases, we made our best judgement of the likely flow direction based on the morphology of subglacial lineations, and marked the uncertainty with a note in the flowset shapefile (Data S1).

We identified 359 pairs of cross-cutting landforms ('critical cross-cuts') which indicate the relative-age sequences of our flowsets. They represent cross-cuts between 342 unique flowsets. The remaining 269 flowsets are floating in the relative-age sequence (Fig. S6), being spatially isolated or lacking cross-cutting landforms with other flowsets. Twenty-eight critical cross-cuts were marked as 'lower confidence', where the relative-age sequence of cross-cutting landforms was uncertain. The relative-age sequence of flowsets (illustrated in Fig. 5) is synthesised in Table S1, which also contains information on flowset assignments to interpreted stages of ice flow evolution, described later.

We classified 456 flowsets (~75% of total) as isochronous, 72 (~12%) as time-transgressive, and 24 (~4%) as meltwater route-directed (Table 3, Fig. 11). The remaining 59 (~10%) flowsets had insufficient landform information to assign a glaciodynamic classification. While isochronous sheet flow fragments and isochronous valley-confined flowsets are the most numerous, they each account for small percentages of the cumulative flowset area (3% and 1%, respectively). The most extensive glaciodynamic signatures, as a proportion of the cumulative flowset area are isochronous sheet flow (43%), isochronous divergent flow (19%), time-transgressive flowline migration (15%) and time-transgressive thinning (11%). Seven time-transgressive thinning flowsets exhibited supplementary signatures of flowline migration or retreat (Table 3).

Isochronous flowsets occur throughout the domain (Fig. 11A). Isochronous sheet flow dominates over central Sweden and N Finland and also extends across Finland into NW Russia. Sheet flow also occurs over the Scandinavian mountains in the Trøndelag region of Norway. Isochronous divergent flowsets are largely concentrated in S Sweden and south-central Finland, with some smaller divergent flowsets located closer to the Scandinavian mountains in Sweden and Norway and in S Norway. Isochronous convergent and valley-confined flow dominates over the Scandinavian mountains and along the Norwegian coast. Some convergent flowsets also occur around the Gulf of Bothnia, but sheet flow is the most dominant signature here. Isochronous sheet fragments are distributed throughout the domain.

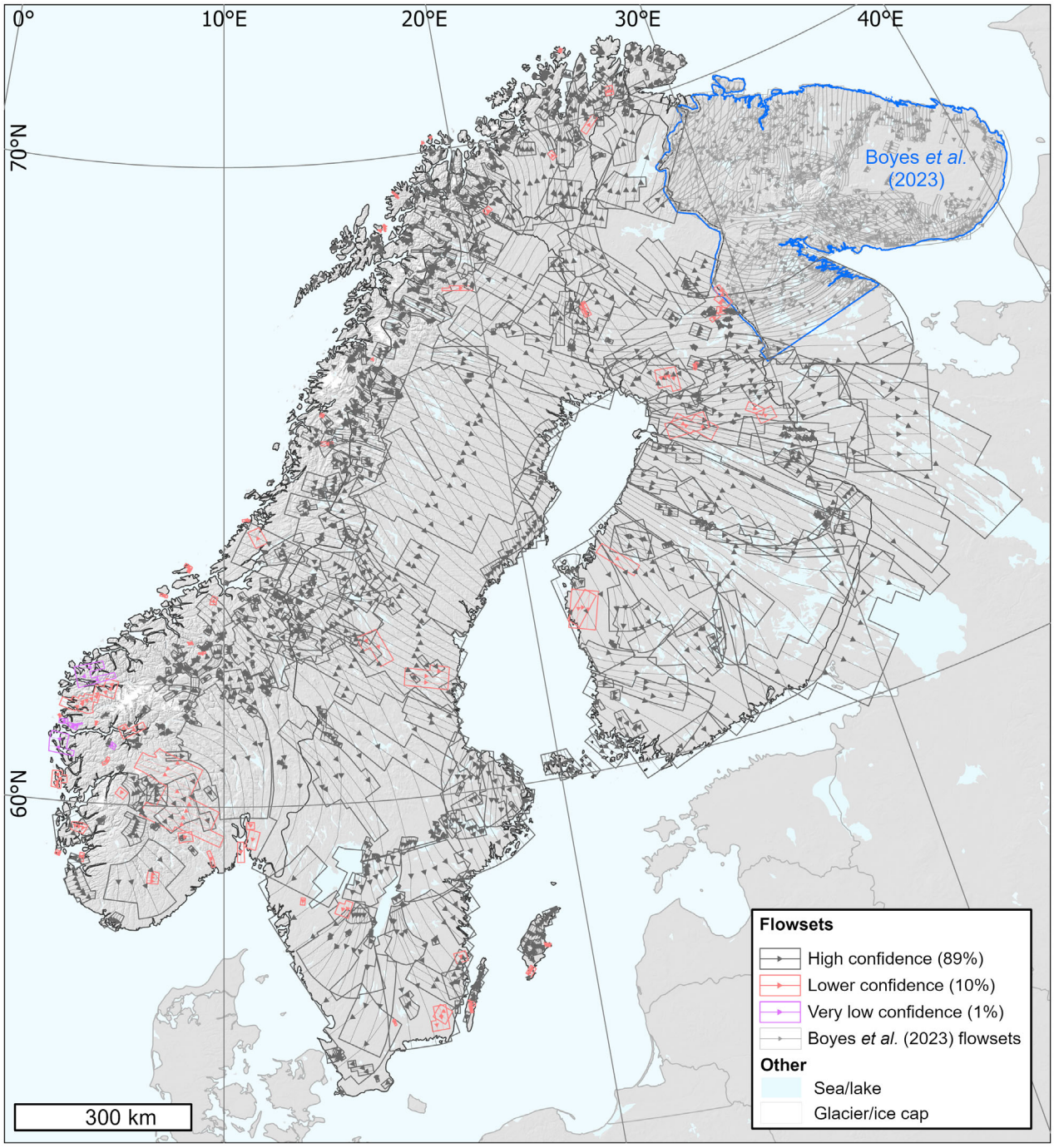

Fig. 10. Map of flowsets generated over Norway, Sweden, Finland, and extending into Russian Karelia. Flowsets are colourised by confidence. See Data S1 for shapefile data. Also shown are flowsets over the Kola Peninsula and Russian Lapland (blue outline) from Boyes *et al.* (2023). The map is best viewed at full scale in Fig. S5. Flowsets that are 'floating' in the relative-age sequence (i.e. which lack cross-cutting relationships with other flowsets) are shown in Fig. S6. Flowsets colourised by the influence of topography on their internal ice flow vectors are shown in Fig. S7, and flowsets colourised by their glaciodynamic classifications are shown in Fig. S8. Data credit for shaded-relief basemap: Airbus, USGS, NGA, NASA, CGIAR, NLS, OS, NMA, Geodatastyrelsen, GSA, GSI and the GIS User Community.

Time-transgressive flowsets exhibit strong spatial clustering (Fig. 11B). Flowsets with signatures of flow-line migration occur predominantly over NE Sweden, N Norway, and northern-central Finland, with additional significant examples on the SW coasts of Sweden and Norway. Flowsets with signatures of thinning occur predominantly in S Norway, south-central Sweden and among E–W oriented flowsets in the Scandinavian

Table 3. Statistics for flowset glaciodynamic classifications and relationships of their constituent subglacial lineations to bed topography. Note that percentages do not sum to 100% due to rounding. Those 'relationship to topography' sub-classes for which no flowsets were identified are not included in the table.

Flowset classification	Number of flowsets	% of all flowsets (n = 611)	% Flowset cumulative area (cumulative area = 1.59 × 106 km^2)	Relationship to topography	Number of flowsets in topographic subclass
Isochronous—sheet flow	65	11%	43%	Ignore	31
				Sense	34
Isochronous—sheet-flow fragment	130	21%	3%	Ignore	52
				Sense	78
Isochronous—convergent	38	6%	2%	Ignore	1
				Sense	32
				Funnel	5
Isochronous—divergent	64	10%	19%	Ignore	26
				Sense	38
Isochronous—convergent and divergent	3	<1%	<1%	Sense	2
				Funnel	1
Isochronous—valley-confined	156	26%	1%	Ignore[2]	6
				Sense[2]	99
				Follow[2]	51
Time-transgressive—flowline migration	15	2%	15%	Ignore	4
				Sense	11
Time-transgressive—behind retreating ice margin	15	2%	4%	Sense	15
Time-transgressive—thinning[1]	41	7%	11%	Sense	34
				Funnel	1
				Follow	6
Time-transgressive—thickening	1	<1%	<1%	Sense	1
Meltwater route directed	24	4%	<1%	Ignore	11
				Sense	13
Unknown	59	7%	<1%	Ignore	22
				Sense	25
				Unknown	12

[1]Within the time-transgressive—thinning class, 4 flowsets showed notable supplementary signatures of time-transgressive flowline migration, and 3 showed notable supplementary signatures of time-transgressive retreat.
[2]By definition, valley-confined flowsets follow broad-scale topography. Hence, for valley-confined flowsets, the topographic characterisations shown here refer to the relationship to local topography on the valley floor.

mountains. A single flowset interpreted to represent ice thickening was identified in S Norway (fs284). Flowsets with signatures of ice retreat occur predominantly in S Sweden and south-central Finland, with an additional significant example extending into Norway from N Finland.

We identified a small number of meltwater-route-directed flowsets (Fig. 11C), predominantly in central Finland (Fig. 8H) with additional examples in N Norway and S Finland. These flowsets have small areas (maximum = 278 km^2, median = 57 km^2), and are at the limits of our linkage- and flowset-mapping resolutions. Meltwater-route-directed flowsets account for <1% of the cumulative flowset area. We briefly explore the implications for ice-flow patterns of this new glaciodynamic classification (see 'Data and methods') before we reconstruct ice flow-pattern evolution at the ice-sheet scale. Meltwater-route-directed flowsets often appear in groups, as discrete flowsets arranged along (and in some cases on both sides of) major subglacial meltwater corridors represented by tunnel valleys and/or eskers (e.g. Dewald *et al.* 2022). They are particularly abundant along a 55 km-long portion of a major subglacial meltwater corridor in E Finland (Fig. 8H), with the characteristic deviations in subglacial lineation orientations varying consistently along the sinuous profile of the meltwater route. Such flowsets appear similar to features interpreted by Dowling *et al.* (2016) as representing ice flow into ice-marginal calving bays. Punkari (1994) also observed local deviations of glacial striae towards meltwater routes within larger deglacial flow patterns. We thus interpret our meltwater-route-directed flowsets as representing localised diversions of ice and/or subglacial meltwater flow towards major corridors of subglacial meltwater drainage. Such diversions could be driven by localised variations in the basal hydraulic gradient and/or in the ice margin geometry over the outlets of subglacial drainage conduits (be they lake or land-terminating ice-margin embayments). In the meltwater-route-directed flowsets we observe, the lineation imprints lack cross-cutting and hence could represent localised isochronous flow events. However, given the probable time-transgressive nature of meltwater corridor formation behind retreating ice margins (e.g. St-

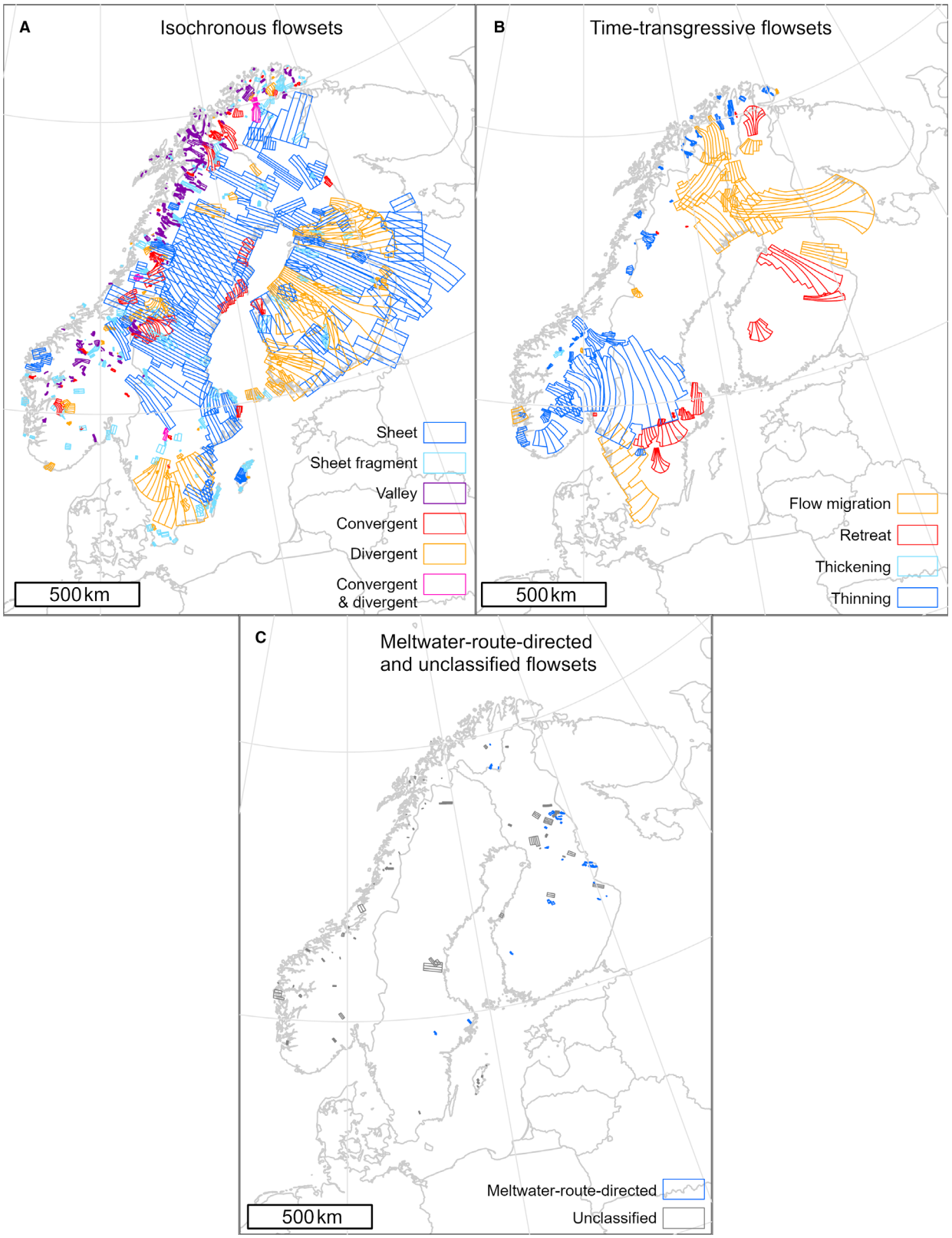

Fig. 11. Flowset glaciodynamic classifications. A. Isochronous flowsets, colourised by subclassifications described in Table 2 and Fig. 8. B. Time-transgressive flowsets, colourised by subclassifications described in Table 2 and Fig. 8. Note that the primary classifications are shown here. Some time-transgressive flowsets had secondary classifications (e.g. evidence for retreat in addition to thinning), which are recorded in the flowset shapefile (Data S1). C. Meltwater-route-directed and unclassified flowsets. See Fig. S8 for a larger map of flowset glaciodynamic classification.

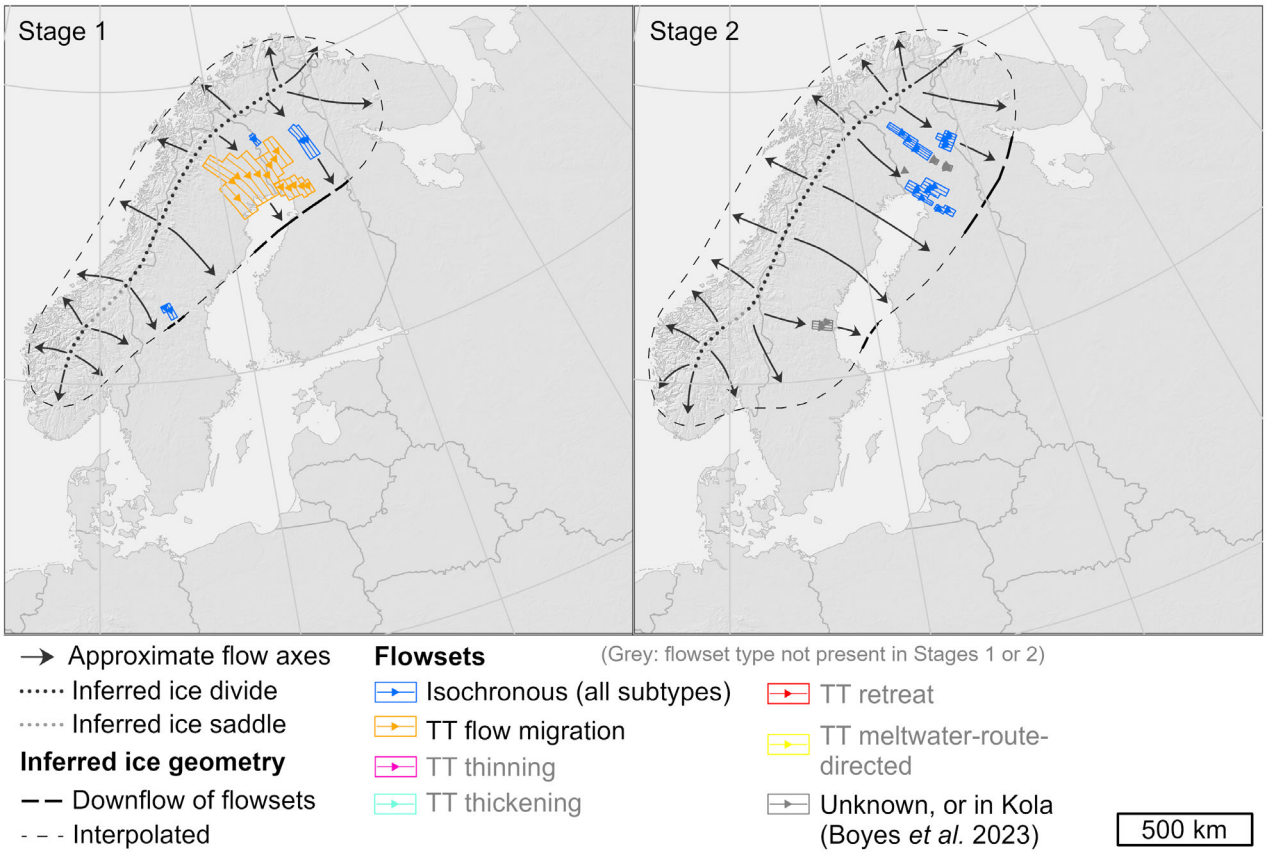

Fig. 12. Stages 1 and 2 of our ice flow-pattern reconstruction. Note that the inferred ice geometries illustrated by dashed lines (which we term 'ice bounding lines') are not precise ice margin positions; rather they depict a generalised size and shape of the ice sheet inferred based on flow-pattern information. We interpret these stages as recording bedform signatures of a pre-MIS-2 (likely MIS 4 or older) ice sheet, which were preserved through the advance and retreat of the last SIS. TT denotes time-transgressive flowsets (see 'Data and methods', and Table 2). See Fig. S9 for A3 versions of the stage maps, and Fig. S10 for A3 versions with individual flowset IDs referred to in the text. Data S2 contains larger A0 maps of flowsets colourised by stage, and Data S1 contains the shapefile data for each stage. Data credit for shaded-relief basemap: Airbus, USGS, NGA, NASA, CGIAR, NLS, OS, NMA, Geodatastyrelsen, GSA, GSI and the GIS User Community.

Onge 1984; Kleman & Borgström 1996; Lewington *et al.* 2020; Dewald *et al.* 2022; Vérité *et al.* 2024) and the occurrence of multiple meltwater route-directed flowsets along significant lengths of individual meltwater routes (Fig. 8H), we do not ascribe either an isochronous or time-transgressive classification to this flowset class. We deemed that these flowsets should not be used for reconstructing ice-sheet-scale flow patterns because, according to our hypothesis, the orientations of their constituent subglacial lineations relate to local variations in subglacial hydraulic pressure gradients and could deviate from the regional ice flow direction by up to 90°, effectively parallel to the regional ice margin. As a result, while we use cross-cutting relationships of these flowsets to inform our interpretation of the minimum size of the ice sheet in the stages in which they appear, we do not use them as a basis for constructing ice-sheet-scale flow patterns.

The orientations of subglacial lineations in a majority of flowsets exhibit some degree of sensitivity to bed topography (Table 3). There are 156 isochronous valley-confined flowsets, which follow broad-scale topography though display varying degrees of topographic sensitivity to local variations within their host valley floors. Of the 455 remaining flowsets, 32% comprise subglacial lineations whose orientations ignore underlying topography, while 62% sense topography, 2% funnel down topography from wider catchments and 1% closely follow topography (but are not valley-confined). 3% of flowsets were deemed to have insufficient information for topographic classification.

Ice sheet flow-pattern evolution over Fennoscandia

We reconstructed 25 interpretative stages of SIS flow-pattern evolution (Figs 12, 13, S9, S10, Tables S1, S2, Data S1, S2). These stages honour the cross-cutting relationships indicated by critical cross-cuts, and the guiding principles for ice-sheet-scale flow-pattern reconstruction (see 'Data and methods'). They include two stages which

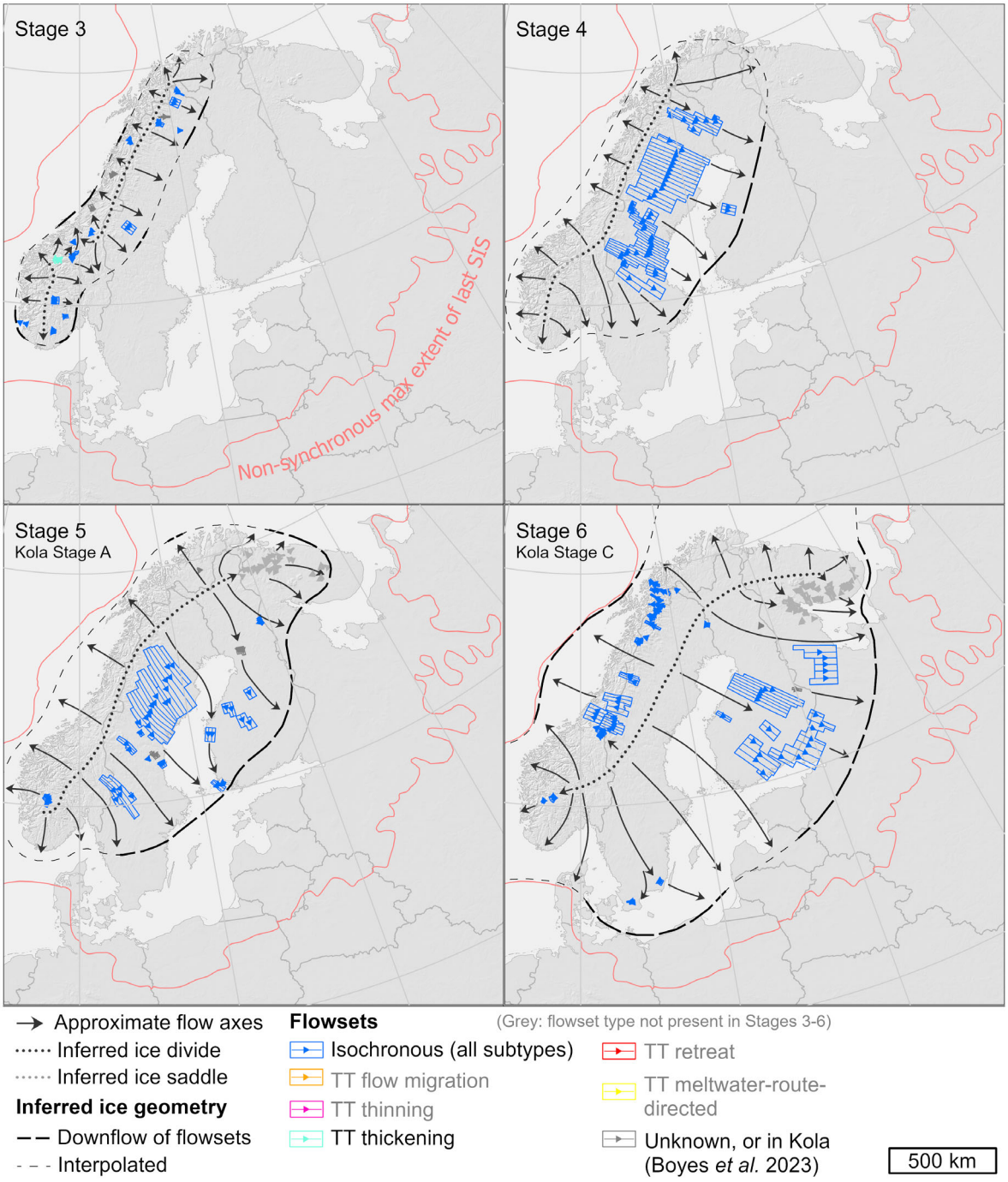

Fig. 13. Stages of flow-pattern evolution of the last SIS, reconstructed based on subglacial lineations over Norway, Sweden, Finland and NW Russia. Note that the inferred ice geometries illustrated by dashed lines (which we term 'ice bounding lines') are not precise ice margin positions; rather they depict a generalised size and shape of the ice sheet inferred based on flow-pattern information. The red line is the non-synchronous maximum extent of the last SIS (see Hughes *et al*. 2016). Grey flowsets over the Kola Peninsula and Russian Lapland are from Boyes *et al*. (2023; correlations to their stages are noted in the relevant panel). TT denotes time-transgressive flowsets (see 'Data and methods', Table 2). In areas lacking flowsets in any given stage, reconstruction was performed by interpolating between areas with flowsets, while also considering the 'memory' of the preceding stage and knowledge of the evolutionary trajectory required to achieve the configuration in the subsequent stage. Flow axes extending into the ice sheet periphery, beyond our mapping domain (i.e. S and E of the Baltic Sea), are highly generalised and based solely on reconstructed ice flow from the ice sheet interior. Similar to Kleman *et al*. (1997), we do not attempt to reconstruct details of flow out to the highly crenulated and time-asynchronous maximum extent of the last SIS. See Fig. S9 for A3 versions of the stage maps, and Fig. S10 for A3 versions with individual flowset IDs referred to in the text. Data S1 contains shapefile data for each stage. See also Fig. S6 for a map of 'floating' flowsets, which do not have relative age information from cross-cutting subglacial lineations, and Data S2 for larger A0 maps of flowsets colourised by stage. Data credit for shaded-relief basemap: Airbus, USGS, NGA, NASA, CGIAR, NLS, OS, NMA, Geodatastyrelsen, GSA, GSI and the GIS User Community.

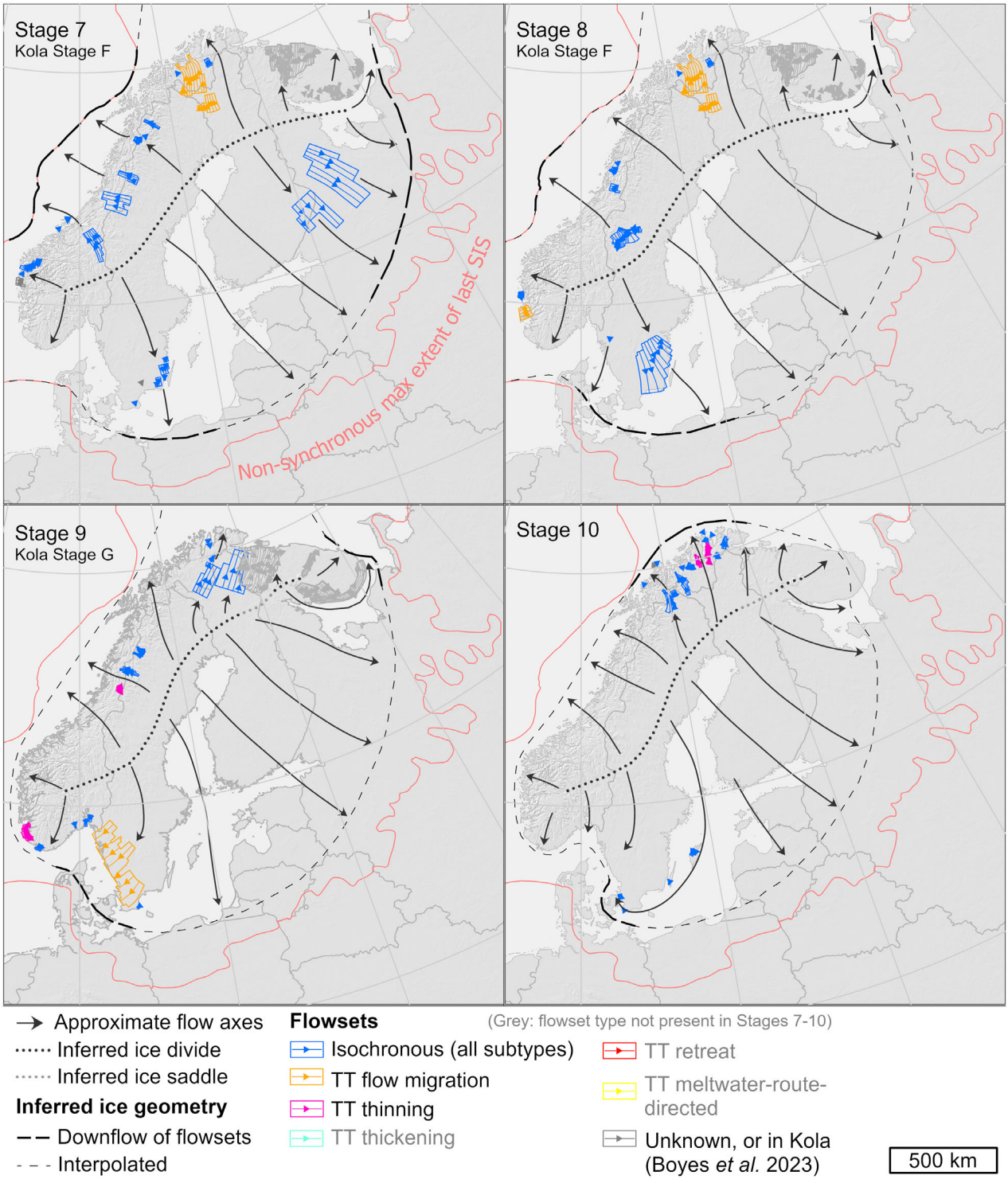

Fig. 13. Continued

we infer may relate to a relatively old ice sheet which preceded the advance of the last (MIS 2) SIS (Fig. 12). We reiterate that the bedform imprints and hence flowset groupings in any given stage may be time-asynchronous and that the bounding lines reconstructed for each stage (see 'Data and methods') represent the approximate ice sheet size and shape evidenced by flowsets, as opposed to specific documented ice margin positions derived from

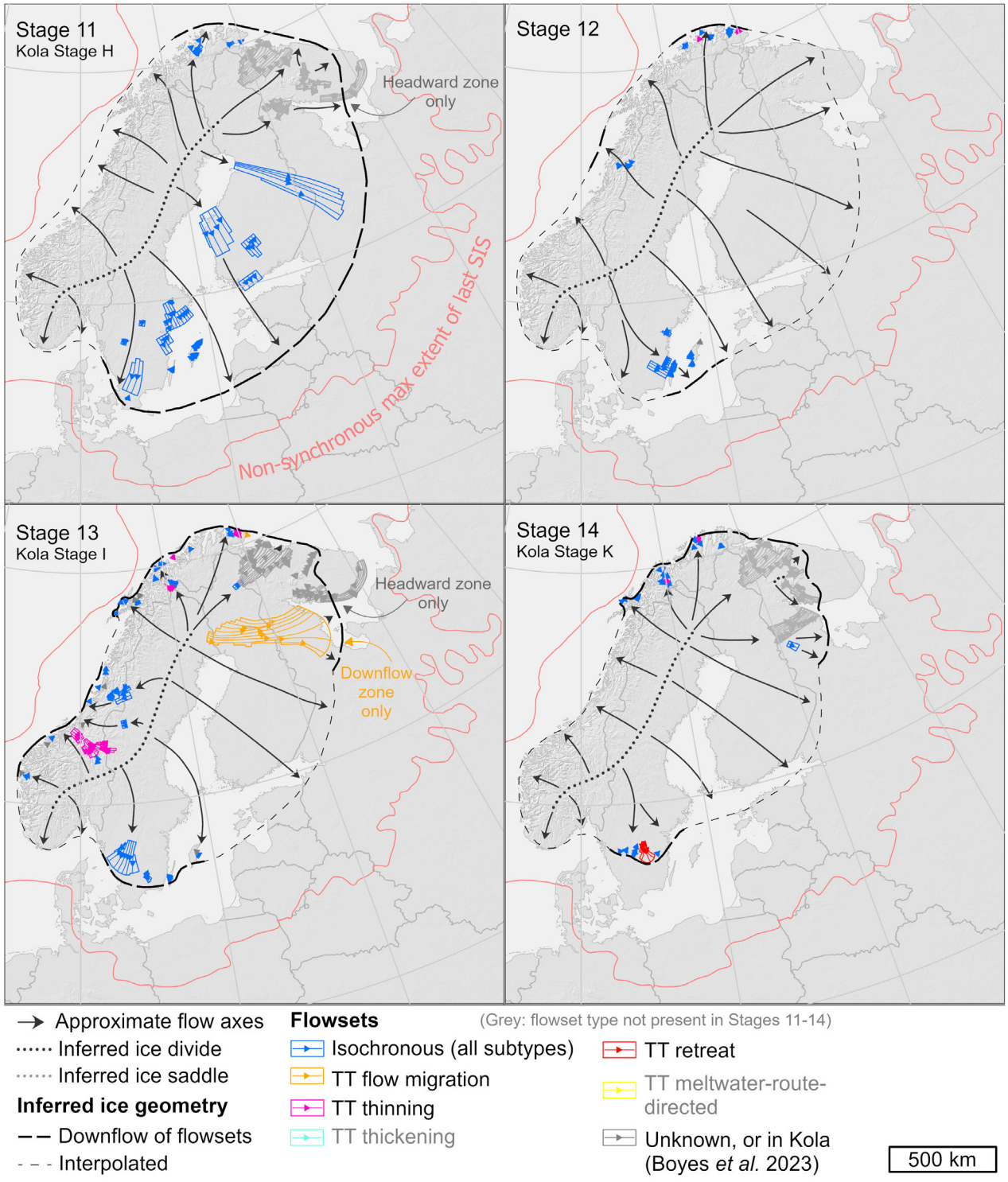

Fig. 13. Continued

mapped moraines or other ice-contact landforms. These boundaries are thus highly schematised, and we do not attempt to force them to follow specific known ice margin positions defined by moraines and other ice-contact landforms, nor to a particular chronological event or associated timing. The actual ice margin positions may have been more extensive and/or more crenulated than depicted in Figs 12 and 13. The sections that follow

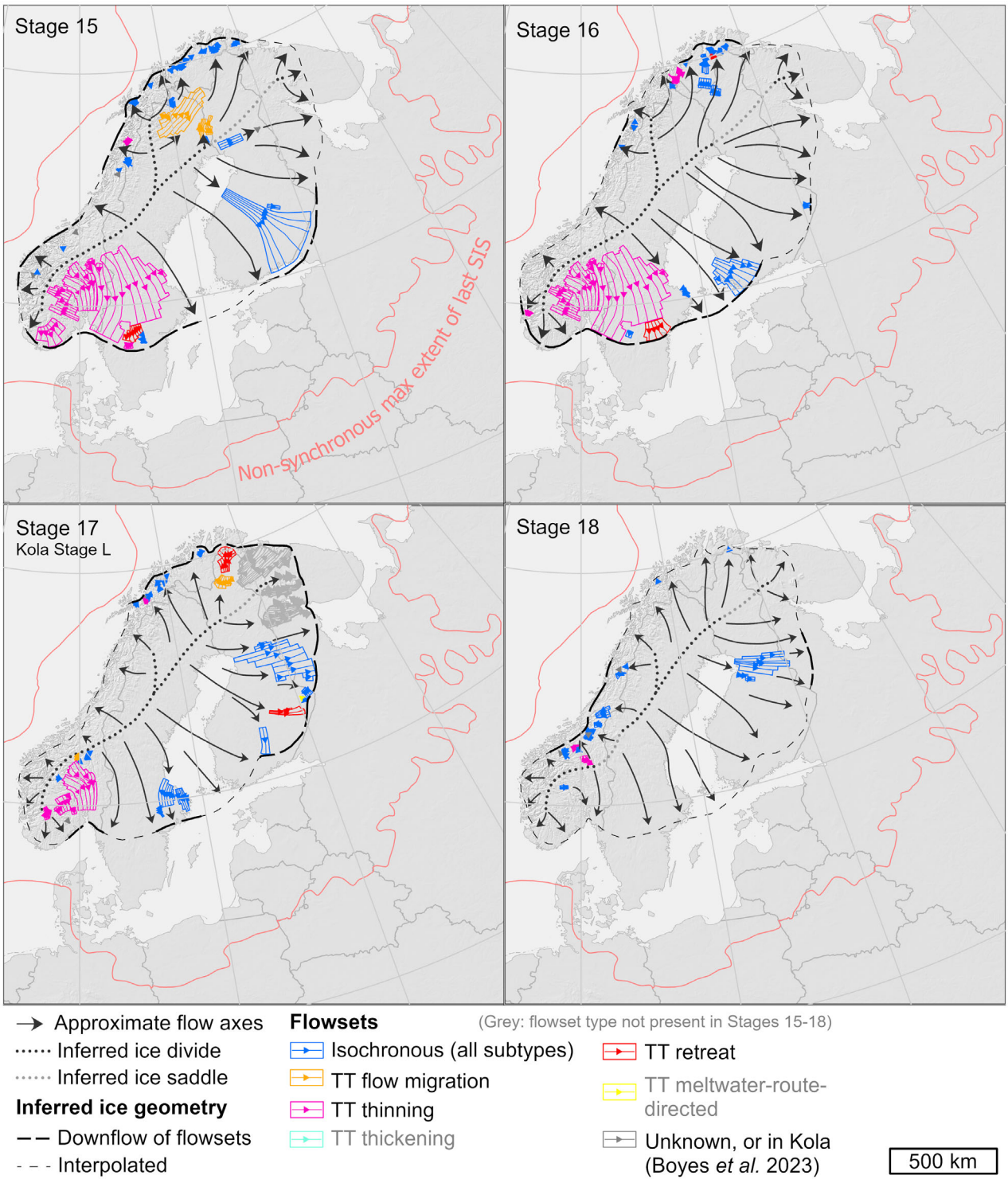

Fig. 13. Continued

include references to individual flowset ID numbers. These can be viewed stage-by-stage in Fig. S10, and in larger maps in Data S2.

An early ice sheet advance (Stages 1–2). – The oldest flowsets in the relative-age sequence record two stages of south-eastward ice flow across N and central Sweden

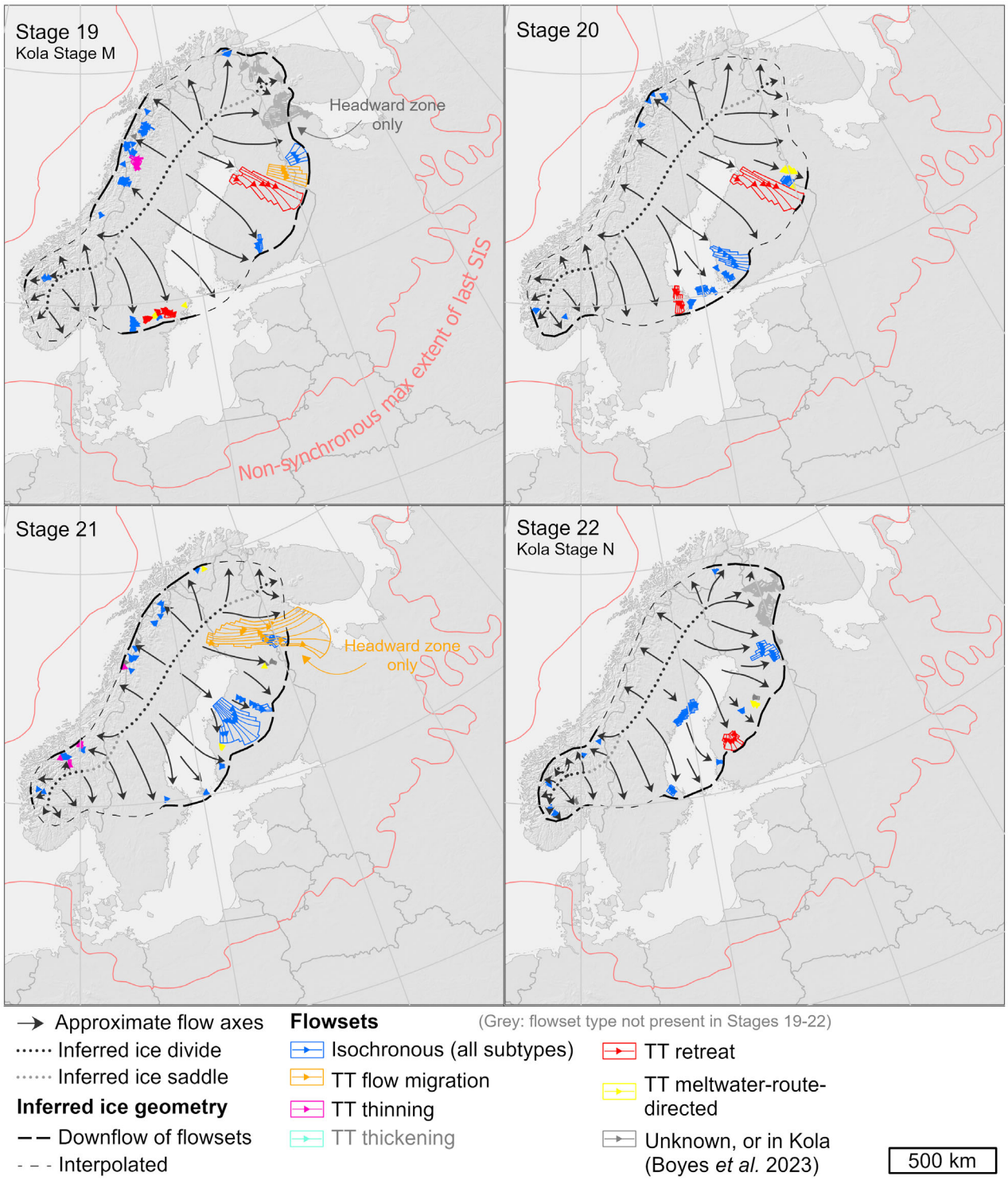

Fig. 13. Continued

and into N Finland. Stage 1 (Figs 12, S10) reflects a consistent pattern of flowsets extending from near to the Scandinavian mountains in N Sweden and across the northern parts of the Gulf of Bothnia (fs63, fs887, fs79, fs80 and fs249). We infer an ice divide over the Scandinavian mountains, potentially connected via a saddle to a second inferred ice dome over high ground in S Norway. In Stage 2, ice flow extended further into Finland,

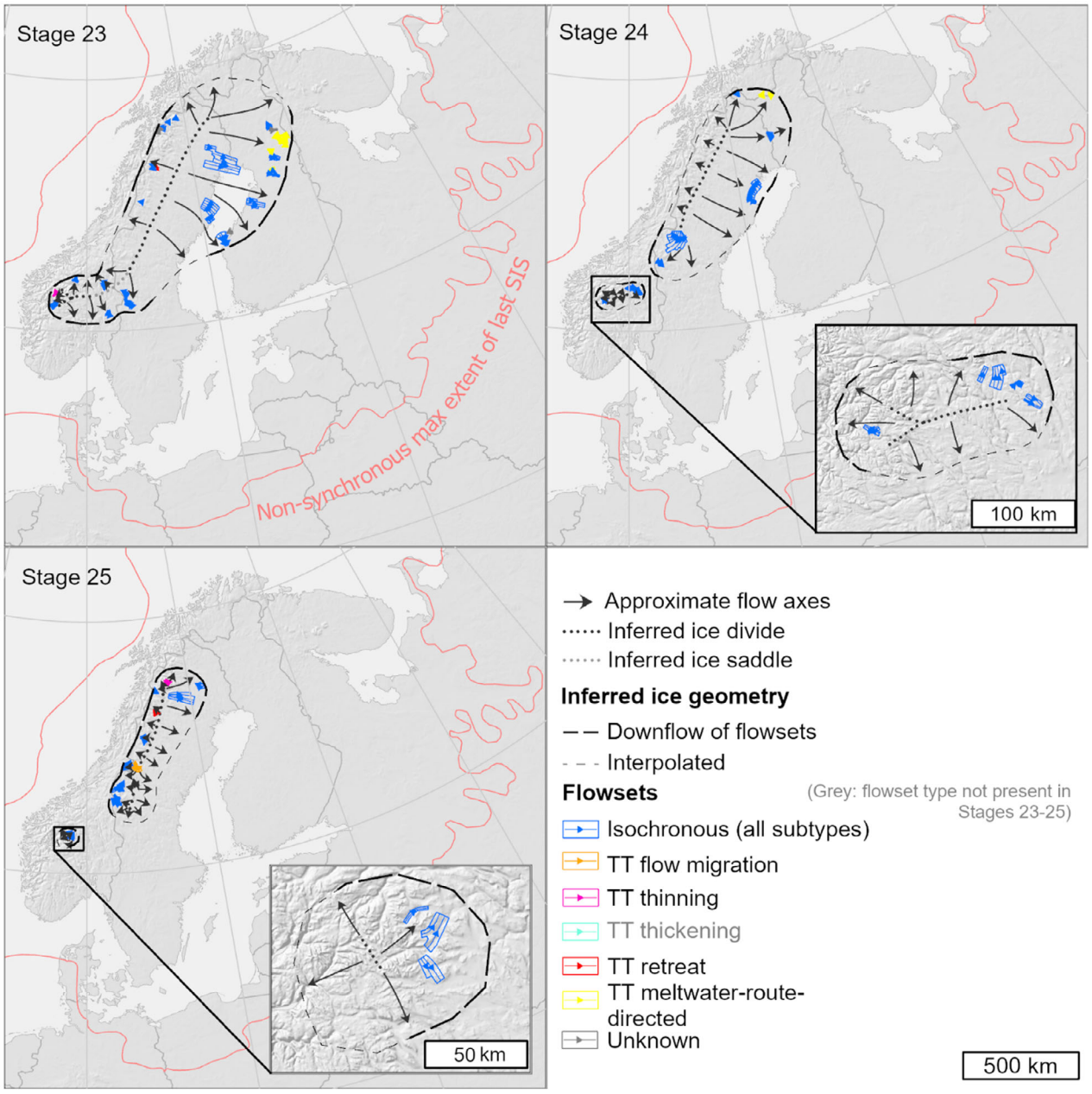

Fig. 13. Continued

and ice flow in central Sweden reoriented towards the topographic depression in the southern part of the Gulf of Bothnia (from fs249 in Stage 1 to fs93 in Stage 2). We note that Stages 1 and 2 are broadly similar to flow patterns identified by Kleman *et al.* (1997) and ascribed to flow of ice sheets during the early Weichselian.

A small ice sheet centred on the Scandinavian mountains (Stage 3). – In Stage 3 (Figs 13, S9, S10), flowsets confined to Norway and W Sweden record a more spatially limited ice flow geometry than Stages 1 and 2, with thinner, more topographically influenced ice centred on the Scandinavian mountains. This leads us to infer that the older Stages 1 and 2 do indeed reflect two evolutionary stages of an earlier ice sheet (e.g. Kleman *et al.* 1997), and that Stage 3 represents the first major imprint of the last SIS preserved in subglacial lineations (see 'Discussion'). Stage 3 flowsets trend away from the spine of the Scandinavian mountains and evoke two ice divides separated by a saddle in S Norway. This flow pattern is consistent with an inferred ice divide in S Norway, which curved along the head of Sognefjord, which likely pro-

vided efficient ice drainage under such a divide configuration. We infer, based on the pattern of flowsets, that S and E Sweden and Finland were ice-free in Stage 3.

Advance of ice to the continental shelf edge, and into NW Russia and the northern European plain (Stages 4–8). – Stage 4 (Figs 13, S9, S10) represents a renewed advance of ice across the Gulf of Bothnia into W Finland. Flowsets in this stage (fs193, fs196, fs197, fs198, fs68, fs245, fs24) represent extensive sheet flow across most of Sweden and necessitate the persistence of an ice divide over the Scandinavian mountains. Assuming enlargement of a southern dome over Norway relative to Stage 3, we infer a simplified N–S-oriented southern divide, connected to the main divide via a saddle.

In Stage 5, ice advanced into S Sweden and Finland, and across the Kola Peninsula and Russian Lapland (stage A flowsets in Boyes *et al*. 2023). A consistent reorientation of extensive sheet flow across Sweden (e.g. fs850, fs202) requires a general rotation of the major eastward flow axis towards the SE, implying a clockwise rotation of the ice divide position. This is consistent with an apparent rotation of the flow axis in S Norway (fs94), which necessitates migration of the ice divide to the southeast of the mountains. The interpreted ice-flow axes and ice sheet geometry were relatively complex in Stage 5, reflecting the interaction of ice flow with the Bothnian and White Sea basins. Following the guiding principle of broad ice sheet symmetry, we assume that the ice extended offshore around the Norwegian coast.

In Stage 6, the zone of major sheet-flow imprints (e.g. fs25, fs7, fs860, fs862, fs855, fs949) shifts from Sweden into Finland and NW Russia. Small flowsets in S Sweden (fs122, fs240) also imply ice flow into the Baltic Sea basin and potentially further south. We correlate Stage 6 with flowsets in stage C of Boyes *et al*. (2023). Southward flow from the Kola Peninsula and Russian Lapland into the White Sea implies the establishment of an east–west-oriented ice divide over the peninsula, which we infer to represent an eastward extension of the main ice divide. Substantial flowsets (e.g. fs254, fs342, fs260, fs757) extend westwards across the Scandinavian mountains from W Sweden to the Norwegian Sea, collectively implying relatively thick ice flowing from a divide east of the mountains. We posit that the SIS may have reached the continental shelf edge around Stage 6 and established its known connections to the BIIS and BKIS to the east and north, respectively.

In Stage 7, westward ice flow continued to pass over the Scandinavian mountains, with additional NW-trending imprints in S Norway (e.g. fs303). Ice likely extended further into NW Russia (fs948, fs611) and south of the Baltic Sea. Northward flow extended across N Norway from Finland (e.g. fs149, fs82) and across the Kola Peninsula and Russian Lapland (correlated with Boyes *et al*. 2023 stage F flowsets) towards the Barents Sea. This suggests a further clockwise rotation of the position of the ice divide, migrating towards the northern tip of the Gulf of Bothnia and extending across Finland and NW Russia into the White Sea.

Stage 8 suggests a relatively stable pattern of ice flow relative to Stage 7, but with a transition to divergent ice flow (fs232) in S Sweden suggesting a minor change in ice geometry within and beyond this region.

Initial deglaciation (Stages 9–16). – We infer that Stage 9 (Figs 13, S9, S10) correlates approximately with the commencement of extensive deglaciation of the SIS. Eight subsequent stages describe the evolution of the ice sheet through deglaciation towards the well-established YD ice sheet limits. Stage 9 captures a series of significant regional ice flow reconfigurations. Ice flow across S Sweden reoriented westward towards Kattegat (fs901). In central Norway, valley-confined flow imprints (fs756, fs399, fs400) suggest ice thinning over the Scandinavian mountains, potentially associated with retreat from the continental shelf. Northward flow persisted towards the Barents Sea, with a slight clockwise rotation of this flow axis (e.g. fs165, fs158, fs172, and Boyes *et al*. 2023 stage G flowsets). This leads us to infer a significant shortening of the northern extent of the primary ice divide and its migration back towards Sweden. A secondary divide could have persisted over high ground in the Kola Peninsula (as inferred in the correlated stage G of Boyes *et al*. 2023), connected to the main divide by a saddle.

Our flowsets alone do not give a particularly strong indication of the geometry of ice flow during break up of ice in the North Sea and detachment of the SIS from the BIIS. However, we infer that these events occurred around Stage 9, allowing accommodation space for minor reconfiguration of ice flow around the S coast of Sweden in Stage 10. In Stage 10, ice flow trended through the Baltic Sea basin (evidenced by fs106 and fs114 on Gotland and Öland, respectively), and curved around the southern tip of Sweden into Kattegat (fs121 and fs893). Time-transgressive thinning signatures in N Norway during Stage 10 (fs151 and fs562) lead us to infer that the nearby connection with the BKIS was weakened and/or lost around the time that these flow patterns were inscribed.

Stage 11 summarises broadly divergent ice flow over S Sweden, with ice flow trending across—as opposed to along—the Baltic Sea; evidenced by a reorientation of flowsets on Gotland and Öland, and S mainland Sweden (fs105, fs110, fs116, fs243, fs224). Ice continued to flow across Finland (fs878, fs21, fs861, fs859) into NW Russia south of the Baltic Sea. We infer loss of the secondary ice divide over NW Russia; north-westward ice flow across Russian Lapland (Boyes *et al*. 2023 stage H flowsets) instead emanated from the end of the primary divide over N Sweden, and ice flow locally curved around the high ground in the Kola Peninsula. Stage 12 captures flow reorientation and reconfiguration in S Sweden as the

ice retreated up and across the Baltic Sea towards the SE coasts of Gotland and Öland. Small, valley-confined, convergent, and time-transgressive thinning flowsets on the N coast of Norway (e.g. fs188, fs144, fs824, fs140, fs828) indicate that the ice margin was likely close to the present-day coastline, perhaps beginning to retreat into the fjords in some locations.

In Stage 13, we reconstruct a lobate ice geometry over S Sweden (e.g. fs233) with the ice margin approaching Gotland and Öland (e.g. fs113 and fs111). Small, topographically controlled and time-transgressive thinning flowsets along large parts of the central and N Norwegian coasts suggest that the ice margin was near the coast (e.g. fs141, fs962, fs990, fs499). A pattern of flowsets with axes converging towards Trondheim from the Scandinavian mountains (e.g. fs264, fs500, fs985, fs300, fs317), including flowsets with time-transgressive thinning signatures, suggests that the ice was thinning but continuing to source from a divide position east of the mountains and draining towards Trondheimsfjord; efficient topographically directed drainage may have helped to capture ice flow from the divide to the NE. Retreating ice over the Kola Peninsula continued to radiate from the primary divide (Boyes *et al*. 2023 stage I flowsets). We include a large, W–E-trending, but notably time-transgressive flowset (fs55) which extends from N Finland to the White Sea in this stage. We explain the cross-cutting relationships and complex bedform imprints recording time-transgressive flowline migration within fs55 by the formation of its down-flow (eastern) portion (which represents ice flowing into the White Sea) around Stage 13, and the later formation of its up-flow (western) portion—which cross-cuts flowsets assigned to Stage 15 (fs612, fs54, and fs944)—in Stage 21. This interpretation of fs55 (see Example 2 in Sheet 1 of Table S1) is compatible with the reconstructed sequence of flow changes between Stages 13 and 21. Fs55 correlates with a flowset from Boyes *et al*. (2023) over NW Russia, which we include in Stage 14 alongside a small flowset that superposes fs55 and evokes a minor reconfiguration of the local flow axis as the ice retreated towards the coast of the White Sea. In Stage 14, ice continued to retreat across S Sweden, generating divergent lobate flow imprints of time-transgressive retreat (fs238) near the margin. A minor ice divide over the Kola Peninsula is inferred to account for southward ice flow towards the White Sea. This is a modification of the correlated stage K from Boyes *et al*. (2023); they interpret topographically influenced ice flow as resulting from the lowering of the ice sheet surface.

Stage 15 represents a major reconfiguration of the flow-pattern geometry of the northern SIS. A group of N- and NE-oriented flowsets (fs612, fs70, fs69, fs146, fs385), the largest of which represent time-transgressive flowline migration, leads us to infer that a branched ice divide developed over N Sweden. One ice divide branch extended north into the Scandinavian mountains over N Sweden, while the other terminated near the northern coast of the Gulf of Bothnia. Ice flow converged between these branches (fs612, fs70, fs69, fs146, fs385) before curving towards the N Norwegian coast, where small topographically influenced flowsets (e.g. fs679, fs181, fs864) suggest that the ice margin was retreating through the fjords. In S Finland, an isochronous divergent flowset (fs11) sources from the western branch of the ice divide and corresponds to the Finnish Lake District ice lobe (Fig. S11; see e.g. Putkinen *et al*. 2017 and 'Discussion'). Extensive bedform signatures of time-transgressive ice sheet thinning (fs297, fs927, fs403, fs445) and retreat (fs213) are also observed over S Sweden and S Norway. Bedforms in the headward zones of such flowsets may have formed somewhat later than those in their down-flow zones and trace back to an ice divide position centred closer to the Scandinavian mountains.

In Stage 16, topographically influenced flowsets suggest continued drainage of ice through the N Norwegian fjords (e.g. fs627, fs553). A second isochronous divergent flowset (fs4) corresponding to the Baltic Sea ice lobe (Fig. S11; see e.g. Lunkka *et al*. 2021; Putkinen *et al*. 2017) extends across SW Finland from the Bothnian coast to the approximate position of the major Salpausselkä I ice-marginal zone.

Ice flow evolution around the Younger Dryas, and subsequent ice sheet demise (Stages 17–25). – Stage 17 (correlated with stage L flowsets from Boyes *et al*. 2023) is one of two stages for which we considered the well-established limit of the SIS associated with the YD (Andersen *et al*. 1995a; Rainio *et al*. 1995; Hughes *et al*. 2016: fig. 8; Boyes *et al*. 2023, 2024; Mangerud *et al*. 2023b; see 'Data and methods'). In Stage 17 (Figs 13, S9, S10), two flowsets cross-cut the lateral margins of the divergent ice lobe represented by fs11 in Stage 15. These flowsets (fs5 and fs857), which we informally describe as 'lateral lobe feathers', terminate around the Salpausselkä II ice-marginal zone (Fig. S11), with the northernmost 'feather' recording subsequent time-transgressive ice-margin retreat. A smaller time-transgressive retreat flowset with a divergent flow pattern also extends into N Norway from Finland (fs160). Stage 17 is the only stage among the deglacial stages in which we found it necessary to invoke a small outward extension of our reconstructed ice geometry (i.e. potentially necessitating a local ice readvance). This extension relates to a large isochronous flowset (fs43) which extends across central Finland to the approximate position of the Rugozero ice-marginal zone (e.g. Rainio *et al*. 1995; Boyes *et al*. 2024) in NW Russia. The overall flowset pattern in the northern SIS is best explained by a lengthening and slight westward migration of the western branch of the ice divide that formed in Stage 15.

Stage 18 represents a minor flow reconfiguration, with the onset of divergent, eastward-trending flow over cen-

tral Finland (fs38). Flowsets over S Norway indicate renewed ice flow convergence into the area south of Trondheimsfjord (e.g. fs977, fs748, fs747, fs969, fs 311) leading us to infer separation of the ice divide over S Norway with convergent flow from a saddle connecting this and the main divide. We also invoke a small westward migration of the divide in S Norway (i.e. away from the spine of the Scandinavian mountains), which could be explained, for example, by ice-sheet thickening during the YD.

In Stage 19, flowsets over central Finland and Russian Karelia (fs41, fs946, fs879) reflect a divergent flow pattern which extended to the approximate location of the Kalevala ice-marginal zone (e.g. Ekman & Iljin 1991; Rainio *et al*. 1995; Boyes *et al*. 2024). This includes a small, isochronous divergent ice lobe (fs879) and a large time-transgressive (retreat) flowset (fs41) with a divergent flow pattern reflecting subsequent retreat of the ice margin into the Gulf of Bothnia. In Russian Lapland (where we correlate our Stage 19 with stage M flowsets from Boyes *et al*. 2023), ice flow diverged towards the Barents Sea coast and the White Sea. We infer that the eastern branch of the main divide completely degraded by Stage 19 (having shortened somewhat through Stages 17 and 18), an interpretation supported by numerous topographically controlled flowsets (e.g. fs376, fs372, fs763, fs269), including time-transgressive thinning signatures, which trend north-west along valleys through the Scandinavian mountains. In Sweden, small flowsets (e.g. fs214, 215, fs701, fs208) with locally variable, but broadly southward flow directions also record flow of thin, topographically influenced ice, and time-transgressive retreat (e.g. fs700 and fs208) north of the Middle Swedish End Moraine Zone (see e.g. Johnson *et al*. 2019). These include two meltwater-route-directed flowsets (fs206 and fs702).

In Stage 20, flowsets over SW Finland, Åland, and SE Sweden (fs3, fs9, fs100, fs98, fs703, fs225) imply a divergent, lobate flow pattern over the southern part of the Gulf of Bothnia, with the isochronous divergent flowset, fs3, in SW Finland, terminating around the Salpausselkä III ice-marginal zone (Fig. S11). This correlates with the Baltic Sea ice lobe in Finland (e.g. Putkinen *et al*. 2017; Lunkka *et al*. 2021). In Stage 21, this lobate pattern persisted as ice retreated towards the Finnish coast, generating space for adjacent lobate flow corresponding to the Näsijärvi ice lobe (e.g. Punkari 1980; Lunkka *et al*. 2021) to the NE (fs1, fs2, and fs15; Fig. S11), which extended from the Bothnian coast to just beyond the Central Finnish Ice-Marginal Formation (e.g. Repo & Tynni 1971; Lunkka *et al*. 2021) (see 'Discussion). We infer that the headward zone of fs55 (the down-flow portion of which is attributed to Stage 15) formed over N Finland during Stage 21.

In Stage 22, a small lobate flowset (fs16) superimposes the downflow end of fs15, terminating near to the Central Finnish Ice-Marginal Formation (Fig. S11); it contains signatures of time-transgressive ice retreat from this position. We also observe signatures of isochronous flow converging towards the Gulf of Bothnia from E Sweden (fs92). This suggests that ice flow became more sensitive to the topographic influence of the Bothnian Sea basin as the SIS thinned and retreated, with the flow axis reorienting along the Gulf of Bothnia and flowing towards Åland. Small flowsets on the coasts of Finland and Sweden (fs46 and fs220) indicate continuation of divergent, lobate flow over this area. We also infer that ice retreat continued towards a secondary ice divide in S Norway. We suggest the topographic influence of Sognefjord likely resulted in the formation of a secondary divide branching north-westward. Over Russian Lapland (where we correlate our Stage 22 with stage N flowsets from Boyes *et al*. 2023), ice flow likely radiated from the northern end of the main ice divide over Scandinavia.

Stages 23–25 describe the deglaciation of the Scandinavian mountains. Stage 23 is the final stage in which we reconstruct a contiguous ice mass. We infer a spatially irregular ice sheet geometry, with a relatively small ice dome over S Norway, connected to the major divide in Sweden (east of the Scandinavian mountains) via a saddle. Ice flowed from the main divide across Sweden (fs60 and fs90) and the Gulf of Bothnia into N and W Finland (fs61, fs36, fs12, fs20), with several meltwater-route-directed flowsets (e.g. fs59, fs614, fs645) occurring in N Finland. In S Norway, time-transgressive thinning and valley-confined signatures (e.g. fs712, fs719) suggest ice flow convergence down Sognefjord from the branched divide established in Stage 22.

In Stage 24, flow patterns indicate that the ice sheet fragmented into an E–W oriented ice dome over S Norway, with the main ice sheet centred over central Sweden. The retreat of the now-independent ice mass over S Norway may have progressed at a different rate than the main ice sheet. Flowsets such as fs253 and fs72 suggest that ice flowed radially from both ends of the main ice sheet divide. The last preserved subglacial bedform imprint into the Gulf of Bothnia from central Sweden is the south-eastward oriented fs649; its convergent form suggests ice may have been flowing into an embayment as ice retreated across this area.

Stage 25 is the final stage in our reconstructed sequence of SIS flow evolution. Valley-confined flowsets in S Norway suggest that the independent ice mass here retreated towards high ground in the core of the southern Norwegian massif, near the head of Sognefjord. The main ice sheet remained centred over Sweden, with flowsets (e.g. fs89, fs84, fs268) indicating a final ice divide position to the east of the Scandinavian mountains and aligned approximately with them. The configuration of fs262—a flowline migration flowset—suggests that the main ice sheet divide split in Stage 25. Ice flow imprints appear to converge from a short southern and longer northern ice divide towards a major topographic low between massifs of the Scandinavian mountains east

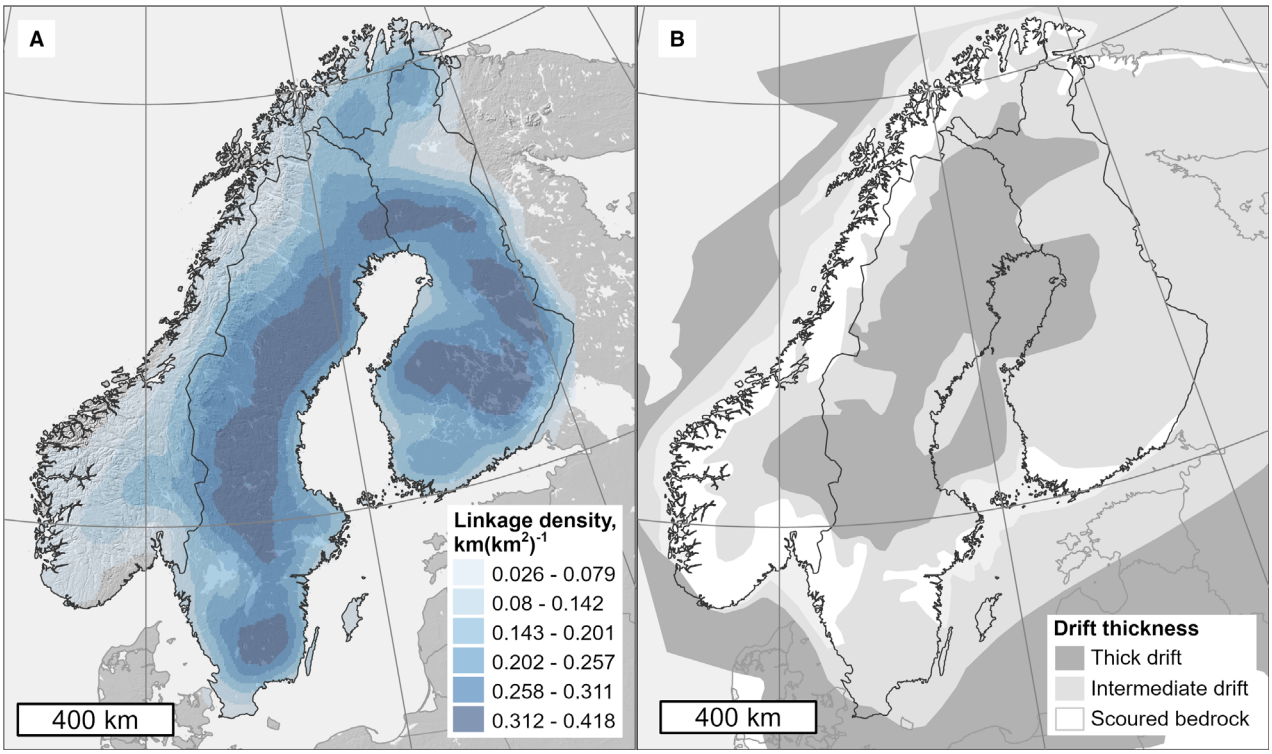

Fig. 14. A. Spatial variations in the density of lineation linkages (in km $(km^2)^{-1}$, calculated within a 75 km search radius) over Norway, Sweden and Finland, on a shaded-relief basemap. The locations of contemporary lakes are shown. B. Thickness and distribution of so-called 'drift' (surficial sediment) redrawn from Kleman *et al.* (2008). Data credit for panel A basemap: Airbus, USGS, NGA, NASA, CGIAR, NLS, OS, NMA, Geodatastyrelsen, GSA, GSI and the GIS User Community.

of Trondheimfjord. Fs258 suggests ice drained through this topographic low. Inward pinching of the reconstructed ice bounding line in this area (Fig. 13) may foreshadow fragmentation of the main ice sheet shortly after Stage 25. Ice draining to the west of the southern divide of the main ice sheet (fs329 and fs848) in Stage 25 was controlled by large valleys through the southern massif of the Scandinavian mountains.

Discussion

Subglacial bedforms as imprints of palaeo-ice flow

Our mapping demonstrates that macro-scale subglacial lineations cover around 81% of the land surface area of Norway, Sweden and Finland (based on the cumulative area covered by at least one flowset). Our sampled mapping leads us to estimate that there are at least several million subglacial lineations in Fennoscandia. Fields of bedforms exist almost everywhere where sediment exists (Figs 6, 14). However, they are not unique to regions with sediment cover; a considerable number of macro-scale glacially streamlined landforms are also expressed in bedrock, albeit less commonly and in lower densities than in areas of thick sediment cover (Fig. 14; Dowling *et al.* 2015).

The new metre-scale bare-earth DTMs we exploited represent an order-of-magnitude improvement in the resolution of remote-sensing data (primarily aerial and satellite images) available for the seminal ice-sheet-scale flow-pattern reconstructions of the late 20th and early 21st centuries (e.g. Dongelmans 1996; Kleman *et al.* 1997; Boulton *et al.* 2001), which also had to contend with the obscuration of the land surface by vegetation. The improved clarity of >metre-scale landforms in the new DTMs is partly what has enabled us to delimit 611 flowsets: an order of magnitude more discrete ice-flow patterns than were reconstructed by Kleman *et al.* (1997: fig. 4) who delimited 56 'flow-trace fans' across Fennoscandia (Fig. 3B). Table S3 provides a detailed comparison between the flow trace fans of Kleman *et al.* (1997) and our 611 flowsets, which we constructed independently using a 'no preconceptions' philosophy. Of the 41 fans which occur at least partially within our core study domain (Norway, Sweden and Finland), 88% comprise flow patterns which are captured or partially captured by our flowsets. Of those fans which are not (n = 5), or only partially captured (n = 14), the majority were identified by Kleman *et al.* (1997) solely on the basis of glacial striae and/or till fabrics. Importantly, however, all represent flow directions that are compatible with the broader flow geometries recon-

structed in at least one of the stages of our flow-pattern reconstruction. Hence, for our study area, 100% of the flow patterns depicted by Kleman *et al.* (1997) are captured within the flow patterns we identify (see Table S3 for detailed remarks for individual fans). We return to a comparison of their reconstructed relative-age sequencing later in the discussion.

Many of our flowsets subdivide flow patterns identified by Kleman *et al.* (1997) into discrete components, with the sequencing of our flowsets through our reconstructed stages revealing greater nuance in the relative timings of those discrete flow events (Table S3). For example, Kleman *et al.* (1997) inferred that their fan 1 likely compounded imprints of both deglacial and older ice flow; we confirm this, delimiting 33 discrete flowsets consistent with Fan 1, which occur between Stages 4 and 24 of our reconstruction (Table S3). Similarly, Kleman *et al.* (1997) noted that their fan 18 compounds numerous topographically influenced flow imprints across the Scandinavian mountains and flowing through the Norwegian fjords; we delimit 47 flowsets consistent with Fan 18, which occur between Stages 6 and 25 of our reconstruction (Table S3). In other cases, we separate flow patterns identified by Kleman *et al.* (1997) into discrete imprints occurring over a narrower range of stages; for example, we identify 10 flowsets which broadly correspond to Fan 48 (a lobate fan extending across central Finland, and into Russian Karelia), which occur within Stages 17–19 and 23 of our reconstruction (Table S3). We additionally identify more widespread subglacial lineation imprints of some flow patterns represented by Kleman *et al.* (1997), particularly during stages attributed to ice sheet advance (Table S3, Fig. S10). Other flowsets add new flow patterns and directions, particularly at local-to-regional scales and especially in Norway, which were not represented in the Kleman *et al.* (1997) reconstruction.

It is striking that 43% of the cumulative area of our flowsets represents spatially extensive isochronous sheet flow (Table 3, Figs 11A, S8), which is either topographically unconstrained or only partially influenced by the topography of the ice sheet bed (Table 3, Fig. S7). These topographically insensitive isochronous sheet flowsets are interpreted to represent ice flow up to hundreds of kilometres into the ice sheet interior; many occur during ice sheet advance stages, while others appear to have formed during deglaciation (Fig. 13). Flowsets hosting bedforms which likely formed a relatively short distance (~10s kms) inwards of a retreating ice margin (time-transgressive retreat, isochronous divergent, and meltwater route-directed flowsets) account for ~23% of the cumulative area of all flowsets delineated across Fennoscandia. The distances from the ice margin at which other types of flowset (~34% of cumulative flowset area) are likely to have formed are more case-specific and often ambiguous or context-dependent. Along with earlier studies (e.g. Sollid & Sørbel 1994; Dongelmans 1996; Kleman *et al.* 1997; Clark *et al.* 2000), this balance underlines that the historic view (e.g. Boulton *et al.* 1985 and references therein) that drumlins form only within tens of kilometres of deglaciating ice margins is unfounded.

Shifting flow patterns and ice divide positions

Arguably, it is the locations of ice divides (which occur in the thickest areas of an ice sheet) and the associated flow-pattern geometry that exert first-order controls on where ice can flow at sub-continental scales and where ice margins can be sustained.

In Fig. 15, we summarise the migration of the main ice divides required to satisfy our flowset groupings and relative chronology through 25 stages of ice flow evolution. A broadly N–S-oriented ice divide is centred over the Scandinavian mountains through Stages 1–3. During ice sheet advance (Stages 3–7), the main divide migrated eastward, hinging clockwise and moving up to 500 km away from the Scandinavian mountains and positioned over relatively flat and low-lying regions of E Sweden and N Finland, extending to the Kola Peninsula and the White Sea. Our data thus reinforces the broad pattern and trajectory of divide movement that has become accepted based on field observations and satellite imagery (Vorren 1977; Lundqvist 1986; Kleman *et al.* 1997) and reproduced in some numerical modelling experiments (e.g. Siegert & Dowdeswell 2004; Clason *et al.* 2014; Patton *et al.* 2016, 2017; Gudlaugsson *et al.* 2017; Arnold & Sharp 2002; Jungdal-Olesen *et al.* 2024). Our inference that the major centre of mass of the SIS around the LGM was located close to the coast of the Gulf of Bothnia in Sweden is in agreement with previous reconstructions (Kleman *et al.* 1997: fig. 11; see also our Fig. 2), and with post-glacial uplift rates, which show maximum rates of uplift over the city of Umeå (just southeast of our Stage 7 ice divide; Vestøl *et al.* 2019).

It has long been understood that the SIS evolved asymmetrically as a result of the high-elevation Scandinavian mountains (the location of ice sheet initiation) being located close to the continental shelf edge to the west, but also having neighbouring extensive lowland plains across which ice could advance eastwards (Larsen *et al.* 2016; Patton *et al.* 2016, 2017). To the east of the main divide, two generally preferred flow directions are evident: towards the SE and towards the SSE (Fig. 9). The change between them is mostly explained by the eastward migration of the primary divide so that ice flow over lowland Sweden and Finland shifted clockwise. The lack of intermediate flow directions between these two modes is intriguing; perhaps rapid divide migration occurred between these two semi-stable configurations, or an unknown control on bedform generation and/or preservation arises through periods of divide migration.

Ice-divide migration of the magnitude that we reconstruct (up to ~500 km) is at the upper extreme of distances reconstructed for other ice sheets. The Keewatin

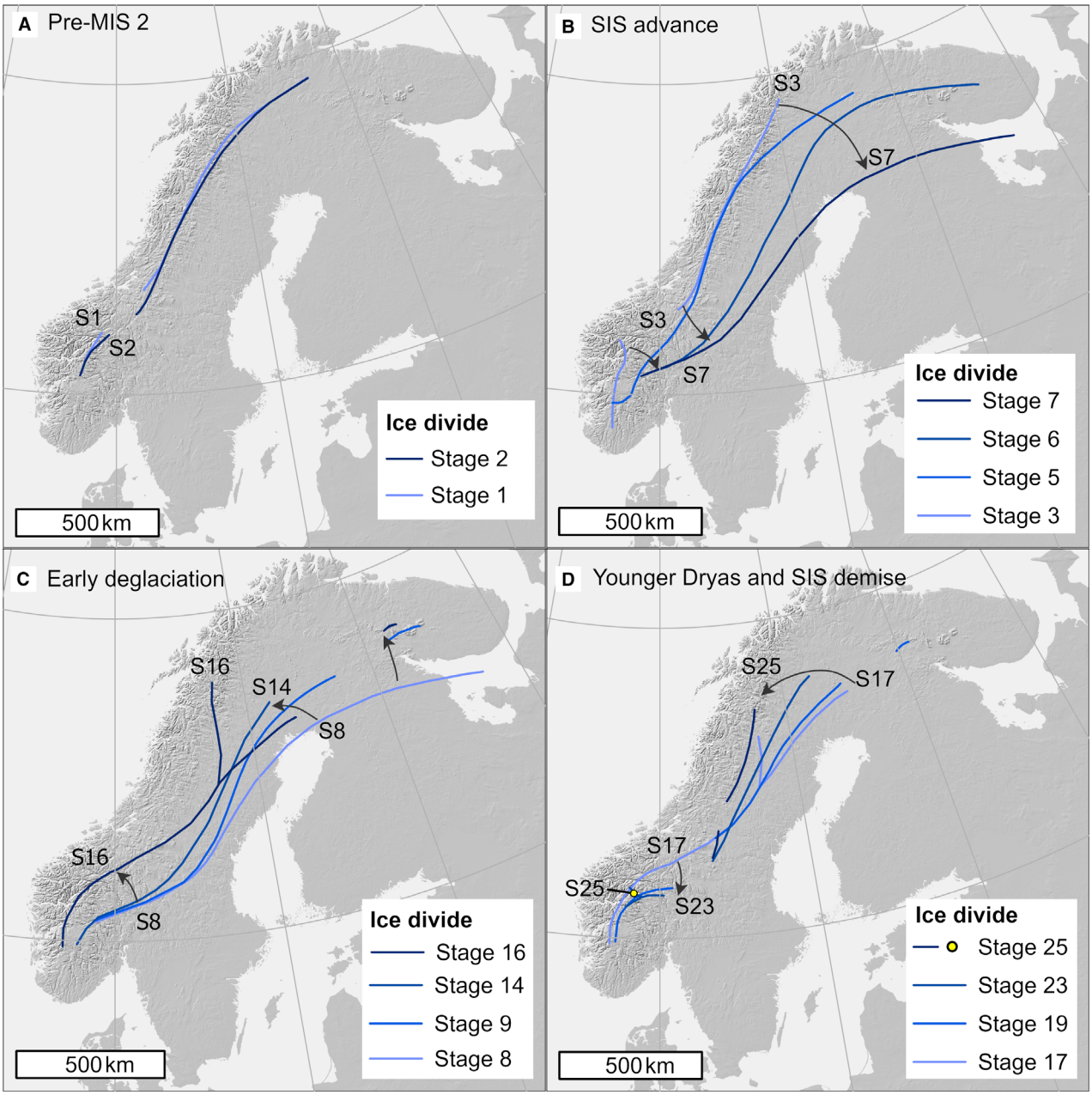

Fig. 15. Migration and configuration changes of ice-sheet divide(s) over Fennoscandia, approximated from patterns of subglacial lineations. End-members of ice-divide positions, and select intermediate positions are shown to illustrate major migration sequences (schematically represented by arrows) through reconstructed stages (S) of ice flow evolution. A. Stages 1 and 2, attributed to an older, pre-MIS-2 ice sheet. B. Advance of the last SIS towards the LGM. C. Early deglaciation of the last SIS. D. Around the YD, and towards the demise of the ice sheet. See Fig. S9 to view larger maps of the reconstructed migration of the ice divide through Stages 1–25, and Data S1 for shapefile data of ice divides. Data credit for basemap: Airbus, USGS, NGA, NASA, CGIAR, NLS, OS, NMA, Geodatastyrelsen, GSA, GSI and the GIS User Community.

ice divide of the much larger Laurentide Ice Sheet is similarly reconstructed to have migrated 500 km (Dyke & Prest 1987; McMartin & Henderson 2004), but the migration distances of the Quebec-Labrador divide (Rice *et al.* 2024) and divides of other ice sheets such as the Cordilleran Ice Sheet (Dulfer *et al.* 2022) and the BIIS (Clark *et al.* 2022) were much shorter (up to 100 km). The large ice divide migration of the SIS reconstructed here must have profoundly affected the ice sheet dynamics, surface profiles and extent and its influence on atmospheric circulation patterns (e.g. Fyke *et al.* 2018).

Our flow-pattern reconstruction suggests an important role of the position of the continental shelf edge in affecting the thickness of ice attained over different parts of the Scandinavian mountains. Figures 16 and S7 illustrate a northward trend along the Scandinavian moun-

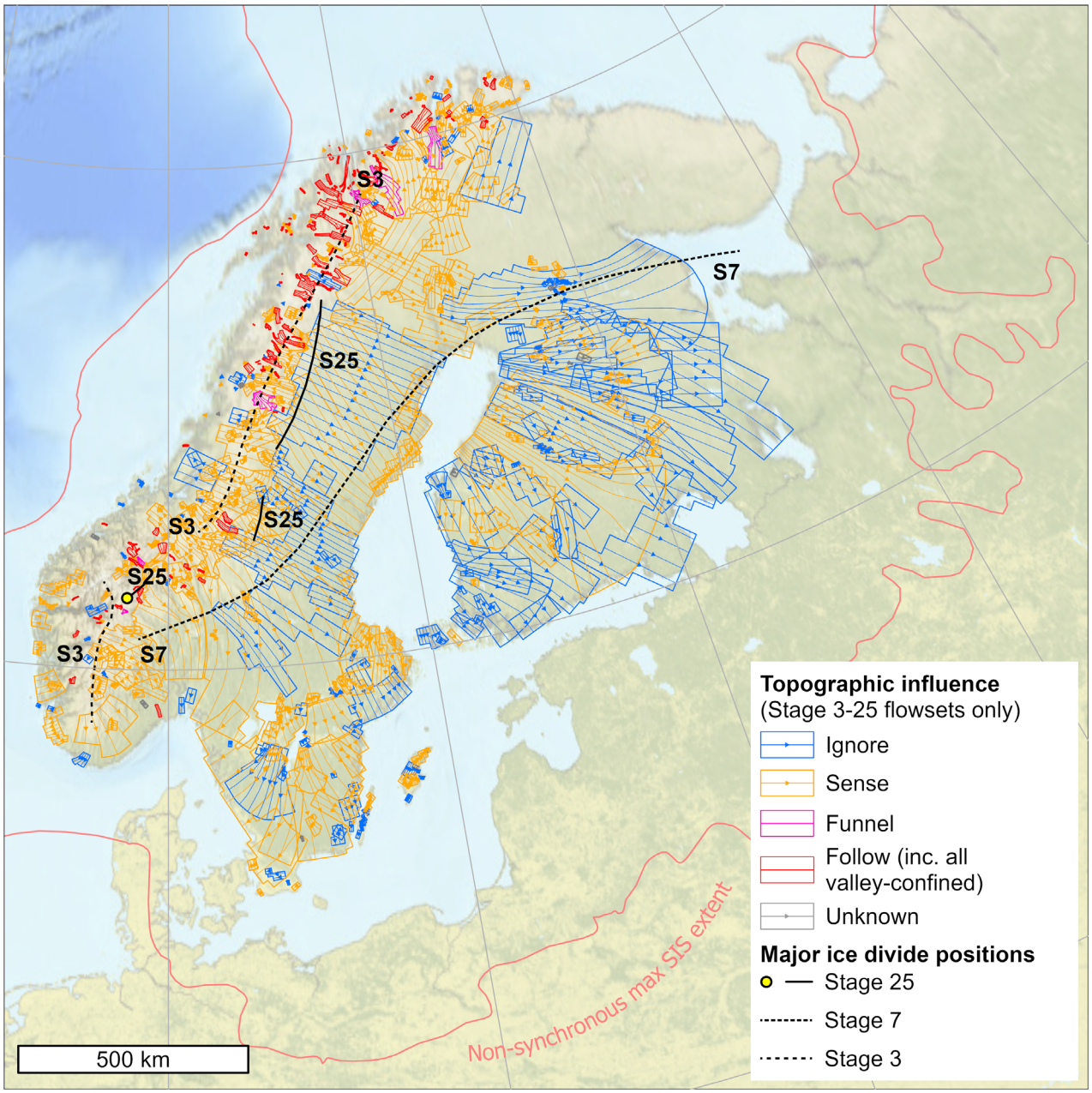

Fig. 16. The influence of topography on ice-flow patterns within flowsets that we associate with the advance and retreat of the last ice sheet over Scandinavia (our Stages 3–25). Thick ice over low-relief areas should produce patterns that mostly ignore topographic bumps and valleys, whereas the converse should produce flow patterns that tend to follow the topography. This means that our flowset categorisations according to topographic influence reveal qualitative information on relative ice thickness, a vital source of information for building reconstructions of ice sheets. The extreme positions of the ice divide (Stage 3 to the west, and Stage 7 to the east) are shown, as well as the inferred ice divide position in Stage 25, just before the final demise of the ice sheet. The non-synchronous maximum extent of the last SIS is also shown (from Hughes *et al.* 2016). Note that while our flowset classifications in Table 3 distinguish valley-confined flowsets into those which ignore, sense, or follow local topography on the valley floor, valley-confined flowsets follow broad-scale topography by definition; hence they are grouped with flowsets which follow topography in this visualisation. See Fig. S7 for a larger map of flowsets colourised by topographic sensitivity, including flowsets ascribed to Stages 1 and 2 of our reconstruction. Data S1 contains the shapefile data for flowsets and ice divides. Basemap data credit: General Bathymetric Chart of the Oceans (GEBCO); NOAA National Centers for Environmental Information (NCEI).

tains in the sensitivity of ice-flow patterns to bed topography. Our relative-age sequencing suggests that this trend existed throughout the evolution of the ice sheet, including when the ice sheet was approaching its largest size (e.g. Stage 6, Figs 13, S9, S10). During this stage, ice flow near Trondheimfjord was topographically unconstrained, while further north, towards Tromsø, ice flow channelled through major valleys. We posit that this

trend is explained by the northward reduction in the distance between the Scandinavian mountains and the continental shelf edge (narrowest close to Andøya), resulting in steeper ice surface slopes to the north. Ice may therefore have flowed faster, and been evacuated to the ocean more efficiently, where the continental shelf edge was closer, preventing the ice from attaining sufficient thickness to flow independently of bed topography, even when the ice sheet was at its maximum extent. These patterns demonstrate the complex interplay between the size and shape of ice sheets, the ice divide geometry, thickness, bed topographies and terminus environments in influencing the ice flow dynamics.

As the ice sheet retreated from its maximum extent, the ice divide swung back to the west, with a larger migration distance in the NE compared to the SW (Fig. 15C, D). This is consistent with the clustering of time-transgressive flowline migration flowsets over N Finland, Sweden and E Norway (Figs 11B, S8). The magnitude of ice divide migration we reconstruct is broadly similar to that reconstructed by Kleman *et al.* (1997: fig. 7), though our easternmost reconstructed ice divide position (Stage 7 in Fig. 16) extends further east, across Finland and into Russian Lapland. Similar is true of the model simulations by Patton *et al.* (2016), which have a branched divide around the head of the White Sea, but do not reproduce the maximum eastern extent of the ice sheet; delivery of ice to those regions may necessitate a divide that indeed extends further east than is simulated in their modelling.

The migration of the ice divide that we reconstruct may explain the low bedform density observed in an area of thick surficial sediment in E Finnish Lapland (Fig. 14). This area was under the broad axis of the ice divide as it migrated southward through N Finland (Stages 5–8, Fig. 15B, consistent with Glückert 1974), then under a persistent saddle connecting the main divide to a local ice dispersal centre over the Kola Peninsula and Russian Lapland (Stages 9–22, Figs 13, 15C, D, S9). Despite the availability of sediment to mould into bedforms, we suggest that long durations under ice divides explain the relative lack of bedforms in this location compared to other thick-sediment regions. This is consistent with inferences of previous workers regarding the preservation of relict landscapes considered to pre-date the last glacial cycle (e.g. Kleman 1992; Fabel *et al.* 2002, 2006; Stroeven *et al.* 2002; Kleman *et al.* 2008; Greenwood *et al.* 2022; Hughes *et al.* 2022; Greenwood & Hughes 2022a, b).

In contrast to the western sectors, the majority of ice flow imprints to the east of the ice divide show little or no influence of local topography on ice flow. This reflects the relatively low topographic relief and the greater thickness that the ice sheet needed to attain in order to extend many hundreds of kilometres over the lowland plains. Most south and eastward-trending flowsets attributed to Stages 3–7 (ice sheet advance) indicate that ice flow direction was not affected by underlying topography, with the exception of flow imprints related to ice advance over the Bothnian depression. In contrast, flowsets attributed to deglacial stages (Stages 9–25) include those that are topographically influenced, likely arising from ice thinning in tandem with retreat.

Our reconstruction shows that the migration of the ice divide during deglaciation was not a simple reversal of that during ice sheet growth. The ice divide did not return to its initial position along the spine of the Scandinavian mountains. Instead, the primary ice divide persisted east of the mountains, over Sweden. The youngest flowsets that we could group into coherent flow geometries show fragmentation of the ice sheet into two independent ice masses at Stages 24 and 25, the largest of which remained centred to the east of the mountains in central Sweden and flowed towards them. These inferences are consistent with recent reconstructions of ice-dammed lakes, which place the final deglaciation of the SIS to the east of the Scandinavian mountains (Høgaas & Longva 2016, 2018; Regnéll *et al.* 2019, 2023; Ploeg & Stroeven 2025).

Progressively smaller ice caps and glaciers likely separated off through the final deglaciation (e.g. Follestad 2003), at smaller scales than we could reconstruct using flowset analysis. Indeed, the reconstructed flow vectors in Stage 25 suggest 'pinching' of the ice geometry west of Trondheimfjord as a precursor to further fragmentation.

While our flow-pattern reconstruction contains significantly more detail than previous ice-sheet-scale reconstructions (e.g. Kleman *et al.* 1997; Boulton *et al.* 2001) and provides more nuance in the sequencing of discrete flow imprints in individual ice-sheet sectors, the broad-scale flow evolution of the SIS is rather similar. All of the ice flow trace fans delimited by Kleman *et al.* (1997), which intersect our study domain are captured either directly by our flowsets or by the broader flow geometries that we reconstruct from them (Table S3). For 92% of these fans, there is agreement between our reconstruction and Kleman *et al.* (1997) in the broad phases of ice flow evolution (i.e. pre-dating the last SIS, advance of the last SIS, around LGM, or last deglaciation) in which the major corresponding flow geometries appear (see Table S3 for detailed remarks). There are only two Kleman *et al.* (1997) fans (fans 25 and 39) which represent flow geometries attributed to a different phase of ice sheet evolution in our reconstruction (Table S3); both were interpreted by Kleman *et al.* (1997) to have formed prior to the last deglaciation on the basis of a lack of co-aligned eskers indicative of subglacial meltwater drainage. However, we propose that subglacial lineations and eskers can form at different times during deglaciation and find that both are consistent with ice flow geometries attributed to the last deglaciation. Our flowset fs84 (Stage 25) aligns with Fan 25 of Kleman *et al.* (1997) and, though it is slightly smaller, is also compatible with the reconstructed flow geometry in

Stage 24. Fan 39 of Kleman *et al.* (1997) is compatible with the flow geometry in Stages 17 and 18. Notably, our major flowset (fs43), which aligns closely with Fan 39 is that which necessitates an outward expansion of the inferred minimum ice sheet bounding line in Stage 17 and is interpreted as evidence for a readvance in this region around the YD cold interval. This may explain why Kleman *et al.* (1997) identified no eskers associated with Fan 39 (Table S3).

That our flow-pattern reconstruction independently verifies that of Kleman *et al.* (1997) is testament to the high quality and robustness of that study and other attempts to reconstruct the evolution of SIS flow at the ice-sheet scale (e.g. Dongelmans 1996; Boulton *et al.* 2001), incorporating both remote sensing and field-based techniques. The new details revealed by our reconstruction augment our understanding of the SIS. Of note is the occurrence of a branched ice divide during deglaciation, which develops at Stage 15, followed by a return to a single divide (consistent with retreat and thinning lowering the ice surface) by Stage 19, when it connects via saddles to an ice dome over S Norway and a local ice dispersal centre over Russian Lapland. Some of the geometries of the ice dispersal centres depicted in the reconstruction of Kleman *et al.* (1997: figs 7, 11) would also likely necessitate branched divide configurations, including for more expansive ice sheet geometries than in our reconstructed Stage 15. Our flowsets additionally necessitate a small branch in the ice divide over S Norway in Stages 22 and 23.

The branched ice divide configuration of Stage 15 provides the simplest explanation for the flow patterns and relative-age sequencing of a group of north and northeast-trending flowsets centred over N Sweden (fs146, fs70, fs612, fs69, fs385; Fig. S10). The subglacial lineations in these flowsets have similar morphologies, which suggest they may have formed under similar conditions. The largest flowsets (fs146, fs70 and fs612) contain evidence of time-transgressive flowline migration, which is consistent with their formation during a reconfiguration of the ice divide. Fs146, fs70 and fs612 (in Stage 15) are positioned close to the northern end of the main ice divide as configured in the preceding Stage 14; they converge towards an axis that is directed away from this location and west of a saddle that connects the Stage 15 ice divide to a local ice-dispersal centre to the NE.

The branched divide in Stage 15 also accounts for SW-trending flowsets observed over Norway in Stage 18 (e.g. fs271, fs977). By Stage 19, this SW-trending flow direction is replaced by NW-trending flow influenced by valleys which cross the spine of the Scandinavian mountains. Hence, we infer that the western branch of the ice divide of Stage 15 gradually degraded through Stages 16–18 as ice drained through the mountains, until ice once again originated from a singular primary divide over N Sweden in Stage 19. This requires further exploration, for example, with ice flow modelling and via the integration of additional landform evidence; however, it demonstrates the potential that flowset analyses unlock for understanding the complexity of ice sheet dynamics and their evolution through time.

Remarks on ice streams

There is a large body of literature on how subglacial bedforms and flowset characteristics can be used to identify palaeo-ice streams (e.g. Stokes & Clark 1999; Stokes *et al.* 2007; Stokes 2018). The identification of specific palaeo-ice stream imprints is beyond the scope of this work, but we make some general observations about our reconstructed flow patterns in relation to major hypothesised ice streams of the SIS.

Several of our flowsets relate to well-documented lobate ice-flow patterns trending southeast over Finland (Fig. S11), which have been interpreted as fast-flowing ice streams (e.g. fs11, fs15, fs3, fs4; Punkari 1980, 1994; Kleman *et al.* 1997; Putkinen *et al.* 2017; Lunkka *et al.* 2021). The imprint of the Lake District ice lobe over S Finland (corresponding to Fan 46 in Kleman *et al.* 1997—see Table S3) predominantly corresponds to a divergent isochronous flowset (fs11) which extends to the edge of our mapping area at the Finnish Baltic coast and is associated with Stage 15 (Figs 13, S10, S11). Whereas Fan 46 in Kleman *et al.* (1997) terminates at the Salpausselkä I ice-marginal zone, the coherent divergent pattern of subglacial lineations we observe extends beyond this (Fig. S11). The terminations of small flowsets, which overprint the lateral margins of fs11 (fs857 and fs5) and occur in Stage 17 of our reconstruction correspond to the Salpausselkä II ice-marginal zone. Hence, while fs856 and fs5 provide evidence that some subglacial lineations formed as the ice margin crossed the Salpausselkä ice-marginal zone, the major subglacial lineation imprint in fs11 may instead reflect a similarly aligned but somewhat more expansive lobate ice-flow pattern. The major divergent imprints of subglacial meltwater routes which do terminate along the Salpausselkä ice-marginal formations (e.g. Putkinen *et al.* 2017; Dewald *et al.* 2022), therefore likely represent an asynchronous landform imprint which largely postdates the major subglacial lineation imprint in this area.

A readvance of ~10s km has been invoked for the Salpausselkä II ice-marginal zone based on observations of small subglacial lineations superimposed on ice-marginal glaciofluvial deposits (Lunkka *et al.* 2021). Despite being much less aerially extensive than fs11, our small flowsets fs857 and fs5, which overprint the lateral margins of fs11, terminate at Salpausselkä II (fs857 being a time-transgressive retreat flowset; Fig. S11). Distinct clusters of lineated glaciofluvial deposits identified by Lunkka *et al.* (2021: fig. 3) occur within the boundaries of these flowsets, with more scattered occurrences in the intervening area. Hence, while reconstructing ice-margin readvances was not a goal of our study, it is

possible that our flowsets fs857 and fs5 (attributed to Stage 17) relate to a local readvance to the area around Salpausselkä II (and in the case of fs857, subsequent time-transgressive retreat from this position). While our data do not necessitate local expansion of the generalised ice sheet bounding line in this region, other flowsets in Stage 17 do necessitate an expansion of the bounding line towards the Rugozero ice-marginal zone further north, likely representing a readvance. Hence, our results are broadly compatible with previous work attempting to resolve the relative timing of ice-marginal deposits in this sector (e.g. Putkinen 2011; Lunkka *et al*. 2021; Boyes *et al*. 2024).

Together, fs5 and fs857 depict a retreated configuration of the Lake District lobe (fs11) in Stage 15. Similar 'lateral feather' flowsets (fs2, fs1) overprint the northeastern edge of fs11 further up its trunk (Fig. S11). We find that this is most consistent as the eastward extension of a later lobate ice-flow pattern (fs15) which was centred to the west of the earlier Lake District Lobe in Stage 21, having a broadly similar but somewhat more expansive geometry to the Näsijärvi ice lobe associated with the Central Finnish Ice-Marginal Formation (e.g. Punkari 1980; Lunkka *et al*. 2021; Figs 13, S11).

The imprint of the Baltic Sea ice lobe over S Finland within the region of the Salpausselkä ice-marginal zone (e.g. Lunkka *et al*. 2021) appears to be divisible into two isochronous flow patterns: one (fs4) which terminates around Salpausselkä I in Stage 16, and a superimposed imprint (fs3) which appears to represent a retreated configuration terminating around Salpausselkä III in Stage 20 (Figs 13, S11). In this stage, several flowsets (fs3, fs4, fs98, fs9, fs225, fs100, fs703; Fig. S10) depict a coherent pattern of lobate flow over the mouth of the Gulf of Bothnia, extending from SW Finland, across the Åland Islands and into E Sweden, as was previously recognised by Kleman *et al*. (1997).

There has been significant discussion regarding the influence of the Bothnian and Baltic Sea basins on the configuration, continuity and longevity of ice streaming through these areas (e.g. De Geer 1884; Punkari 1980, 1994, 1997; Holmlund & Fastook 1995; Boulton *et al*. 2001; Stokes & Clark 2001; Lundqvist 2007; Greenwood *et al*. 2015, 2017, 2023; Szuman *et al*. 2024). Greenwood *et al*. (2023), in particular, provide a comprehensive synthesis of the development of ideas and evidence for the Baltic Ice Stream along the axis of the Baltic Sea. Although we provide no new data on ice flow in these now-submarine regions, a convergent flowset at the Swedish Bothnian coast in Stage 22 (fs92) trends southwards into the Gulf of Bothnia; this flowset correlates to southward-trending landforms analysed offshore by Greenwood *et al*. (2015, 2017), that define the track of an ice stream which broadly follows the topographic axis of the Bothnian basin but does not span its full width (Greenwood *et al*. 2015, 2017).

It is notable that other flowsets which deflect through the Gulf of Bothnia imply that significant topographic influence of the basin only occurred when we infer relatively thin ice advancing or retreating across the area (i.e. during advance in Stage 5; fs850, fs18, fs10; then during deglaciation through Stages 17–22; e.g. fs217, fs225, fs703, fs98, fs92). Most other observed imprints adjacent to the Gulf of Bothnia appear to require flow across, as opposed to along its axis. This suggests that the topographic influence of the Gulf of Bothnia diminished as the ice sheet expanded and did not resume until the ice margin retreated back towards this area late in the deglaciation. Through much of the peak glaciation, the Gulf of Bothnia was near to the ice divide. Recent work to examine the offshore landform record in the Baltic Sea (Greenwood *et al*. 2015, 2023; Szuman *et al*. 2024) has revealed multiple superimposed imprints of both streaming and non-streaming ice flow, which progressively back-stepped through this basin during deglaciation. We concur with these interpretations. While we do interpret SW-trending flowsets on the Baltic Sea islands of Gotland and Öland in Stage 10 (fs106, fs114; Figs 13, S10) as having been fed by ice that flowed through the Gulf of Bothnia, this does not necessarily imply a long, spatially continuous ice stream operated along the entire flow axis shown in Stage 10. Ice streams previously identified from imprints in the Baltic and Bothnian basins (Greenwood *et al*. 2015, 2017, 2023; Szuman *et al*. 2024) likely operated at various times between Stages 10 and 22 of our flow-pattern reconstruction. There is no new information in our flowsets with which to assess the hypothesis invoked by Lundqvist (2007) that readvances occurred during the generalised retreat of ice through this offshore area.

Ice streams are also thought to have operated in other sectors of the SIS, with many extending offshore (e.g. Ottesen *et al*. 2002, 2005, 2008, 2016; Winsborrow *et al*. 2010). While we have not connected our flowsets to offshore landform records, some could represent upstream tributaries of large marine-terminating ice streams flowing through cross-shelf troughs when the SIS extended beyond the present-day coastline (Ottesen *et al*. 2002, 2005, 2008, 2016). Others may represent upice tributaries of offshore ice streams such as the Bjørnøyrenna ice stream (e.g. fs149 via Ingøydjupet Trough, as in Winsborrow *et al*. 2010), and the Norwegian Channel (Norskrenna) ice stream. Flowsets which could relate to these ice streams mostly occur in our inferred LGM SIS Stages 7–8 (e.g. fs303, fs260, and fs149). Numerous other ice streams may have operated in the later stages of our reconstruction including to the southeast of the ice divide over Sweden and Finland. Many of our fjord-directed flowsets along the Norwegian coast likely also represent short-lived pathways of former outlet glaciers during late-stage deglaciation (e.g. fs390, fs397). More work is required to identify the detailed distributions of ice stream imprints across

the SIS, to connect terrestrial and marine flow patterns and to assess the timing of ice streaming and its wider significance and influence on ice sheet dynamics and ice loss.

Placing ice flow stages in approximate time

We do not currently have means to directly date ice-flow patterns recorded by lineations formed in the subglacial environment (Kleman & Borgström 1996; Kleman *et al*. 2006). However, we can use landform superimposition (Clark 1993, 1997) to build a relative age sequence of events, and then use this sequence alongside other evidence to make broad inferences about the potential timing of events in our flow-pattern sequence (e.g. Kleman *et al*. 1997). Our flow-pattern stages are almost certainly not equally spaced in time, nor can we comment on the longevity of each stage. Nevertheless, we make some tentative inferences about their general timing and pacing.

During the last glacial cycle (~120 000 years) the SIS advanced and retreated multiple times; most extensively during MIS 2 (29–14 ka), but also during MIS 4 (71–57 ka) and early Weichselian stadials MIS 5d and 5b (109 and 87 ka) (Svendsen *et al*. 2004; Batchelor *et al*. 2019; Gowan *et al*. 2021; ages based on Lisiecki & Raymo 2005). The extent and evolution of the SIS during the MIS 3 (57–30 ka) interstadial has been a subject of significant debate (e.g. Houmark-Nielsen & Kjær 2003; Alexanderson *et al*. 2010; Houmark-Nielsen 2010; Wohlfarth 2010; Möller *et al*. 2013, 2020; Lüthgens *et al*. 2020; Kleman *et al*. 2021; Mangerud *et al*. 2023a). However, over the last decade, it has become generally accepted that the SIS retreated into the Scandinavian mountains before advancing to achieve its maximum areal extent around 20–21 ka (Hughes *et al*. 2016; Kleman *et al*. 2021; Mangerud *et al*. 2023a).

Based on the relative chronology and pattern of our flowsets, we interpret that most can plausibly be explained within a single ice sheet advance and retreat cycle, and represent the evolution of the ice sheet through MIS 2. However, 13 of our flowsets are interpreted to have formed prior to this, and may represent flow imprints of earlier ice sheet(s). This is consistent with previous inferences that some Fennoscandian subglacial lineations represent Early Weichselian ice flow (e.g. Hirvas *et al*. 1988; Kleman *et al*. 1997). The flow patterns and cross-cutting relationships of these older flowsets (low down in the relative-age sequence) allow us to separate and group them into two different flow stages (Stages 1 and 2; Fig. 12), which depict the growth of a spatially-extensive ice sheet, and which are difficult to reconcile with later flow events in a single advance-retreat cycle. For example, Stage 3, depicts a relatively small and thin ice sheet centred on the Scandinavian mountains (Fig. 13). Thereafter, our reconstruction (Fig. 13) depicts the growth of a large, topographically unconstrained ice sheet that was centred over E Sweden and N Finland by Stages 7–8.

Cross-cutting relationships indicate that fs63 (Stage 1; Figs 12, S10) formed prior to the hummocky Veiki moraines (Hoppe 1952; Lagerbäck 1988), which have recently been dated to within MIS 3 (~56–39 ka; Alexanderson *et al*. 2022). Together with other evidence (see Mangerud *et al*. 2023a), we therefore suggest Stages 1 and 2 may represent ice-flow patterns of an ice sheet at least as old as MIS 4, and possibly older. In N Sweden and Finland the geometry of Stage 1 flowsets is similar to the flow patterns depicted in the first stage of the Kleman *et al*. (1997: figs 5, 11) reconstruction, which they assigned to MIS 5d–5a (110 ka). We do not see a clear parallel to our Stage 2 represented in their reconstruction, though our Stages 3, 4, and 5 have some similarities to the ice sheet geometries they associate to between 100 and 65 ka (Kleman *et al*. 1997: figs 6, 11), particularly in terms of the placement of the ice divides. It is interesting to note that we reconstruct similar early ice-flow patterns and divide positions based on relative-age sequencing and glaciological interpretations of subglacial lineation flowsets, despite the fact that most of the pre-LGM flow patterns of Kleman *et al*. (1997) are based on fans derived solely from striae and/or till fabrics (see Table S3). Both reconstructions therefore capture more than one cycle of ice advance and retreat centred on the Scandinavian mountains before the development of the LGM SIS, though with slightly different inferred timing. An important distinction is that, based on their glaciodynamic interpretations, Kleman *et al*. (1997) suggest that the ice-flow patterns they ascribe to 100 ka represent recession relative to the ice extent at 110 ka. Here, we present similar ice flow configurations (our Stages 3–5) as part of a plausible sequence that may document ice-sheet advance towards the LGM. If we accept that Stages 1 and 2 relate to an MIS 4 or older glaciation, then our Stage 3 can be placed at the end of MIS 3 or start MIS 2. This appears consistent with both empirical data and modelling, which suggest a limited ice extent in MIS 3 and growth of the MIS 2 ice sheet from ice fields centred on the Scandinavian mountains (Lambeck *et al*. 2010; Hughes *et al*. 2016; Mangerud *et al*. 2023a; Jungdal-Olesen *et al*. 2024).

Flow in Stages 7–8 (Figs 13, S9, S10) is consistent with the ice sheet extending westward onto the Norwegian continental shelf, eastward and southward into the Russian and European plains (i.e. beyond the Baltic Sea), and converging with the BIIS (from Stage 6) and BKIS (from Stage 7). These connections are loosely constrained by chronological evidence to ~27–18 and ~25–15 ka (Hughes *et al*. 2016; Brendryen *et al*. 2020; Clark *et al*. 2022; Sejrup *et al*. 2022), respectively. We therefore suggest that these stages approximate the interior flow configuration and ice divide position when the SIS reached its peak areal LGM extent, constrained to 21–20 ka (Hughes *et al*. 2016). However, we note that

Stages 7 and 8 potentially represent the ice-flow patterns of the SIS interior through several thousand years, and that the local maximum extent of different sectors of the ice sheet margin was achieved at different times (e.g. Hughes *et al*. 2016; Stroeven *et al*. 2016). Our postulated LGM ice reconstruction (Stages 7–8) is similar to that proposed at 22 ka by Kleman *et al*. (1997; Fig. 7), though we extend the main ice divide further east and north (Figs 3C, 13).

Stage 8 (Figs 13, S9, S10) is followed by a progressive and consistent back-stepping of flow imprints across Fennoscandia, and a general increase in the topographic sensitivity of flowsets; hence we suggest that Stage 9 represents the onset of extensive deglaciation. From Stages 10 to 11, flowsets extending from N Norway to the Barents Sea start to exhibit significant topographic sensitivity consistent with separation from the BKIS. Overall, most of our stages, and 70% of our flowsets document the ice-flow patterns during deglaciation (from *c*. 15 ka), which is not unexpected given that these subglacial lineations have higher preservation potential.

We used the well-established extent of the SIS associated with the YD (e.g. Andersen *et al*. 1995a; Mangerud *et al*. 2023b; Boyes *et al*. 2024) to suggest that Stages 16–18 represent the approximate flow patterns around the time of this climatic cooling (12.7–11.6 ka; Rasmussen *et al*. 2014). Stages 9–16 thus capture the evolution of ice flow through initial deglaciation prior to the YD (Figs 13, S9, S10). We do not place more precise timing on these stages, though by Stages 13–15 it is reasonable to infer that ice had retreated from S Sweden and back to the approximate position of the present-day Norwegian coastline, accompanied by widespread ice sheet thinning with development of a branched divide across the northern sector of the SIS by Stage 15. This implies a possible timing of *c*. 18–13 ka for Stages 9–16 (Hughes *et al*. 2016; Stroeven *et al*. 2016).

Stage 17 is the only deglacial stage where we found it necessary—based on flowsets and their relative sequencing alone—to infer a spatially restricted re-advance of the ice margin. This re-advance (of unconstrained distance) extends towards the position of the Rugozero ice-marginal zone in NW Russia, which has been associated with the YD (Rainio *et al*. 1995; Stroeven *et al*. 2016; Boyes *et al*. 2024). This is consistent with other evidence for a readvance of up to tens of kilometres at multiple sites around the SIS margin (e.g. Mangerud *et al*. 2016, 2019; Høgaas *et al*. 2018; Romundset *et al*. 2019; Lunkka *et al*. 2021), as a response to this cold interval which interrupted the general trajectory of climate warming. We re-emphasise that we do not generally attempt to correlate flowsets with specific ice-marginal landforms, and elsewhere, our flowsets do not require us to invoke readvances at any time during deglaciation, including during the YD. However, this does not necessarily mean readvances did not occur, simply that the incorporation of other lines of evidence and/or more detailed mapping, is needed to identify them and their precise timing, with security.

Taking Stages 16–18 as representing ice-flow patterns around the YD, subsequent stages relate to ice flow evolution into the Early Holocene (from 11.6 ka; Rasmussen *et al*. 2014). Our Stages 17–23 (Figs 13, S9, S10) illustrate significant dynamism in the flow pattern across S Finland and southern parts of the Gulf of Bothnia (Stages 21–23; e.g. fs92, fs90; Greenwood *et al*. 2017), and likely represent flow-pattern changes over relatively short periods compared to the rest of the sequence. This dynamism was likely facilitated by large volumes of surface melt and the continued development of proglacial ice-dammed lakes during retreat (e.g. Regnéll *et al*. 2023, 2024). It may also simply reflect better preservation of discrete landform imprints that can be separated into coherent broader flow patterns with detailed relative age information; that is, that we capture greater dynamism as the landform record is better preserved.

Based on the understanding that the final demise of the SIS occurred before 9.5 ka (Hughes *et al*. 2016; Stroeven *et al*. 2016; Regnéll *et al*. 2019, 2023, 2024), Stages 18–25 represent flow-pattern changes that occur in less than 2000 years. The scenario of final ice sheet demise presented in Stages 23–25 is likely to be over-generalised and could be significantly enhanced, revised and extended with the incorporation of additional evidence, such as ice-marginal landforms and dating (e.g. Mangerud *et al*. 2019; Regnéll *et al*. 2023). This is because relatively thin ice retreating through the rugged topography of the Scandinavian mountains and Norwegian fjord systems likely resulted in highly complex, dynamic, and locally variable flow patterns, with lower potential for generating coherent flowset records. The temporal evolution of the geometry of the independent ice masses may have proceeded with different relative timings; hence the geometries of the ice masses illustrated in Stages 24 and 25 may be asynchronous (cf. Nesje & Matthews 2024; Regnéll *et al*. 2024).

While we have reconstructed most of our flow signatures into plausible ice sheet configurations as a series of stages through the last glacial (MIS 2; Late Weichselian), it is important to note that this is merely the simplest interpretation. Some of the flowsets may record events from prior glaciations. Additional work to connect flowsets with till stratigraphy and well-dated ice-marginal landforms is required to build a more precise chronology of flow evolution.

Logical next steps

The bedform-derived flow patterns presented here form one of a suite of key ingredients required to generate a fully integrated empirical whole-ice-sheet reconstruction incorporating multiple lines of evidence. Additional ingredients for such a reconstruction include (i) subgla-

cial meltwater routes (e.g. Dewald *et al*. 2022), (ii) ice-marginal landforms, (iii) compilations of landform evidence, reduced to flowsets, from beyond our core study area and offshore (e.g. Ottesen *et al*. 2005; Winsborrow *et al*. 2010; Sejrup *et al*. 2022; Greenwood *et al*. 2023; Diemont 2024; Szuman *et al*. 2024) and (iv) a compilation of relevant ages (e.g. Hughes *et al*. 2016; Stroeven *et al*. 2016). In addition, our flow-pattern reconstruction could be further refined, and the level of detail enhanced, with future inclusion of flow indicators such as glacial striae (e.g. Mangerud *et al*. 2019) and erratics. In generating our flow-pattern reconstruction independently of other sources of empirical information we provide a valuable tool for independently verifying and testing interpretations from other bodies of evidence. We release our flow-pattern reconstruction data (Data S1) to enable such analyses, and to allow the data to be re-analysed and re-interpreted as new, complementary, or contradictory evidence arises.

We do not foresee that further improvements in the quality and resolution of digital terrain models for Norway, Sweden or Finland would provide meaningful improvements in the detail of ice-sheet-scale flow-pattern information. However, new local-to-regional-scale studies based on complete landform mapping—as opposed to sampled mapping undertaken here—have significant potential to reveal new information about the behaviour of the ice sheet within individual sectors and regions (e.g. Boyes *et al*. 2023); our ice-sheet-scale reconstruction may be useful for identifying particular areas of interest over which to target such studies. As an example, the new meltwater-route-directed flowsets we identify (e.g. Fig. 8H) are small in area, and our sampling approach to landform mapping means that the examples we identify are not likely to be an exhaustive catalogue of this type of landform imprint. An extensive search for such features (including in existing landform maps, e.g. Putkinen *et al*. 2017), and detailed analysis of them, could reveal new information about the interactions of subglacial meltwater and subglacial bedform evolution. We outline below some logical next steps for ice-sheet-scale analysis.

Integration with ice sheet periphery and offshore records. – A logical next step is to augment our mapped flow patterns with similar information offshore, and to the S and E, extending from the core area of the ice sheet to its periphery. As noted by previous workers (e.g. Boulton *et al*. 2001; Larsen *et al*. 2016), the nature of the landform record around the onshore portions of the ice sheet south and east of the Baltic Sea, and in parts of Russia, is notably different from that of our study area. The availability of high-quality, high-resolution DTMs in these areas is also far more limited. This transition broadly correlates with the boundary of the Fennoscandian Shield (Fig. 1) and aligns approximately with the south-easternmost extent of spatially contiguous flow imprints we observe extending into NW Russia from Finland (Fig. 10). The S and E periphery of the SIS (extending from Denmark to Arctic Russia) is the subject of a coordinated parallel study by Diemont (2024), which could be integrated with the flow-pattern reconstruction we present here.

Integration with records of ice margin positions, meltwater drainage and dating. – In reconstructing past ice sheets, most attention has typically focussed on how ice-marginal landforms (including e.g. moraines, ice-marginal channels, and eskers) inform the pattern and timing of deglaciation (e.g. Stroeven *et al*. 2016). Other approaches have focussed on reconciling catalogues of dates to reconstruct ice sheet extent through time (e.g. 'time-slice' reconstructions of Dyke & Prest 1987; Dyke *et al*. 2003; Hughes *et al*. 2016; Dalton *et al*. 2023). Only rare attempts have combined such ice-marginal or extent analyses at the ice-sheet scale with flow patterns generated across the ice sheet bed, including up to several hundreds of kilometres inboard of the margins (e.g. Kleman *et al*. 1997; Boulton *et al*. 2001). We have focussed on the latter in this paper, with a logical next step to combine information on the internal flow geometry with ice-marginal records. It would then be possible to combine evidence from the landform record with information from published compilations of age constraints on ice advance and retreat (e.g. Hughes *et al*. 2016) to generate a fully integrated reconstruction of ice sheet evolution incorporating flow patterns, ice margin positions and absolute age constraints, similar to that undertaken for the BIIS, for example, by Clark *et al*. (2022).

Comparison with other lines of evidence of palaeo-ice flow. – We focused on subglacial bedforms as indicators of spatially extensive palaeo-ice sheet flow, purposefully keeping our reconstruction separate from other lines of evidence such as glacial striae on bedrock, clast fabrics in glacial deposits (till) or the dispersal of erratics. There is a large body of information on these that could be investigated to test or add to our flowsets and interpretations (e.g. Kjær *et al*. 2003; Donner 2005), but we note some difficulties in seeking matches because the processes are not entirely equivalent. Erratics, for example, do not typically record flowlines with the ice sheet, but rather cumulative transport trajectories taken as flow geometries adjusted over time, potentially over successive glaciations (e.g. Kleman *et al*. 2008). Having separated discrete flow patterns into flowsets and interpreted the adjustments of flow trajectories over time, it may now be possible to develop better predictions of the potential erratic transport trajectories. Our lineation linkage data could provide a valuable reference dataset for filtering out signals of local-scale flow variability in compilations of glacial striae (e.g. Kleman 1990) in order to extract regional signals of ice flow. The compatibility between our reconstructed ice-flow geometries

and those flow patterns identified by Kleman *et al*. (1997) using striae and/or till fabrics (see Table S3) suggests that glacial striae and till fabric data may not significantly modify our reconstructed ice-sheet-scale flow patterns. However, testing this inference is an important future task, and would additionally provide opportunities to increase the level of detail pertaining to regional-scale flow variations (e.g. Mangerud *et al*. 2019).

Integration into data-model comparison approaches. – Comparisons between numerical models of palaeo-ice sheets and empirical observations of the landform record they left behind are becoming increasingly common (e.g. Lambeck *et al*. 2010; Clason *et al*. 2014; Patton *et al*. 2016, 2017; Seguinot *et al*. 2016; Gandy *et al*. 2021; Ely *et al*. 2024). Ideally, data-model comparison experiments would consider multiple lines of geochronological and geomorphological evidence (Ely *et al*. 2021), but most thus far have focussed on reconciling the extent and timing of ice margins and relative sea level records (e.g. Tarasov *et al*. 2012; Ely *et al*. 2019; Gowan *et al*. 2021). Tools and approaches for comparing ice flow directional observations with model simulations exist (e.g. Näslund *et al*. 2003; Hättestrand *et al*. 2004; Li *et al*. 2007; Napieralski *et al*. 2007; Archer *et al*. 2023) but have often been underused in ice sheet modelling experiments. One could envisage a number of different data model comparison experiments using the datasets we provide; the limited availability and accessibility such datasets has so far presented a significant barrier to conducting such experiments. Any modeller wishing to compare simulations to the data presented here should be mindful of the assumptions behind each data product. Flowsets have proved a valuable tool in palaeoglacial inversion, but are cartographically simplified representations of ice flow, which often generalize (and thus may obscure) more complex ice flow dynamics. This is particularly true of time-transgressive flowsets, which represent the compound vectors of dynamic ice flow events that can include significant local-to-regional-scale changes in ice flow orientation. Comparisons between models and flowsets may be sufficient for modellers working with coarse-resolution continental-scale models (e.g. Patton *et al*. 2017). However, those focusing on more detailed comparisons between empirically interpreted and modelled flow directions may wish to use the new lineation linkages product. The linkages contain less interpretation than flowsets, and are closer in scale than raw lineation mapping to the resolutions of numerical model grids (typically kilometres to tens of kilometres); hence, they are of a spatial scale and level of abstraction that is potentially useful for current data-model comparison approaches. Perhaps eventually, improvements in the fidelity of modelling may even permit the use of numerical simulations to assess the plausibility of empirical interpretations of ice flow reflected in our flowsets and groupings of flowsets into ice-sheet-scale flow patterns.

Wider implications and utility of flow-pattern information

Together, streamlined subglacial landforms provide an underpinning linearity and patterning to Fennoscandian landscapes, which has relevance beyond palaeoglaciological reconstruction. Such patterning is particularly influential, for example, to lowland hydrology. Data on the distributions, orientations, and sequencing of subglacial landforms, such as those generated herein, are useful resources for investigating subglacial bedform formation processes, the volume and distributions of sediments, the geotechnical properties of substrates and for informing mineral exploration. Furthermore, extensive mapping of diverse subglacial lineations and ice flow orientations is a critical step towards training machine-learning algorithms to automatically extract ice flow information from glacial landform patterns.

Glacio-isostatic adjustment and sea level change. – It is not possible to understand rates and variations in contemporary sea level across Fennoscandia and Europe, or to robustly predict future changes, without accounting for the glacial rebound (land uplift) following ice-mass unloading as the SIS disappeared (e.g. Spada 2017). Our reconstruction of ice divide migration (e.g. Figs 12, 13, 15) is relevant because the divides strongly influence where the mass of ice is distributed across an ice sheet domain, in turn influencing glacio-isostatic adjustment and affecting sea level. Future work reconciling ice sheet modelling with flowsets (e.g. using tools such as that developed by Archer *et al*. 2023) could provide a history of ice thickness changes to help improve sea level forecasts over the coming centuries (e.g. Palmer *et al*. 2018).

Improving understanding of contemporary ice sheets. – The responses of present-day ice sheets to contemporary climate forcing are likely occurring against a backdrop of longer term ice-flow evolution; they may still be responding to dynamic changes in ice flow over timescales of millennia (Albrecht *et al*. 2020; Yang *et al*. 2022). Current practices of 'spinning up' ice sheet models based on present-day ice-flow fields and using this as a basis to forecast future ice sheet evolution are likely to omit such long-term influences (Yan *et al*. 2013). Ice flow indicators are currently underused in numerical ice-sheet modelling approaches, despite providing critical information on ice-flow patterns and strong constraints on divide configurations during the life cycles of ice sheets. It is hoped that the new information we provide on the flow-pattern evolution of the SIS will help stimulate methods and investigations which use palaeo-ice flow in numerical modelling to advance understanding of ice sheet behaviours, including those of contemporary ice sheets in Greenland and Antarctica.

Implications for erratics and mineral exploration. – Ice sheets erode their beds, including rocks hosting vital rare-earth minerals (e.g. lithium, gold, tellurium), and disperse materials down-flow. A common technique in mineral exploration is to identify key geochemical traces in samples of till, and then to use local ice flow history to suggest the upstream location of the source rock from which it was eroded (e.g. McClenaghan *et al*. 2023). However, some sources are difficult to find because of changing ice flow directions (Parent *et al*. 1996); hence, the flowset data and relative age sequences presented here could be of use. An ice sheet model simulation optimised to fit with flowset data would be useful for mineral exploration. An early test of its ability would be to assess how well it explains the distribution of known glacial erratics. For the BIIS for example, Veness *et al*. (2025) used such approaches to explain erratic transport.

Conclusions

We present a new reconstruction of the evolution of ice-sheet-scale flow-patterns over Fennoscandia based on systematic mapping of ~240 000 subglacial lineations and lineation fields across Norway, Sweden, Finland and NW Russia. Our reconstruction comprises a sequence of 25 stages depicting distinct ice-sheet-scale flow patterns and the inferences we can make from them about the evolution of the overall size and shape of the ice sheet, including the position and migration of the ice divide(s). We base our reconstruction on 611 flowsets, which delimit discrete ice-flow patterns in the mapped subglacial lineations. Our sequence of stages honours the relative age sequencing of flowsets evidenced by cross-cutting relationships of their constituent subglacial lineations. We integrate our flow-patterns with the recent flow-pattern reconstruction over the Kola Peninsula and Russian Lapland by Boyes *et al*. (2023).

Our reconstruction is the most detailed empirical ice-sheet-scale flow-pattern reconstruction undertaken for the SIS to date and was enabled by a recent revolution in the coverage and availability of high-resolution (1–2 m pixel^{-1}) bare-Earth digital terrain models over Norway, Sweden and Finland. Of our 25 reconstructed stages, 23 depict the evolution of the last (MIS 2; Late Weichselian) SIS; this includes several stages of ice advance towards the LGM and numerous stages of subsequent deglaciation, including the eventual fragmentation of the ice sheet into smaller ice masses during the Early Holocene. It demonstrates that the ice divide of the last SIS migrated up to 500 km during ice-sheet advance, hinging from its initial position over the N Scandinavian mountains to a position across N Finland and extending to the White Sea. During deglaciation, the ice divide migrated westwards back across Finland and N Sweden but did not fully return to the mountains. Instead, the ice sheet fragmented into smaller ice masses, the largest of which was centred to the east of the Scandinavian mountains. Two additional stages in our reconstruction appear to record the flow patterns of an older ice sheet (or multiple ice sheets) over Fennoscandia, perhaps during MIS 4 or earlier.

Our reconstruction independently verifies, augments, and advances on many major properties of the SIS that were inferred by previous studies; this reflects the impressive legacies of earlier attempts to reconcile ice-flow patterns at the ice-sheet scale. Those foundational contributions to understanding the ice sheet—and to the wider discipline of palaeoglaciology—endure to this day. This gives us confidence in the robustness of our reconstruction, which identifies many more stages of ice flow, including during the fragmentation of the ice sheet towards its final demise, and reveals numerous new details of flow-pattern evolution and ice flow relative-age sequencing. Flowset-by-flowset analysis, for example, reveals spatio-temporal patterns in the ratio of ice thickness to local topographic relief as evidenced by the interaction of ice-flow patterns with topographic variations. Such information holds significant potential for informing detailed reconstructions of the three-dimensional properties of the ice sheet through time, particularly if combined with numerical ice sheet modelling and further theoretical work.

We release our flowset data, relative chronology information, and digital files for our flow-pattern reconstruction along with our dataset of ~58 000 lineation linkages, which summarise our detailed landform mapping (Data S1). These datasets have a range of potential uses both within and beyond palaeoglaciology, and we make them available to be scrutinised, re-analysed, augmented, and revised as new evidence, approaches, ideas, and applications arise. We anticipate that our lineation linkage dataset could be particularly valuable for numerical ice-sheet modelling approaches which incorporate empirical data, as they are less interpretative than flowsets but reduce detailed landform-scale information to scales that are comparable to the resolutions of model grids. By releasing our digital data files, we open the possibility for optimising numerical, climate-coupled ice-sheet-model simulations of the SIS to detailed empirical evidence of flow-pattern evolution observed in the landform record. We expect the new information we provide will help to stimulate methods and investigations which use palaeo-ice flow in numerical modelling to advance understanding of the range of behaviours of past and present ice sheets and thereby ensure that we can better predict future responses of the Greenland and Antarctic ice sheets to anthropogenic climate change.

Acknowledgements. – This project benefited from the PalGlac team of researchers with funding from the European Research Council (ERC) under the European Union's Horizon 2020 research and innovation programme to CDC (Grant Agreement No. 787263) and which supported FEGB, HED, BMB and CRD. We thank Robyn Dyson for her thorough work checking the orientations of the lineation linkages,

and Nico Dewald for helping process DTMs. This paper was submitted while FEGB was in receipt of a Leverhulme Trust Early Career Research Fellowship. A NERC independent fellowship (NE/R014574/1) enabled JCE to work on the topic. We are grateful to Niko Putkinen for numerous insightful discussions during our mapping work. We thank Tom Dowling for generously providing data that helped with training mapping assistants. We thank Arjen Stroeven and Nigel Atkinson for providing thorough and insightful reviews. We are grateful to Ívar Örn Benediktsson for handling this manuscript as Guest Editor as well as Jan A. Piotrowski as Editor-in-Chief of Boreas. Finally, we dedicate this paper to Professor Johan Kleman, whose groundbreaking research has inspired generations of palaeoglaciologists and provided much of the motivation for this work.

Author contributions. – Initial conceptualisation and funding acquisition were by CDC, ALCH and JCE. The methodology was developed by FEGB, with inputs from ALCH and CDC. Basemap datasets were processed by FEGB, CRD, BMB and ELML. Lineation mapping was performed by FEGB, ALCH, JCE, ELML, ACS and SH. Linkage mapping in Finland, Sweden and Norway was performed by FEGB and ALCH, and reconnaissance-style linkage mapping in Russian Karelia was performed by BMB. Cross-cutting analysis and relative age sequencing of flowsets were performed by FEGB and HED. The stage reconstructions were generated by FEGB, HED, ALCH, BMB and CDC. FEGB curated the datasets. FEGB, ALCH and CDC drafted the manuscript with assistance from HED and BMB. All authors contributed to scientific discussions during the investigation and/or during revision of the manuscript.

Data availability statement. – Major supporting maps and data tables are included as Figs S1–S11 and Tables S1–S3. Data S1 contains the shapefile datasets for the lineation linkages, critical cross-cuts, flowsets and flow-pattern stage reconstructions. Data S1 includes a detailed README file on the contents of each shapefile. Data S2 includes additional supporting maps.

References

Aario, R. 1977: Associations of flutings, drumlins, hummocks and transverse ridges. *GeoJournal 1*, 65–72. https://doi.org/10.1007/BF00195540.

Albrecht, T., Winkelmann, R. & Levermann, A. 2020: Glacial-cycle simulations of the Antarctic Ice Sheet with the Parallel Ice Sheet Model (PISM) – part 2: parameter ensemble analysis. *The Cryosphere 14*, 633–656. https://doi.org/10.5194/tc-14-633-2020.

Alexanderson, H., Hättestrand, M., Lindqvist, M. A. & Sigfúsdóttir, T. 2022: MIS 3 age of the Veiki moraine in N Sweden – dating the landform record of an intermediate-sized ice sheet in Scandinavia. *Arctic, Antarctic, and Alpine Research 54*, 239–261. https://doi.org/10.1080/15230430.2022.2091308.

Alexanderson, H., Johnsen, T. & Murray, A. S. 2010: Re-dating the Pilgrimstad Interstadial with OSL: a warmer climate and a smaller ice sheet during the Swedish Middle Weichselian (MIS 3)? *Boreas 39*, 367–376. https://doi.org/10.1111/j.1502-3885.2009.00130.x.

Andersen, B. G., Lundqvist, J. & Saarnisto, M. 1995a: The Younger-Dryas margin of the Scandinavian Ice-Sheet – an introduction. *Quaternary International 28*, 145–146. https://doi.org/10.1016/1040-6182(95)00043-i.

Andersen, B. G., Mangerud, J., Søresen, R., Reite, A., Sveian, H., Thoresen, M. & Bergström, B. 1995b: Younger Dryas ice-marginal deposits in Norway. *Quaternary International 28*, 147–169. https://doi.org/10.1016/1040-6182(95)00037-J.

Andrews, J. T. 1982: On the reconstruction of Pleistocene ice sheets: a review. *Quaternary Science Reviews 1*, 1–30. https://doi.org/10.1016/0277-3791(82)90017-8.

Andrews, J. T. & Barry, R. G. 1978: Glacial inception and disintegration during the last glaciation. *Annual Review of Earth and Planetary Science 6*, 205–228. https://doi.org/10.1146/annurev.ea.06.050178.001225.

Anundsen, K. 1990: Evidence of ice movement over Southwest Norway indicating an ice dome over the Coastal District of West Norway. *Quaternary Science Reviews 9*, 99–116. https://doi.org/10.1016/0277-3791(90)90007-W.

Archer, R. E., Ely, J. C., Heaton, T. J., Butcher, F. E. G., Hughes, A. L. C. & Clark, C. D. 2023: Assessing ice sheet models against the landform record: the likelihood of accordant Lineations analysis (LALA) tool. *Earth Surface Processes and Landforms 48*, 2754–2771. https://doi.org/10.1002/esp.5658.

Arnold, N. & Sharp, M. 2002: Flow variability in the Scandinavian ice sheet: modelling the coupling between ice sheet flow and hydrology. *Quaternary Science Reviews 21*, 485–502. https://doi.org/10.1016/S0277-3791(01)00059-2.

Astakhov, V., Shkatova, V., Zastrozhnov, A. & Chuyko, M. 2016: Glaciomorphological map of the Russian Federation. *Quaternary International 420*, 4–14. https://doi.org/10.1016/j.quaint.2015.09.024.

Bahadory, T., Tarasov, L. & Andres, H. 2021: Last glacial inception trajectories for the Northern Hemisphere from coupled ice and climate modelling. *Climate of the Past 17*, 397–418. https://doi.org/10.5194/cp-17-397-2021.

Barry, R. G., Andrews, J. T. & Mahaffy, M. A. 1975: Continental ice sheets: conditions for growth. *Science 190*, 979–981. https://doi.org/10.1126/science.190.4218.979.

Batchelor, C. L., Margold, M., Krapp, M., Murton, D. K., Dalton, A. S., Gibbard, P. L., Stokes, C. R., Murton, J. B. & Manica, A. 2019: The configuration of Northern Hemisphere ice sheets through the Quaternary. *Nature Communications 10*, 3713. https://doi.org/10.1038/s41467-019-11601-2.

Benediktsson, Í. Ö., Aradóttir, N., Ingólfsson, Ó. & Brynjólfsson, S. 2022: Cross-cutting palaeo-ice streams in NE-Iceland reveal shifting Iceland ice sheet dynamics. *Geomorphology 396*, 108009. https://doi.org/10.1016/j.geomorph.2021.108009.

Boulton, G. S. & Clark, C. D. 1990a: A highly mobile Laurentide ice sheet revealed by satellite images of glacial lineations. *Nature 346*, 813–817. https://doi.org/10.1038/346813a0.

Boulton, G. S. & Clark, C. D. 1990b: The Laurentide ice sheet through the last glacial cycle: the topology of drift lineations as a key to the dynamic behaviour of former ice sheets. *Earth and Environmental Science Transactions of the Royal Society of Edinburgh 81*, 327–347. https://doi.org/10.1017/S0263593300020836.

Boulton, G. S., Dongelmans, P., Punkari, M. & Broadgate, M. 2001: Palaeoglaciology of an ice sheet through a glacial cycle: the European ice sheet through the Weichselian. *Quaternary Science Reviews 20*, 591–625. https://doi.org/10.1016/S0277-3791(00)00160-8.

Boulton, G. S., Smith, G. D., Jones, A. S. & Newsome, J. 1985: Glacial geology and glaciology of the last mid-latitude ice sheets. *Journal of the Geological Society 142*, 447–474. https://doi.org/10.1144/gsjgs.142.3.0447.

Boyes, B. M., Linch, L. D., Pearce, D. M. & Nash, D. J. 2023: The last Fennoscandian Ice Sheet glaciation on the Kola Peninsula and Russian Lapland (part 1): ice flow configuration. *Quaternary Science Reviews 300*, 107871. https://doi.org/10.1016/j.quascirev.2022.107871.

Boyes, B. M., Pearce, D. M. & Linch, L. D. 2021: Glacial geomorphology of the Kola Peninsula and Russian Lapland. *Journal of Maps 17*, 497–515. https://doi.org/10.1080/17445647.2021.1970036.

Boyes, B. M., Pearce, D. M., Linch, L. D. & Nash, D. J. 2024: Younger Dryas and Early Holocene ice-margin dynamics in northwest Russia. *Boreas 53*, 346–400. https://doi.org/10.1111/bor.12653.

Brendryen, J., Haflidason, H., Yokoyama, Y., Haaga, K. A. & Hannisdal, B. 2020: Eurasian Ice Sheet collapse was a major source of meltwater pulse 1A 14,600 years ago. *Nature Geoscience 13*, 363–368. https://doi.org/10.1038/s41561-020-0567-4.

Carrivick, J. L., How, P., Lea, J. M., Sutherland, J. L., Grimes, M., Tweed, F. S., Cornford, S., Quincey, D. J. & Mallalieu, J. 2022: Ice-marginal proglacial lakes across Greenland: present status and a possible future. *Geophysical Research Letters 49*, e2022GL099276. https://doi.org/10.1029/2022GL099276.

Catania, G. A., Stearns, L. A., Moon, T., Enderlin, E. & Jackson, R. H. 2020: Future evolution of Greenland's marine-terminating outlet glaciers. *Journal of Geophysical Research: Earth Surface 125*, e2018JF004873. https://doi.org/10.1029/2018JF004873.

Clark, C. D. 1990: *Reconstruction of the behaviour of the Laurentide Ice Sheet using satellite imagery*. Ph.D. thesis, University of Edinburgh, 272 pp. Available at: http://hdl.handle.net/1842/13406.
Clark, C. D. 1993: Mega-scale glacial Lineations and cross-cutting ice-flow landforms. *Earth Surface Processes and Landforms 18*, 1–29. https://doi.org/10.1002/esp.3290180102.
Clark, C. D. 1997: Reconstructing the evolutionary dynamics of former ice sheets using multi-temporal evidence, remote sensing and GIS. *Quaternary Science Reviews 16*, 1067–1092. https://doi.org/10.1016/S0277-3791(97)00037-1.
Clark, C. D. 1999: Glaciodynamic context of subglacial bedform generation and preservation. *Annals of Glaciology 28*, 23–32. https://doi.org/10.3189/172756499781821832.
Clark, C. D., Ely, J. C., Greenwood, S. L., Hughes, A. L. C., Meehan, R., Barr, I. D., Bateman, M. D., Bradwell, T., Doole, J., Evans, D. J. A., Jordan, C. J., Monteys, X., Pellicer, X. M. & Sheehy, M. 2018: BRITICE Glacial Map, version 2: a map and GIS database of glacial landforms of the last British-Irish Ice Sheet. *Boreas 47*, 11–27. https://doi.org/10.1111/bor.12273.
Clark, C. D., Evans, D. J. A., Khatwa, A., Bradwell, T., Jordan, C. J., Marsh, S. H., Mitchell, W. A. & Bateman, M. D. 2004: Map and GIS database of glacial landforms and features related to the last British Ice Sheet. *Boreas 33*, 359–375. https://doi.org/10.1080/03009480410001983.
Clark, C., Greenwood, S. & Evans, D. 2006: Palaeoglaciology of the last British-Irish ice sheet: challenges and some recent developments. *In* Knight, P. (ed.): *Glacier Science and Environmental Change*, 248–264. Blackwell Science, Oxford. https://doi.org/10.1002/9780470750636.ch50.
Clark, C. D., Knight, J. K. & Gray, J. T. 2000: Geomorphological reconstruction of the Labrador Sector of the Laurentide Ice Sheet. *Quaternary Science Reviews 19*, 1343–1366. https://doi.org/10.1016/S0277-3791(99)00098-0.
Clark, C. D. and 37 others 2022: Growth and retreat of the last British–Irish Ice Sheet, 31 000 to 15 000 years ago: the BRITICE-CHRONO reconstruction. *Boreas 51*, 699–758. https://doi.org/10.1111/bor.12594.
Clason, C., Applegate, P. & Holmlund, P. 2014: Modelling Late Weichselian evolution of the Eurasian ice sheets forced by surface meltwater-enhanced basal sliding. *Journal of Glaciology 60*, 29–40. https://doi.org/10.3189/2014JoG13J037.
Dalton, A. S., Dulfer, H. E., Margold, M., Heyman, J., Clague, J. J., Froese, D. G., Gauthier, M. S., Hughes, A. L. C., Jennings, C. E., Norris, S. L. & Stoker, B. J. 2023: Deglaciation of the north American ice sheet complex in calendar years based on a comprehensive database of chronological data: NADI-1. *Quaternary Science Reviews 321*, 108345. https://doi.org/10.1016/j.quascirev.2023.108345.
De Angelis, H. & Kleman, J. 2005: Palaeo-ice streams in the northern Keewatin sector of the Laurentide Ice Sheet. *Annals of Glaciology 42*, 135–144. https://doi.org/10.3189/172756405781812925.
De Geer, G. 1884: Om den skandinaviska landisens andra utbredning. *Geologiska Foreningen i Stockholm Forhandlingar 7*, 436–466.
Dewald, N., Livingstone, S. J. & Clark, C. D. 2022: Subglacial meltwater routes of the Fennoscandian Ice Sheet. *Journal of Maps 18*, 382–396. https://doi.org/10.1080/17445647.2022.2071648.
Diemont, C. R. 2024: *Land-terminating sectors of the last Scandinavian Ice Sheet: a landform-driven reconstruction*. Ph.D. thesis, University of Sheffield, 274 pp.
Dongelmans, P. W. 1996: *Glacial dynamics of the Fennoscandinavian ice sheet: a remote sensing study*. Ph.D. thesis, University of Edinburgh, 252 pp.
Donner, J. 2005: *Quaternary History of Scandinavia*. 212 pp. Cambridge University Press, Cambridge.
Dowling, T. P. F., Alexanderson, H. & Möller, P. 2013: The new high-resolution LiDAR digital height model ('Ny Nationell Höjdmodell') and its application to Swedish Quaternary geomorphology. *GFF 135*, 145–151. https://doi.org/10.1080/11035897.2012.759269.
Dowling, T. P. F., Möller, P. & Spagnolo, M. 2016: Rapid subglacial streamlined bedform formation at a calving bay margin. *Journal of Quaternary Science 31*, 879–892. https://doi.org/10.1002/jqs.2912.
Dowling, T. P. F., Spagnolo, M. & Möller, P. 2015: Morphometry and core type of streamlined bedforms in southern Sweden from high resolution LiDAR. *Geomorphology 236*, 54–63. https://doi.org/10.1016/j.geomorph.2015.02.018.
Dulfer, H. E. & Margold, M. 2021: Glacial geomorphology of the central sector of the Cordilleran Ice Sheet, Northern British Columbia, Canada. *Journal of Maps 17*, 413–427. https://doi.org/10.1080/17445647.2021.1937729.
Dulfer, H. E., Margold, M., Darvill, C. M. & Stroeven, A. P. 2022: Reconstructing the advance and retreat dynamics of the central sector of the last Cordilleran Ice Sheet. *Quaternary Science Reviews 284*, 107465. https://doi.org/10.1016/j.quascirev.2022.107465.
Dyke, A. S. & Prest, V. K. 1987: Late Wisconsinan and Holocene history of the Laurentide Ice Sheet. *Géographie Physique et Quaternaire 41*, 237–263. https://doi.org/10.7202/032681ar.
Dyke, A. S., Moore, A. & Robertson, L. 2003: Deglaciation of North America. *Geological Survey of Canada Open File 1574*. https://doi.org/10.4095/214399.
Ekman, I. & Iljin, V. 1991: Deglaciation, the Younger Dryas end moraines and their correlation in the Karelian A.S.S.R. and adjacent areas. *In* Rainio, H. & Saarnisto, M. (eds.): *Eastern Fennoscandian Younger Dryas End Moraines*, 73–99. Geological Survey of Finland, Field Conference North Karelia, Finland and Karelian ASSR, June 26–July 4, 1991. *Geological Survey of Finland, Guide 32*, Espoo.
Ely, J. C., Clark, C. D., Bradley, S. L., Gregoire, L., Gandy, N., Gasson, E., Veness, R. L. J. & Archer, R. 2024: Behavioural tendencies of the last British–Irish ice sheet revealed by data–model comparison. *Journal of Quaternary Science 39*, 839–871. https://doi.org/10.1002/jqs.3628.
Ely, J. C., Clark, C. D., Hindmarsh, R. C. A., Hughes, A. L. C., Greenwood, S. L., Bradley, S. L., Gasson, E., Gregoire, L., Gandy, N., Stokes, C. R. & Small, D. 2021: Recent progress on combining geomorphological and geochronological data with ice sheet modelling, demonstrated using the last British–Irish ice sheet. *Journal of Quaternary Science 36*, 946–960. https://doi.org/10.1002/jqs.3098.
Ely, J. C., Clark, C. D., Small, D. & Hindmarsh, R. C. A. 2019: ATAT 1.1, the automated timing accordance tool for comparing ice-sheet model output with geochronological data. *Geoscientific Model Development 12*, 933–953. https://doi.org/10.5194/gmd-12-933-2019.
Ely, J. C., Stevens, D., Clark, C. D. & Butcher, F. E. G. 2023: Numerical modelling of subglacial ribs, drumlins, herringbones, and mega-scale glacial lineations reveals their developmental trajectories and transitions. *Earth Surface Processes and Landforms 48*, 956–978. https://doi.org/10.1002/esp.5529.
European Space Agency *GLO-30 Copernicus DEM*. https://doi.org/10.5270/ESA-c5d3d65 (accessed 28.02.2021).
Fabel, D., Fink, D., Fredin, O., Harbor, J., Land, M. & Stroeven, A. P. 2006: Exposure ages from relict lateral moraines overridden by the Fennoscandian ice sheet. *Quaternary Research 65*, 136–146. https://doi.org/10.1016/j.yqres.2005.06.006.
Fabel, D., Stroeven, A. P., Harbor, J., Kleman, J., Elmore, D. & Fink, D. 2002: Landscape preservation under Fennoscandian ice sheets determined from in situ produced ^{10}Be and ^{26}Al. *Earth and Planetary Science Letters 201*, 397–406. https://doi.org/10.1016/S0012-821X(02)00714-8.
Follestad, B. A. 2003: Development of minor late-glacial ice domes east of Oppdal, Central Norway. *Norges Geologiske Undersøkelse Bulletin 441*, 39–49. Available at: https://www.ngu.no/upload/Publikasjoner/Bulletin/Bulletin441_39-49.pdf.
Follestad, B. A. & Fredin, O. 2007: Late Weichselian ice flow evolution in south-central Norway. *Norwegian Journal of Geology 87*, 281–289. Available at: https://geologi.no/images/NJG_articles/Follestad_et_al.pdf.
Fredin, O. 2002: Glacial inception and Quaternary mountain glaciations in Fennoscandia. *Quaternary International 95–96*, 99–112. https://doi.org/10.1016/S1040-6182(02)00031-9.
Fyke, J., Sergienko, O., Löfverström, M., Price, S. & Lenaerts, J. T. M. 2018: An overview of interactions and feedbacks between ice sheets and the Earth system. *Reviews of Geophysics 56*, 361–408. https://doi.org/10.1029/2018RG000600.
Gandy, N., Gregoire, L. J., Ely, J. C., Cornford, S. L., Clark, C. D. & Hodgson, D. M. 2021: Collapse of the last Eurasian ice sheet in the North Sea modulated by combined processes of ice flow, surface melt, and marine ice sheet instabilities. *Journal of Geophysical*

Research: Earth Surface 126, e2020JF005755. https://doi.org/10.1029/2020JF005755.
GEBCO Compilation Group 2024: *GEBCO 2024 Grid*. https://doi.org/10.5285/1c44ce99-0a0d-5f4f-e063-7086abc0ea0f (accessed 03.09.2024).
Glückert, G. 1974: Map of glacial striation of the Scandinavian ice sheet during the last (Wichsel) glaciation in northern Europe. *Bulletin of the Geological Society of Finland 46*, 1–8. https://doi.org/10.17741/bgsf/46.1.001.
Goodship, A. & Alexanderson, H. 2020: Dynamics of a retreating ice sheet: a LiDAR study in Värmland, SW Sweden. *GFF 142*, 325–345. https://doi.org/10.1080/11035897.2020.1822437.
Gowan, E. J., Zhang, X., Khosravi, S., Rovere, A., Stocchi, P., Hughes, A. L. C., Gyllencreutz, R., Mangerud, J., Svendsen, J. I. & Lohmann, G. 2021: A new global ice sheet reconstruction for the past 80 000 years. *Nature Communications 12*, 1199. https://doi.org/10.1038/s41467-021-21469-w.
Greenwood, S. L. & Clark, C. D. 2008: Subglacial bedforms of the Irish ice sheet. *Journal of Maps 4*, 332–357. https://doi.org/10.4113/jom.2008.1030.
Greenwood, S. L. & Clark, C. D. 2009a: Reconstructing the last Irish ice sheet 1: changing flow geometries and ice flow dynamics deciphered from the glacial landform record. *Quaternary Science Reviews 28*, 3085–3100. https://doi.org/10.1016/j.quascirev.2009.09.008.
Greenwood, S. L. & Clark, C. D. 2009b: Reconstructing the last Irish ice sheet 2: a geomorphologically-driven model of ice sheet growth, retreat and dynamics. *Quaternary Science Reviews 28*, 3101–3123. https://doi.org/10.1016/j.quascirev.2009.09.014.
Greenwood, S. L. & Hughes, A. L. C. 2022a: Chapter 29 – Fennoscandia: glacial landforms prior to the Last Glacial Maximum. *In* Palacios, D., Hughes, P. D., García-Ruiz, J. & Andrés, N. (eds.): *European Glacial Landscapes. Maximum Extent of Glaciations*, 213–221. Elsevier, Amsterdam. https://doi.org/10.1016/B978-0-12-823498-3.00044-3.
Greenwood, S. L. & Hughes, A. L. C. 2022b: Chapter 48 – Fennoscandia: glacial landforms from the Last Glacial Maximum. *In* Palacios, D., Hughes, P. D., García-Ruiz, J. M. & Andrés, N. (eds.): *European Glacial Landscapes. Maximum Extent of Glaciations*, 373–379. Elsevier, Amsterdam. https://doi.org/10.1016/B978-0-12-823498-3.00044-3.
Greenwood, S. L., Avery, R. S., Gyllencreutz, R., Regnéll, C. & Tylmann, K. 2023: Footprint of the Baltic ice stream: geomorphic evidence for shifting ice stream pathways. *Boreas 53*, 4–26. https://doi.org/10.1111/bor.12634.
Greenwood, S. L., Clason, C. C., Mikko, H., Nyberg, J., Peterson, G. & Smith, C. A. 2015: Integrated use of LiDAR and multibeam bathymetry reveals onset of ice streaming in the northern Bothnian Sea. *GFF 137*, 284–292. https://doi.org/10.1080/11035897.2015.1055513.
Greenwood, S. L., Clason, C., Nyberg, J., Jakobsson, M. & Holmlund, P. 2017: The Bothnian Sea ice stream: early Holocene retreat dynamics of the south-central Fennoscandian ice sheet. *Boreas 46*, 346–362. https://doi.org/10.1111/bor.12217.
Greenwood, S. L., Hughes, A. L. C. & Winsborrow, M. C. M. 2022: Chapter 28 – the EISC evolution prior to the Last Glacial Maximum. *In* Palacios, D., Hughes, P. D., García-Ruiz, J. M. & Andrés, N. (eds.): *European Glacial Landscapes. Maximum Extent of Glaciations*, 203–211. Elsevier, Amsterdam. https://doi.org/10.1016/B978-0-12-823498-3.00066-2.
Gudlaugsson, E., Humbert, A., Andreassen, K., Clason, C. C., Kleiner, T. & Beyer, S. 2017: Eurasian ice-sheet dynamics and sensitivity to subglacial hydrology. *Journal of Glaciology 239*, 556–564. https://doi.org/10.1017/jog.2017.21.
Hättestrand, C., Gotz, S., Naslund, J.-O., Fabel, D. & Stroeven, A. P. 2004: Drumlin formation time: evidence from northern and central Sweden. *Geografiska Annaler Series A 86*, 155–167. https://doi.org/10.1111/j.0435-3676.2004.00221.x.
Heikkinen, O. & Tikkanen, M. 1989: Drumlins and flutings in Finland: their relationships to ice movement and to each other. *Sedimentary Geology 62*, 349–355. https://doi.org/10.1016/0037-0738(89)90124-3.
Hewitt, I. J. & Creyts, T. T. 2019: A model for the formation of eskers. *Geophysical Research Letters 46*, 6673–6680. https://doi.org/10.1029/2019GL082304.
Hirvas, H., Lagerbäck, R., Mäkinen, K., Nenonen, K., Olsen, L., Rodhe, L. & Thoresen, M. 1988: The Nordkalott project: studies of Quaternary geology in northern Fennoscandia. *Boreas 17*, 431–437. https://doi.org/10.1111/j.1502-3885.1988.tb00560.x.
Høgaas, F. & Longva, O. 2016: Mega deposits and erosive features related to the glacial lake Nedre Glomsjø outburst flood, southeastern Norway. *Quaternary Science Reviews 151*, 273–291. https://doi.org/10.1016/j.quascirev.2016.09.015.
Høgaas, F. & Longva, O. 2018: The early Holocene ice-dammed lake Nedre Glomsjø in mid-Norway: an open lake system succeeding an actively retreating ice sheet. *Norsk Geologisk Tidsskrift 98*, 661–675. https://doi.org/10.17850/njg98-4-08.
Høgaas, F., Olsen, L., Gislefoss, L., Longva, O., Romundset, A. & Sveian, H. 2018: Deglacial patterns and ice-sheet dynamics in the fjords of southern Norland, Norway. *Norwegian Journal of Geology 98*, 1–17. https://doi.org/10.17850/njg98-4-07.
Holmlund, P. & Fastook, J. 1995: A time-dependent glaciological model of the Weichselian ice-sheet. *Quaternary International 27*, 53–58. https://doi.org/10.1016/1040-6182(94)00060-I.
Hoppe, G. 1952: Hummocky moraine regions with special reference to the interior of Norrbotten. *Geografiska Annaler 34*, 1–72. https://doi.org/10.1080/20014422.1952.11904365.
Houmark-Nielsen, M. 2010: Extent, age and dynamics of marine isotope stage 3 glaciations in the southwestern Baltic Basin. *Boreas 39*, 343–359. https://doi.org/10.1111/j.1502-3885.2009.00136.x.
Houmark-Nielsen, M. & Kjær, K. H. 2003: Southwest Scandinavia, 40–15 kyr BP: palaeogeography and environmental change. *Journal of Quaternary Science 18*, 769–786. https://doi.org/10.1002/jqs.802.
Hughes, A. L. C., Clark, C. D. & Jordan, C. J. 2010: Subglacial bedforms of the last British ice sheet. *Journal of Maps 6*, 543–563. https://doi.org/10.4113/jom.2010.1111.
Hughes, A. L. C., Clark, C. D. & Jordan, C. J. 2014: Flow-pattern evolution of the last British ice sheet. *Quaternary Science Reviews 89*, 148–168. https://doi.org/10.1016/j.quascirev.2014.02.002.
Hughes, A. L. C., Gyllencreutz, R., Lohne, Ø. S., Mangerud, J. & Svendsen, J. I. 2016: The last Eurasian ice sheets – a chronological database and time-slice reconstruction, DATED-1. *Boreas 45*, 1–45. https://doi.org/10.1111/bor.12142.
Hughes, A. L. C., Winsborrow, M. C. M. & Greenwood, S. L. 2022: Chapter 47 – European ice sheet complex evolution during the Last Glacial Maximum (29–19 ka). *In* Palacios, D., Hughes, P. D., García-Ruiz, J. M. & Andrés, N. (eds.): *European Glacial Landscapes. Maximum Extent of Glaciations*, 306–372. Elsevier, Amsterdam. https://doi.org/10.1016/B978-0-12-823498-3.00038-8.
Ingólfsson, Ó. & Landvik, J. Y. 2013: The Svalbard–Barents Sea ice-sheet – historical, current and future perspectives. *Quaternary Science Reviews 64*, 33–60. https://doi.org/10.1016/j.quascirev.2012.11.034.
Ives, J., Andrews, J. T. & Barry, R. G. 1975: Growth and decay of the Laurentide ice sheet and comparisons with Fenno-Scandinavia. *Nature 62*, 118–125. https://doi.org/10.1007/BF00623272.
Johnson, M. D., Fredin, O., Ojala, A. E. K. & Peterson, G. 2015: Unravelling Scandinavian geomorphology: the LiDAR revolution. *GFF 137*, 245–251. https://doi.org/10.1080/11035897.2015.1111410.
Johnson, M. D., Wedel, P. O., Benediktsson, Í. & Lenninger, A. 2019: Younger Dryas glaciomarine sedimentation, push-moraine formation and ice-margin behavior in the middle Swedish end-moraine zone west of Billingen, central Sweden. *Quaternary Science Reviews 224*, 105913. https://doi.org/10.1016/j.quascirev.2019.105913.
Joughin, I., Smith, B. E., Howat, I. M., Scambos, T. & Moon, T. 2010: Greenland flow variability from ice-sheet-wide velocity mapping. *Journal of Glaciology 56*, 415–430. https://doi.org/10.3189/002214310792447734.
Jungdal-Olesen, G., Andersen, J. L., Born, A. & Pedersen, V. K. 2024: The influence of glacial landscape evolution on Scandinavian ice-sheet dynamics and dimensions. *The Cryosphere 18*, 1517–1532. https://doi.org/10.5194/tc-18-1517-2024.

Kalm, V. 2012: Ice-flow pattern and extent of the last Scandinavian ice sheet southeast of the Baltic Sea. *Quaternary Science Reviews 44*, 51–59. https://doi.org/10.1016/j.quascirev.2010.01.019.

Kjær, K., Houmark-Nielsen, M. & Richardt, N. 2003: Ice-flow patterns and dispersal of erratics at the southwestern margin of the last Scandinavian ice sheet: signature of palaeo-ice streams. *Boreas 32*, 130–148. https://doi.org/10.1111/j.1502-3885.2003.tb01434.x.

Kleman, J. 1990: On the use of glacial striae for reconstruction of paleo-ice sheet flow patterns – with application to the Scandinavian ice sheet. *Geografiska Annaler: Series A 72*, 217–236. https://doi.org/10.1080/04353676.1990.11880318.

Kleman, J. 1992: The palimpsest glacial landscape in northwestern Sweden – late Weichselian deglaciation landforms and traces of older west-centered ice sheets. *Geografiska Annaler: Series A 74*, 305–325. https://doi.org/10.2307/521429.

Kleman, J. 1994: Preservation of landforms under ice sheets and ice caps. *Geomorphology 9*, 19–32. https://doi.org/10.1016/0169-555X(94)90028-0.

Kleman, J. & Borgström, I. 1996: Reconstruction of paleo-ice sheets: the use of geomorphological data. *Earth Surface Processes and Landforms 21*, 893–909. https://doi.org/10.1002/(SICI)1096-9837(199610)21:10<893::AID-ESP620>3.0.CO;2-U.

Kleman, J., Fastook, J. & Stroeven, A. P. 2002: Geologically and geomorphologically constrained numerical model of Laurentide ice sheet inception and build-up. *Quaternary International 95-96*, 87–98. https://doi.org/10.1016/S1040-6182(02)00030-7.

Kleman, J., Hättestrand, C., Borgström, I., Fabel, D. & Preusser, F. 2021: Age and duration of a MIS 3 interstadial in the Fennoscandian ice sheet core area – implications for ice sheet dynamics. *Quaternary Science Reviews 264*, 107011. https://doi.org/10.1016/j.quascirev.2021.107011.

Kleman, J., Hättestrand, C., Borgström, I. & Stroeven, A. 1997: Fennoscandian palaeoglaciology reconstructed using a glacial geological inversion model. *Journal of Glaciology 43*, 283–299. https://doi.org/10.3189/S0022143000003233.

Kleman, J., Hättestrand, C., Stroeven, A. P., Jansson, K. N., De Angelis, H. & Borgström, I. 2006: Reconstruction of Palaeo-ice sheets – inversion of their glacial geomorphological record. *In* Knight, P. G. (ed.): *Glacier Science and Environmental Change*, 192–198. Blackwell Science Ltd., Oxford. https://doi.org/10.1002/9780470750636.ch38.

Kleman, J., Jansson, K., De Angelis, H., Stroeven, A. P., Hättestrand, C., Alm, G. & Glasser, N. 2010: North American ice sheet build-up during the last glacial cycle, 115–21 kyr. *Quaternary Science Reviews 29*, 2036–2051. https://doi.org/10.1016/j.quascirev.2010.04.021.

Kleman, J., Stroeven, A. P. & Lundqvist, J. 2008: Patterns of Quaternary ice sheet erosion and deposition in Fennoscandia and a theoretical framework for explanation. *Geomorphology 97*, 73–90. https://doi.org/10.1016/j.geomorph.2007.02.049.

Lagerbäck, R. 1988: The Veiki moraines in northern Sweden – widespread evidence of an early Weichselian glaciation. *Boreas 17*, 469–486. https://doi.org/10.1111/j.1502-3885.1988.tb00562.x.

Lambeck, K., Purcell, A., Zhao, J. & Svensson, N.-O. 2010: The Scandinavian ice sheet: from MIS 4 to the end of the Last Glacial Maximum. *Boreas 39*, 410–435. https://doi.org/10.1111/j.1502-3885.2010.00140.x.

Larsen, E., Fredin, O., Lysså, A., Amantov, A., Fjeldskaar, W. & Ottesen, D. 2016: Causes of time-transgressive glacial maxima positions of the last Scandinavian ice sheet. *Norwegian Journal of Geology 96*, 159–170. https://doi.org/10.17850/njg96-2-06.

Leigh, J. R., Evans, D. J. A., Stokes, C. R., Andreassen, L. M. & Carr, R. J. 2021: Glacial and periglacial geomorphology of central Troms and Finnmark county, Arctic Norway. *Journal of Maps 17*, 348–366. https://doi.org/10.1080/17445647.2021.1950580.

Lewington, E. L. M., Livingstone, S. J., Clark, C. D., Sole, A. J. & Storrar, R. D. 2020: A model for interaction between conduits and surrounding hydraulically connected distributed drainage based on geomorphological evidence from Keewatin, Canada. *The Cryosphere 14*, 2949–2976. https://doi.org/10.5194/tc-14-2949-2020.

Li, Y., Napieralski, J., Harbor, J. & Hubbard, A. 2007: Identifying patterns of correspondence between modeled flow directions and field evidence: an automated flow direction analysis. *Computers & Geosciences 33*, 141–150. https://doi.org/10.1016/j.cageo.2006.06.016.

Lidmar-Bergström, K., Elvhage, C. & Ringberg, B. 1991: Landforms in Skåne, south Sweden. Preglacial and glacial landforms analysed from two relief maps. *Geografiska Annaler 73A*, 61–91. https://doi.org/10.1080/04353676.1991.11880333.

Lisiecki, L. E. & Raymo, M. E. 2005: A Pliocene-Pleistocene stack of 57 globally distributed benthic $\delta^{18}O$ records. *Paleoceanography 20*, PA1003. https://doi.org/10.1029/2004PA001071.

Lundqvist, J. 1986: Late Weichselian glaciation and deglaciation in Scandinavia. *Quaternary Science Reviews 5*, 269–292. https://doi.org/10.1016/0277-3791(86)90192-7.

Lundqvist, J. 2007: Surging ice and break-down of an ice dome – a deglaciation model for the Gulf of Bothnia. *GFF 129*, 329–336. https://doi.org/10.1080/11035890701294329.

Lunkka, J. P., Palmu, J. P. & Seppänen, A. 2021: Deglaciation dynamics of the Scandinavian ice sheet in the Salpausselkä zone, southern Finland. *Boreas 50*, 404–418. https://doi.org/10.1111/bor.12502.

Lüthgens, C., Hardt, J. & Böse, M. 2020: Proposing a new conceptual model for the reconstruction of ice dynamics in the SW sector of the Scandinavian ice sheet (SIS) based on the reinterpretation of published data and new evidence from optically stimulated luminescence (OSL) dating. *E&G Quaternary Science Journal 69*, 201–223. https://doi.org/10.5194/egqsj-69-201-2020.

Mangerud, J., Aarseth, I., Hughes, A. L. C., Lohne, Ø. S., Skår, K., Sønstegaard, E. & Svendsen, J. I. 2016: A major re-growth of the Scandinavian ice sheet in western Norway during Allerød-Younger Dryas. *Quaternary Science Reviews 132*, 175–205. https://doi.org/10.1016/j.quascirev.2015.11.013.

Mangerud, J., Alexanderson, H., Birks, H. H., Paus, A., Perić, Z. M. & Svendsen, J. I. 2023a: Did the Eurasian ice sheets melt completely in early Marine Isotope Stage 3? New evidence from Norway and a synthesis for Eurasia. *Quaternary Science Reviews 311*, 108136. https://doi.org/10.1016/j.quascirev.2023.108136.

Mangerud, J., Hughes, A. L. C., Johnson, M. D. & Lunkka, J. P. 2023b: Chapter 46 – The Fennoscandian ice sheet during the Younger Dryas stadial. *In* Palacios, D., Hughes, P. D., García-Ruiz, J. & Andrés, N. (eds.): *European Glacial Landscapes. The Last Deglaciation*, 437–452. Elsevier, Amsterdam. https://doi.org/10.1016/B978-0-323-91899-2.00060-7.

Mangerud, J., Hughes, A. L. C., Sæle, T. H. & Svendsen, J. I. 2019: Ice-flow patterns and precise timing of ice sheet retreat across a dissected fjord landscape in western Norway. *Quaternary Science Reviews 214*, 139–163. https://doi.org/10.1016/j.quascirev.2019.04.032.

Margold, M., Stokes, C. R. & Clark, C. D. 2015: Ice streams in the Laurentide ice sheet: identification, characteristics and comparison to modern ice sheets. *Earth-Science Reviews 143*, 117–146. https://doi.org/10.1016/j.earscirev.2015.01.011.

Margold, M., Stokes, C. R. & Clark, C. D. 2018: Reconciling records of ice streaming and ice margin retreat to produce a palaeogeographic reconstruction of the deglaciation of the Laurentide ice sheet. *Quaternary Science Reviews 189*, 1–30. https://doi.org/10.1016/j.quascirev.2018.03.013.

Mattsson, Å. 1997: Glacial striae, glacigenous sediments and Weichselian ice movements in southernmost Sweden. *Sedimentary Geology 111*, 285–311. https://doi.org/10.1016/S0037-0738(97)00022-5.

McClenaghan, M. B., Paulen, R. C., Smith, I. R., Rice, J. M., Plouffe, A., McMartin, I., Campbell, J. E., Lehtonen, M., Parsasadr, M. & Becket-Brown, C. E. 2023: Review of till geochemistry and indicator mineral methods for mineral exploration in glaciated terrain. *Geochemistry: Exploration, Environment, Analysis 23*, geochem2023-013. https://doi.org/10.1144/geochem2023-013.

McMartin, I. & Henderson, P. J. 2004: Evidence from Keewatin (central Nunavut) for paleo-ice divide migration. *Géographie Physique et Quaternaire 58*, 163–186. https://doi.org/10.7202/008132ar.

Mercer, J. H. 1970: A former ice sheet in the Arctic Ocean? *Palaeogeography, Palaeoclimatology, Palaeoecology 8*, 19–27. https://doi.org/10.1016/0031-0182(70)90076-3.

Möller, P. & Dowling, T. P. F. 2016: Streamlined subglacial bedforms on the Närke plain, south-central Sweden – areal distribution, morphometrics, internal architecture and formation. *Quaternary Science*

Reviews 146, 182–215. https://doi.org/10.1016/j.quascirev.2016.04.007.
Möller, P., Alexanderson, H., Anjar, J. & Björck, S. 2020: MIS 3 sediment stratigraphy in southern Sweden sheds new light on the complex glacial history and dynamics across southern Scandinavia. *Boreas 49*, 389–416. https://doi.org/10.1111/bor.12433.
Möller, P., Anjar, J. & Murray, A. S. 2013: An OSL-dated sediment sequence at Idre, west-central Sweden, indicates ice-free conditions in MIS 3. *Boreas 42*, 25–42. https://doi.org/10.1111/j.1502-3885.2012.00284.x.
Morlighem, M. and 31 others 2017: BedMachine v3: complete bed topography and ocean bathymetry mapping of Greenland from multibeam Echo sounding combined with mass conservation. *Geophysical Research Letters 44*, 11051–11061. https://doi.org/10.1002/2017GL074954.
Morlighem, M. and 36 others 2020: Deep glacial troughs and stabilizing ridges unveiled beneath the margins of the Antarctic ice sheet. *Nature Geoscience 13*, 132–137. https://doi.org/10.1038/s41561-019-0510-8.
Napieralski, J. & Nalepa, N. 2010: The application of control charts to determine the effect of grid cell size on landform morphometry. *Computers & Geosciences 36*, 222–230. https://doi.org/10.1016/j.cageo.2009.06.003.
Napieralski, J., Hubbard, A., Li, Y., Harbor, J., Stroeven, A. P., Kleman, J., Alm, G. & Jansson, K. N. 2007: Towards a GIS assessment of numerical ice-sheet model performance using geomorphological data. *Journal of Glaciology 53*, 71–83. https://doi.org/10.3189/172756507781833884.
Näslund, J. O., Rodhe, L., Fastook, J. L. & Holmlund, P. 2003: New ways of studying ice sheet flow directions and glacial erosion by computer modelling – examples from Fennoscandia. *Quaternary Science Reviews 22*, 245–258. https://doi.org/10.1016/S0277-3791(02)00079-3.
National Land Survey of Finland *Elevation model 2 m*. Available at: https://www.maanmittauslaitos.fi/en/maps-and-spatial-data/datasets-and-interfaces/product-descriptions/elevation-model-2-m (accessed 07.11.2019).
Nesje, A. & Matthews, J. A. 2024: Chapter 14 – Holocene glacial landscapes of the Scandinavian Peninsula. *In* Palacios, D., Hughes, P. D., Jomelli, V. & Tanarro, L. M. (eds.): *European Glacial Landscapes. The Holocene*, 245–274. Elsevier, Amsterdam. https://doi.org/10.1016/B978-0-323-99712-6.00020-9.
Niemelä, J., Ekman, I. & Lukashov, A. (eds.) 1993: *Quaternary deposits of Finland and northwestern part of Russian Federation and their resources* (scale 1:1,000,000). Geological Survey of Finland, Helsinki.
Nikarmaa, T., Lunkka, J. P. & Putkinen, N. 2017: Factors affecting the dynamics of the North Karelian/Oulu ice lobe, Central Finland, during the last deglaciation – a LiDAR and DEM interpretation of subglacial lineation patterns. *Bulletin of the Geological Society of Finland 89*, 100–120. https://doi.org/10.17741/bgsf/89.2.003.
Nordkalott Project 1986a: *Ice flow directions, Northern Fennoscandia (Map of Quaternary Geology Sheet 5, Scale 1:1,000,000)*. Geological Surveys of Finland, Norway and Sweden.
Nordkalott Project 1986b: *Ice flow indicators, northern Fennoscandia (Map of Quaternary Geology Sheet 3, Scale 1:1,000,000)*. Geological Surveys of Finland, Norway and Sweden.
Nordkalott Project 1986c: *Glacial geomorphology, northern Fennoscandia (Map of Quaternary Geology Sheet 2, Scale 1:1,000,000)*. Geological Surveys of Finland, Norway and Sweden.
Norwegian Mapping Authority, Kartverket 2023: Nasjonal detaljert høydemodel. Available at: https://hoydedata.no/LaserInnsyn2/ (accessed 04.02.2023).
Oerlemans, J. 2002: On glacial inception and orography. *Quaternary International 95–96*, 5–10. https://doi.org/10.1016/S1040-6182(02)00031-9.
Öhrling, C., Peterson, G. & Johnson, M. D. 2020: Glacial geomorphology between Lake Vänern and Lake Vättern, southern Sweden. *Journal of Maps 16*, 776–789. https://doi.org/10.1080/17445647.2020.1820386.
Ottesen, D., Batchelor, C. L., Bjarnadóttir, L. R., Wiberg, D. H. & Dowdeswell, J. A. 2022: Glacial landforms reveal dynamic ice-sheet behaviour along the mid-Norwegian margin during the last glacial-deglacial cycle. *Quaternary Science Reviews 285*, 107462. https://doi.org/10.1016/j.quascirev.2022.107462.
Ottesen, D., Dowdeswell, J. A. & Rise, L. 2005: Submarine landforms and the reconstruction of fast-flowing ice streams within a large quaternary ice sheet: the 2500-km-long Norwegian-Svalbard margin (57° [Unicode_Missing] 80°N). *GSA Bulletin 117*, 1033–1050. https://doi.org/10.1130/B25577.1.
Ottesen, D., Dowdeswell, J. A., Rise, L., Rokoengen, K. & Henriksen, S. 2002: Large-scale morphological evidence for past ice-stream flow on the mid-Norwegian continental margin. *Geological Society, London, Special Publications 203*, 245–258.
Ottesen, D., Stokes, C. R., Bøe, R., Rise, L., Longva, O., Thorsnes, T., Olesen, O., Bugge, T., Lepland, A. & Hestvik, O. B. 2016: Landform assemblages and sedimentary processes along the Norwegian Channel ice stream. *Sedimentary Geology 338*, 115–137. https://doi.org/10.1016/j.sedgeo.2016.01.024.
Ottesen, D., Stokes, C. R., Rise, L. & Olsen, L. 2008: Ice-sheet dynamics and ice streaming along the coastal parts of northern Norway. *Quaternary Science Reviews 27*, 922–940. https://doi.org/10.1016/j.quascirev.2008.01.014.
Palmer, M., Howard, T., Tinker, J., Lowe, J., Bricheno, L., Calvert, D., Edwards, T., Gregory, J., Harris, G., Krijnen, J., Pickering, M., Roberts, C. & Wolf, J. 2018: *UKCP18 Marine Report*. Available at: https://www.metoffice.gov.uk/pub/data/weather/uk/ukcp18/science-reports/UKCP18-Marine-report.pdf (accessed 05.09.2024).
Parent, M., Paradis, S. J. & Doiron, A. 1996: Palimpsest glacial dispersal trains and their significance for drift prospecting. *Journal of Geochemical Exploration 56*, 123–140. https://doi.org/10.1016/0375-6742(96)00011-8.
Patton, H., Andreassen, K., Bjarnadóttir, L. R., Dowdeswell, J. A., Winsborrow, M. C. M., Noormets, R., Polyak, L., Auriac, A. & Hubbard, A. 2015: Geophysical constraints on the dynamics and retreat of the Barents Sea ice sheet as a paleobenchmark for models of marine ice sheet deglaciation. *Reviews of Geophysics 53*, 1051–1098. https://doi.org/10.1002/2015rg000495.
Patton, H., Hubbard, A., Andreassen, K., Auriac, A., Whitehouse, P. L., Stroeven, A. P., Shackleton, C., Winsborrow, M., Heyman, J. & Hall, A. M. 2017: Deglaciation of the Eurasian ice sheet complex. *Quaternary Science Reviews 169*, 148–172. https://doi.org/10.1016/j.quascirev.2017.05.019.
Patton, H., Hubbard, A., Andreassen, K., Winsborrow, M. & Stroeven, A. P. 2016: The build-up, configuration, and dynamical sensitivity of the Eurasian ice-sheet complex to Late Weichselian climatic and oceanic forcing. *Quaternary Science Reviews 153*, 97–121. https://doi.org/10.1016/j.quascirev.2016.10.009.
Perry, J. E. H. 1998: *Reconstructing the character of the eastern sector of the Scandinavian Ice Sheet using Remote Sensing*. Ph.D. thesis, University of Edinburgh, 195 pp. Available at: http://hdl.handle.net/1842/15632.
Peterson Becher, G., Blomdin, R., Goodfellow, B. W., Ising, J., Mikko, H., Ransed, G., Regnéll, C., Smith, C. & Öhrling, C. 2024: *Beskrivning till Jordartskarta över centrala Jämtlands län K754*. 214 pp. Sveriges Geologiska Undersökning, Uppsala. Available at: https://resource.sgu.se/dokument/publikation/k/k754beskrivning/k754-beskrivning.pdf.
Peterson, G., Johnson, M. D. & Smith, C. A. 2017: Glacial geomorphology of the south Swedish uplands – focus on the spatial distribution of hummock tracts. *Journal of Maps 13*, 534–544. https://doi.org/10.1080/17445647.2017.1336121.
Petrini, M., Colleoni, F., Kirchner, N., Hughes, A. L. C., Camerlenghi, A., Rebesco, M., Lucchi, R. G., Forte, E., Colucci, R. R. & Noormets, R. 2018: Interplay of grounding-line dynamics and sub-shelf melting during retreat of the Bjørnøyrenna ice stream. *Scientific Reports 8*, 7196. https://doi.org/10.1038/s41598-018-25664-6.
Ploeg, K. & Stroeven, A. P. 2025: History and dynamics of Fennoscandian ice sheet retreat, contemporary ice-dammed lake evolution, and faulting in the Torneträsk area, northwestern Sweden. *The Cryosphere 19*, 347–373. https://doi.org/10.5194/tc-19-347-2025.
Porter, C., Morin, P., Howat, I., Noh, M. J., Bates, B., Peterman, K., Keesey, S., Schlenk, M., Gardiner, J., Tomko, K., Willis, M., Kelleher, C.,

Cloutier, M., Husby, E., Foga, S., Nakamura, H., Platson, M., Wethington, M., Williamson, C., Bauer, G., Enos, J., Arnold, G., Kramer, W., Becker, P., Doshi, A., D'Souza, C., Cummens, P., Laurier, F. & Bojesen, M. 2018: ArcticDEM. Version 3. Harvard Dataverse, V1. https://doi.org/10.7910/DVN/OHHUKH (accessed 16.01.2024).

Principato, S. M., Moyer, A. N., Hampsch, A. G. & Ipsen, H. A. 2016: Using GIS and streamlined landforms to interpret palaeo-ice flow in northern Iceland. *Boreas 45*, 470–482. https://doi.org/10.1111/bor.12164.

Punkari, M. 1980: The ice lobes of the Scandinavian ice sheet during the deglaciation in Finland. *Boreas 9*, 307–310. https://doi.org/10.1111/j.1502-3885.1980.tb00710.x.

Punkari, M. 1984: The relations between glacial dynamics and tills in the eastern part of the Baltic Shield. *Striae 20*, 49–54.

Punkari, M. 1994: Function of the ice streams in the Scandinavian ice sheet: analyses of glacial geological data from southwestern Finland. *Earth and Environmental Science Transactions of the Royal Society of Edinburgh 85*, 283–302. https://doi.org/10.1017/S0263593300000054.

Punkari, M. 1997: Glacial and glaciofluvial deposits in the interlobate areas of the Scandinavian ice sheet. *Quaternary Science Reviews 16*, 741–753. https://doi.org/10.1016/S0277-3791(97)00020-6.

Putkinen, N. 2011: *Late Weichselian deglaciation chronology and palaeoenvironments in northern Karelia, NW Russia*. Ph.D. thesis, The Geological Survey of Finland, 21 pp.

Putkinen, N., Eyles, N., Putkinen, S., Ojala, A. E. K., Palmu, J. P., Sarala, P., Väänänen, T., Räisänen, J., Saarelainen, J., Ahtonen, N., Rönty, H., Kiiskinen, A., Rauhaniemi, T. & Tervo, T. 2017: High-resolution LiDAR mapping of glacial landforms and ice stream lobes in Finland. *Bulletin of the Geological Society of Finland 89*, 64–81. https://doi.org/10.17741/bgsf/89.2.001.

Putniņš, A. & Henriksen, M. 2017: Reconstructing the flow pattern evolution in inner region of the Fennoscandian ice sheet by glacial landforms from Gausdal Vestfjell area, south-central Norway. *Quaternary Science Reviews 163*, 56–71. https://doi.org/10.1016/j.quascirev.2017.03.008.

Rainio, H., Saarnisto, M. & Ekman, I. 1995: Younger Dryas end moraines in Finland and NW Russia. *Quaternary International 28*, 179–192. https://doi.org/10.1016/1040-6182(95)00051-J.

Rasmussen, S. O., Bigler, M., Blockley, S. P., Blunier, T., Buchardt, S. L., Clausen, H. B., Cvijanovic, I., Dahl-Jensen, D., Johnsen, S. J., Fischer, H., Gkinis, V., Guillevic, M., Hoek, W. Z., Lowe, J. J., Pedro, J. B., Popp, T., Seierstad, I. K., Steffensen, J. P., Svensson, A. M., Vallelonga, P., Vinther, B. M., Walker, M. J. C., Wheatley, J. J. & Winstrup, M. 2014: A stratigraphic framework for abrupt climatic changes during the last glacial period based on three synchronized Greenland ice-core records: refining and extending the INTIMATE event stratigraphy. *Quaternary Science Reviews 106*, 14–28. https://doi.org/10.1016/j.quascirev.2014.09.007.

Regnéll, C., Greenwood, S. L., Mangerud, J. & Hughes, A. L. C. 2024: Chapter 13 – Early Holocene glacial landscapes and final-stage deglaciation of the Fennoscandian ice sheet. *In* Palacios, D., Hughes, P. D., Jomelli, V. & Tanarro, L. M. (eds.): *European Glacial Landscapes. The Holocene*, 225–244. Elsevier, Amsterdam. https://doi.org/10.1016/B978-0-323-99712-6.00008-8.

Regnéll, C., Mangerud, J. & Svendsen, J. I. 2019: Tracing the last remnants of the Scandinavian ice sheet: ice-dammed lakes and a catastrophic outburst flood in northern Sweden. *Quaternary Science Reviews 221*, 105862. https://doi.org/10.1016/j.quascirev.2019.105862.

Regnéll, C., Peterson Becher, G., Öhrling, C., Greenwood, S. L., Gyllencreutz, R., Blomdin, R., Brendryen, J., Goodfellow, B. W., Mikko, H., Ransed, G. & Smith, C. 2023: Ice-dammed lakes and deglaciation history of the Scandinavian ice sheet in central Jämtland, Sweden. *Quaternary Science Reviews 314*, 108219. https://doi.org/10.1016/j.quascirev.2023.108219.

Repo, R. & Tynni, R. 1971: Observations on the quaternary geology of an area between the 2nd Salpausselkä and the ice-marginal formation of central Finland. *Bulletin of the Geological Society of Finland 43*, 185–202. https://doi.org/10.17741/bgsf/43.2.005.

Rice, J. M., Paulen, R. C., Campbell, H. E. & Ross, M. 2024: The surficial geology record of ice stream catchment dynamics and ice-divide migration in the Quebec-Labrador sector of the Laurentide Ice Sheet. *Quaternary Science Advances 13*, 100123. https://doi.org/10.1016/j.qsa.2023.100123.

Romundset, A., Lakeman, T. R. & Høgaas, F. 2019: Coastal lake records add constraints to the age and magnitude of the Younger Dryas ice-front oscillation along the Skagerrak coastline in southern Norway. *Journal of Quaternary Science 34*, 112–124. https://doi.org/10.1002/jqs.3085.

Salonen, V. P. 1986: Glacial transport distance distribution of surface boulders in Finland. *Bulletin of the Geological Survey of Finland 388*, 57 pp.

Sarala, P. & Räisänen, J. 2017: Evolution of the eastern part of the Kuusamo Ice Lobe, based on geomorphological interpretation of high-resolution LiDAR data. *Bulletin of the Geological Society of Finland 89*, 82–99. https://doi.org/10.17741/bgsf/89.2.002.

Seguinot, J., Rogozhina, I., Stroeven, A. P., Margold, M. & Kleman, J. 2016: Numerical simulations of the Cordilleran ice sheet through the last glacial cycle. *The Cryosphere 10*, 639–664. https://doi.org/10.5194/tc-10-639-2016.

Sejrup, H. P., Hjelstuen, B. O., Patton, H., Esteves, M., Winsborrow, M., Rasmussen, T. L., Andreassen, K. & Hubbard, A. 2022: The role of ocean and atmospheric dynamics in the marine-based collapse of the last Eurasian ice sheet. *Nature Communications Earth and Environment 3*, 119. https://doi.org/10.1038/s43247-022-00447-0.

Siegert, M. J. & Dowdeswell, J. A. 2004: Numerical reconstructions of the Eurasian ice sheet and climate during the Late Weichselian. *Quaternary Science Reviews 23*, 1273–1283. https://doi.org/10.1016/j.quascirev.2003.12.010.

Smith, M. J. & Clark, C. D. 2005: Methods for the visualization of digital elevation models for landform mapping. *Earth Surface Processes and Landforms 30*, 885–900. https://doi.org/10.1002/esp.1210.

Smith, M. J. & Knight, J. 2011: Palaeoglaciology of the last Irish ice sheet reconstructed from striae evidence. *Quaternary Science Reviews 30*, 147–160.

Smith, M. J., Knight, J., Field, K. S. & Harrison, S. 2008: Glacial striae observations for Ireland compiled from historic records. *Journal of Maps 4*, 378–398.

Sollid, J. L. & Sørbel, L. 1994: Distribution of glacial landforms in southern Norway in relation to the thermal regime of the last continental ice sheet. *Geografiska Annaler: Series A, Physical Geography 76*, 25–35. https://doi.org/10.2307/521317.

Sollid, J. L. & Torp, B. 1984: *Glasialgeologiske kart over Norge (Nasjonalatlas for Norge, Scale 1:1,000,000)*. Oslo Universitet, Geografisk Institutt, Oslo.

Spada, G. 2017: Glacial isostatic adjustment and Contemporary Sea level Rise: an overview. *In* Cazenave, A., Champollion, N., Paul, F. & Benveniste, J. (eds.): *Integrative Study of the Mean Sea Level and Its Components*, 155–187. *Space Sciences Series of ISSI 58*. Springer, Cham. https://doi.org/10.1007/978-3-319-56490-6_8.

Stoker, B. J., Dulfer, H. E., Stokes, C. R., Brown, V. H., Clark, C. D., Ó Cofaigh, C., Evans, D. J. A., Froese, D., Norris, S. L. & Margold, M. 2025: Ice flow dynamics of the northwestern Laurentide ice sheet during the last deglaciation. *The Cryosphere 19*, 869–910. https://doi.org/10.5194/tc-19-869-2025.

Stokes, C. R. 2018: Geomorphology under ice streams: moving from form to process. *Earth Surface Processes and Landforms 43*, 85–123. https://doi.org/10.1002/esp.4259.

Stokes, C. R. & Clark, C. D. 1999: Geomorphological criteria for identifying Pleistocene ice streams. *Annals of Glaciology 28*, 67–74. https://doi.org/10.3189/172756499781821625.

Stokes, C. R. & Clark, C. D. 2001: Palaeo-ice streams. *Quaternary Science Reviews 20*, 1437–1457. https://doi.org/10.1016/S0277-3791(01)00003-8.

Stokes, C. R. & Clark, C. D. 2002: Are long subglacial bedforms indicative of fast ice flow? *Boreas 31*, 239–249. https://doi.org/10.1111/j.1502-3885.2002.tb01070.x.

Stokes, C. R., Clark, C. D., Lian, O. B. & Tulaczyk, S. 2007: Ice stream sticky spots: a review of their identification and influence beneath contemporary and palaeo-ice streams. *Earth-Science Reviews 81*, 217–249. https://doi.org/10.1016/j.earscirev.2007.01.002.

Stokes, C. R., Tarasov, L., Blomdin, R., Cronin, T. M., Fisher, T. G., Gyllencreutz, R., Hättestrand, C., Heyman, J., Hindmarsh, R. C. A., Hughes, A. L. C., Jakobsson, M., Kirchner, N., Livingstone, S.

J., Margold, M., Murtin, J. B., Noormets, R., Peltier, W. R., Peteet, D. M., Piper, D. J. W., Preusser, F., Renssen, H., Roberts, D. H., Roche, D. M., Saint-Ange, F., Stroeven, A. P. & Teller, J. T. 2015: On the reconstruction of palaeo-ice sheets: recent advances and future challenges. *Quaternary Science Reviews 125*, 15–49. https://doi.org/10.1016/j.quascirev.2015.07.016.

St-Onge, D. A. 1984: Surficial deposits of the Redrock Lake area, District of Mackenzie. *Geological Survey of Canada Current Research Paper 84-1A*, 271–278. https://doi.org/10.4095/119675.

Stroeven, A. P., Fabel, D., Hättestrand, C. & Harbor, J. 2002: A relict landscape in the centre of the Fennoscandian glaciation: cosmogenic radionuclide evidence of tors preserved through multiple glacial cycles. *Geomorphology 44*, 145–154. https://doi.org/10.1016/S0169-555X(01)00150-7.

Stroeven, A. P., Hättestrand, C., Kleman, J., Heyman, J., Fabel, D., Fredin, O., Goodfellow, B. W., Harbor, J. M., Jansen, J. D., Olsen, L., Caffee, M. W., Fink, D., Lundqvist, J., Rosqvist, G. C., Strömberg, B. & Jansson, K. N. 2016: Deglaciation of Fennoscandia. *Quaternary Science Reviews 147*, 91–121. https://doi.org/10.1016/j.quascirev.2015.09.016.

Svendsen, J. I., Alexanderson, H., Astakhov, V. I., Demidov, I., Dowdeswell, J. A., Funder, S., Gataullin, V., Henriksen, M., Hjort, C., Houmark-Nielsen, M., Hubberten, H. W., Ingólfsson, Ó., Jakobsson, M., Kjær, K. H., Larsen, E., Lokrantz, H., Lunkka, J. P., Lysså, A., Mangerud, J., Matiouchkov, A., Murray, A., Möller, P., Niessen, F., Nikolskaya, O., Polyak, L., Saarnisto, M., Siegert, C., Siegert, M., Spielhagen, R. F. & Stein, R. 2004: Late Quaternary ice sheet history of northern Eurasia. *Quaternary Science Reviews 23*, 1229–1271. https://doi.org/10.1016/j.quascirev.2003.12.008.

Swedish Ordnance Survey, Lantmäteriet *National Elevation Model, version 1*. Latest Version. Available at: https://www.lantmateriet.se/en/geodata/geodata-products/product-list/elevation-model-download/ (accessed 30.09.2019).

Szuman, I., Kalita, J. Z., Diemont, C. R., Livingstone, S. J., Clark, C. D. & Margold, M. 2024: Reconstructing dynamics of the Baltic ice stream complex during deglaciation of the last Scandinavian ice sheet. *The Cryosphere 18*, 2407–2428. https://doi.org/10.5194/tc-18-2407-2024.

Szuman, I., Kalita, J. Z., Ewertowski, M. W., Clark, C. D. & Livingstone, S. J. 2021: Dynamics of the last Scandinavian Ice Sheet's southernmost sector revealed by the pattern of ice streams. *Boreas 50*, 764–780. https://doi.org/10.1111/bor.12155.

Tarasov, L., Dyke, A. S., Neal, R. M. & Peltier, W. R. 2012: A data-calibrated distribution of deglacial chronologies for the north American ice complex from glaciological modeling. *Earth and Planetary Science Letters 315–316*, 30–40. https://doi.org/10.1016/j.epsl.2011.09.010.

Veness, R. L. J., Clark, C. D., Ely, J. C., Knight, J. L., Igneczi, A. & Bradley, S. L. 2025: Modelling erratic dispersal accounting for shifting ice flow geometries: a new method and explanations of erratic dispersal of the British-Irish ice sheet. *Journal of Quaternary Science 40*, 944–957. https://doi.org/10.1002/jqs.3720.

Vérité, J., Livingstone, S. J., Ravier, E., McMartin, I., Campbell, J., Lewington, E. L. M., Dewald, N., Clark, C. D., Sole, A. J. & Storrar, R. D. 2024: Conceptual model for the formation of bedforms along subglacial meltwater corridors (SMCs) by variable ice-water-bed interactions. *Earth Surface Processes and Landforms 49*, 170–196. https://doi.org/10.1002/esp.5725.

Vestøl, O., Ågren, J., Steffen, H., Kierulf, H. & Tarasov, L. 2019: NKG2016LU: a new land uplift model for Fennoscandia and the Baltic Region. *Journal of Geodesy 93*, 1759–1779. https://doi.org/10.1007/s00190-019-01280-8.

Vorren, T. O. 1977: Weichselian ice movement in South Norway and adjacent areas. *Boreas 6*, 247–257. https://doi.org/10.1111/j.1502-3885.1977.tb00292.x.

Vorren, T. O. 1979: Weichselian ice movements, sediments and stratigraphy on Hardanger-vidda, South Norway. *Norges Geologiske Undersøkelse Bulletin 350*, 1–117. Available at: https://hdl.handle.net/11250/2675076.

van der Wateren, F. M. 1995: Structural geology and sedimentology of push moraines: processes on soft sediment deformation in a glacial environment and the distribution of glaciotectonic styles. *Mededelingen Rijks Geologische Dienst 54*, 168.

Winsborrow, M. C. M., Andreassen, K., Corner, G. D. & Laberg, J. S. 2010: Deglaciation of a marine-based ice sheet: late Weichselian palaeo-ice dynamics and retreat in the southern Barents Sea reconstructed from onshore and offshore glacial geomorphology. *Quaternary Science Reviews 29*, 424–442. https://doi.org/10.1016/j.quascirev.2009.10.001.

Wohlfarth, B. 2010: Ice-free conditions in Sweden during marine oxygen isotope stage 3? *Boreas 39*, 377–398. https://doi.org/10.1111/j.1502-3885.2009.00137.x.

Yan, Q., Zhang, Z., Gao, Y., Wang, H. & Johannessen, O. M. 2013: Sensitivity of the modeled present-day Greenland ice sheet to climatic forcing and spin-up methods and its influence on future sea level projections. *Journal of Geophysical Research: Earth Surface 118*, 2174–2189. https://doi.org/10.1002/jgrf.20156.

Yang, H., Krebs-Kanzow, U., Kleiner, T., Sidorenko, D., Rodehacke, C. B., Shi, X., Gierz, P., Niu, L., Gowan, E. J., Hinck, S. & Liu, X. 2022: Impact of paleoclimate on present and future evolution of the Greenland ice sheet. *PLoS One 17*, e0259816. https://doi.org/10.1371/journal.pone.0259816.

Supporting Information

Additional Supporting Information to this article is available at http://www.boreas.dk.

Data S1. Shapefile datasets including the following: (1) lineation linkages for Norway, Sweden and Finland; (2) reconnaissance-style lineation linkages for Russian Karelia; (3) flowsets, including the bounding polygons and flowlines; (4) critical cross-cuts, including a points shapefile containing IDs of the corresponding flowsets and relative-age information, and a polyline file containing the crestlines of the relevant cross-cutting lineations; and (5) shapefiles for flow-pattern Stages 1–25, including flowsets separated by stage, the ice-sheet-scale flow axes, ice divides, ice saddles (for the relevant stages) and the bounding line depicting the inferred ice geometry. All shapefiles use a Lambert Azimuthal Equal Area projection with a central meridian centred on 10°E and a latitude of origin of 90°. The datum is WGS 1984. The projection is included as a .prj file. A README file is included, containing details of individual shapefiles, the fields in their attribute tables and instructions for accessing their attributes without GIS software.

Data S2. Ten A0 maps intended to provide greater clarity of individual flowsets ascribed to each stage of our flow pattern reconstruction. Maps are provided both with and without flowset ID labels. The flowsets are colourised according to the stage to which we assign them in our flow pattern reconstruction. There are two versions of each of the following maps, one version with flowset ID labels and one version without. Flowsets_S1_2_PreMIS2: Flowsets in Stages 1 and 2 of our reconstruction, which we interpret as relating to an older pre-MIS 2 ice

sheet over Fennoscandia. Flowsets_S3_8_Advance: Flowsets in Stages 3–8, which we interpret as depicting the advance of the last Scandinavian Ice Sheet. Flowsets_S9_16_Deglac1: Flowsets in Stages 9–16, which we interpret as depicting the initial deglaciation ('Deglac1') of the last Scandinavian Ice Sheet. Flowsets_S17_25_Deglac2: Flowsets in Stages 17–25, which we interpret as depicting the deglaciation of the last Scandinavian Ice Sheet from around the Younger Dryas and since ('Deglac2'). Flowsets_BtwnStages_NoStage: Flowsets that, based on the relative-age chronology indicated by cross-cutting subglacial lineations detailed in Table S1, fall between stages of our reconstruction and we interpret as representing small, local-scale variations in flow that do not relate to major ice-flow reconfiguration at the ice-sheet scale. Also included are the 60 small flowsets for which we were unable to assign a stage.

Fig. S1. A0 map showing the orientations of subglacial lineation crestlines (n = 210 909) and grain (n = 30 342) mapped in Steps 1 and 2 of our multi-scale sampled mapping approach. Hashed areas show areas where DTMs did not provide coverage at the time of Steps 1 and 2 mapping; these were carefully in-filled during Step 3 when DTMs became available; such areas are largely in high-relief areas where subglacial lineations are sparse. Data credit for shaded-relief basemap: Airbus, USGS, NGA, NASA, CGIAR, NLS, OS, NMA, Geodatastyrelsen, GSA, GSI and the GIS User Community.

Fig. S2. Schematic example of a location where, according to the guiding principles we employed during our flow-pattern reconstruction, it is necessary to invoke migration of the ice divide to explain flowsets which are close to one-another and host subglacial lineations which indicate opposing ice flow directions. A. Two flowsets in Sweden generated in our study (fs96 in red and fs196 in blue) with such a configuration. According to our guiding principles, they cannot be explained during a single phase of ice flow. B. The older of the two flowsets (according to the sequence indicated by cross-cutting lineations in each of the flowsets), which requires an ice divide to the west. C. The younger of the two flowsets, which requires that the ice divide migrated to the east relative to the position in B. The ice divide positions in B and C are for illustration only.

Fig. S3. A0 map of lineation linkages over Norway, Sweden and Finland (n = 53 433) and NW Russia (n = 4355), colourised by orientation. The map includes lineation linkages generated in step 3 of our multi-scale mapping approach over Norway, Sweden and Finland, reconnaissance-style linkages extending into and beyond Russian Karelia. Also shown are lineation linkages from Boyes *et al*. (2023) over the Kola Peninsula and Russian Lapland. Note, the specific approaches to linkage generation differ somewhat between our study and that of Boyes *et al*. (2023). For visual clarity, orientations are represented on a 0–180° colour scale; the shapefile dataset contains orientations between 0 and 360°. The small DTM gaps that existed in Norway during mapping Steps 1 and 2 were carefully filled in during the generation of lineation linkages, as DTM coverage became available. Data credit for shaded-relief basemap: Airbus, USGS, NGA, NASA, CGIAR, NLS, OS, NMA, Geodatastyrelsen, GSA, GSI and the GIS User Community.

Fig. S4. A0 map of lineation linkages over Norway, Sweden and Finland (n = 53 433) and NW Russia (n = 4355), colourised by ascribed confidence rating. The map includes lineation linkages generated in Step 3 of our multi-scale mapping approach over Norway, Sweden and Finland, reconnaissance-style linkages extending into and beyond Russian Karelia and lineation linkages from Boyes *et al*. (2023) over the Kola Peninsula and Russian Lapland. Note, the specific approaches to linkage generation differ somewhat between our study and that of Boyes *et al*. (2023), and confidence rankings are not shown for those linkages. In our linkage data, medium-to-high confidence linkages generally represent very clearly streamlined landforms, be they in thick sediments, regions with thin sediment cover or expressed in exposed bedrock. Low-confidence lineation linkages generally represent landform fields that could represent a former ice flow direction but are, for example, (i) less pronounced (often being subtle, low-relief features), (ii) strongly modified by later cross-cutting subglacial lineations or (iii) exhibit relatively weak streamlining in an area where bedrock structure is visible in the surface topography, thus reducing confidence that the streamlining is truly glacial in origin. The final confidence category ('very low confidence') represents landforms that we suspect to be best explained as bedrock structure, but for which there are some hints of glacial streamlining. The vast majority of the latter category were not used to generate flowsets, particularly where they occurred in isolation from lineation linkages with higher levels of confidence. Data credit for shaded-relief basemap: Airbus, USGS, NGA, NASA, CGIAR, NLS, OS, NMA, Geodatastyrelsen, GSA, GSI and the GIS User Community.

Fig. S5. A0 map of flowsets generated over Norway, Sweden, Finland and extending into NW Russia. Flowsets are colourised by ascribed confidence. Flowsets

over the Kola Peninsula and Russian Lapland (blue outline) are from Boyes *et al*. (2023). Flowsets were given high, lower or very-low-confidence classifications (89%, 10% and 1% of the total number of flowsets, respectively) if, for example, they hosted a significant proportion of lineation linkages with the corresponding confidence classification, hosted sparse lineation linkages, or occurred in areas where bedrock structure made the identification of glacially streamlined features more challenging. The ice flow direction was deemed somewhat uncertain for a small number of flowsets (19), accounting for 0.05% of the cumulative flowset area. In these cases, we made our best judgement of the likely flow direction based on the morphology of subglacial lineations, and marked the uncertainty with a note in the flowset shapefile dataset. Data credit for shaded-relief basemap: Airbus, USGS, NGA, NASA, CGIAR, NLS, OS, NMA, Geodatastyrelsen, GSA, GSI and the GIS User Community.

Fig. S6. A0 map showing the 269 'floating' flowsets which lack relative-age information from cross-cutting subglacial lineations. The flowsets are colourised according to ascribed flowset confidence (see also Fig. S5). Many such flowsets were incorporated into stages of our flow-pattern reconstruction (Fig. 13 and Table S1) following the guiding principles and pattern group approach outlined in 'Data and methods'. Data credit for shaded-relief basemap: Airbus, USGS, NGA, NASA, CGIAR, NLS, OS, NMA, Geodatastyrelsen, GSA, GSI and the GIS User Community.

Fig. S7. A0 map of all flowsets colourised according to the influence of topography on ice flow vectors within flowsets. Thick ice over low-relief areas should produce patterns that mostly ignore topographic bumps and valleys, whereas the converse should produce flow patterns that tend to follow the topography. This means that our flowset categorisations according to topographic influence reveal qualitative information on relative ice thickness, a vital source of information for building reconstructions of ice sheets. Note that while the classifications therein distinguish valley-confined flowsets into those which ignore, sense, or follow local topography on the valley floor, valley-confined flowsets follow broad-scale topography by definition; hence they are grouped with flowsets which follow topography in this visualisation. Data credit for shaded-relief basemap: Airbus, USGS, NGA, NASA, CGIAR, NLS, OS, NMA, Geodatastyrelsen, GSA, GSI and the GIS User Community.

Fig. S8. A0 map of all flowsets colourised according to the inferred glaciodynamic context evidenced by the configurations of their constituent subglacial lineations. See Table 2, Fig. 8 and 'Data and methods' in main manuscript for an explanation of the different categories. Note that the primary classifications are shown here. Some time-transgressive flowsets had secondary classifications (e.g. evidence for retreat in addition to thinning), which are recorded in the flowset shapefile (Data S1). Data credit for shaded-relief basemap: Airbus, USGS, NGA, NASA, CGIAR, NLS, OS, NMA, Geodatastyrelsen, GSA, GSI and the GIS User Community.

Fig. S9. A multi-page PDF compiling A3 versions of the 25 individual stages of ice-flow pattern evolution shown in Figs 12 and 13 of the main manuscript. Grey flowsets over the Kola Peninsula and Russian Lapland are from Boyes *et al*. (2023). Correlated stage letters from Boyes *et al*. 2023 are noted in the relevant panel. See main manuscript for description and interpretation of stages. The red line in Stages 3–25 shows the maximum-achieved asynchronous extent of the last SIS (see e.g. Hughes *et al*. 2016). See Fig. S10 for replicas of these maps with individual flowset IDs referred to in the text. See also Data S2 for larger (A0) maps of flowsets grouped by assigned stage. Data credit for shaded-relief basemap: Airbus, USGS, NGA, NASA, CGIAR, NLS, OS, NMA, Geodatastyrelsen, GSA, GSI and the GIS User Community.

Fig. S10. A multi-page PDF compiling A3 versions of the 25 individual stages of ice-flow pattern evolution shown in Figs 12 and 13 of the main manuscript, with the addition of individual flowset ID labels. Grey flowsets over the Kola Peninsula and Russian Lapland are from Boyes *et al*. (2023). Correlated stage letters from Boyes *et al*. (2023) are noted in the relevant panel. The red line in Stages 3–25 shows the maximum-achieved asynchronous extent of the last SIS (see e.g. Hughes *et al*. 2016). See main manuscript for description and interpretation of stages. See also Data S2 for larger (A0) maps of flowsets grouped by assigned stage. Data credit for shaded-relief basemap: Airbus, USGS, NGA, NASA, CGIAR, NLS, OS, NMA, Geodatastyrelsen, GSA, GSI and the GIS User Community.

Fig. S11. Selected key flowsets (coloured according to assigned stage in our flow pattern reconstruction) in southern Finland which correlate with notable candidate ice streams (so-called 'ice lobes') that are widely discussed in the literature (e.g. Putkinen

et al. 2017; Lunkka *et al*. 2021; and references therein). For clarity, several small flowsets in the relevant stages are not visualised; see Stages 15–22 in Figs S9 and S10. Also shown are schematic representations of the local ice-bounding lines from our flow pattern reconstruction, and the locations of notable ice-marginal formations: the Salpausselka I, II and III ice marginal zones (SS-I, SS-II and SS-III, respectively), and the Central Finnish Ice Marginal Formation (CFIMF). In some cases, our flowsets extend somewhat beyond these positions; in these cases, the subglacial lineation imprints likely formed some time before the ice margin reached the associated ice-marginal formation. This reflects the palimpsest nature of glacial landscapes, in which spatially associated features such as subglacial lineations and moraines can form at different times. It is not an aim of our study to correlate specific flowsets or ice flow pattern stages to specific ice-marginal landforms, but we include these notable ice-marginal zones in the map to aid visualisation of the concepts and locations discussed in the main text (see 'Remarks on Ice Streams').

Table S1. Table of flowset relative ages, as indicated by cross-cutting and superposition relationships between their constituent subglacial lineations and the first stage of flow-pattern evolution to which we assign each flowset based on that information. 'Floating' flowsets which lack cross-cutting information are included where flow pattern allowed them to be assigned to a stage. The first sheet of this file contains instructions on interpreting the table, including two 'worked examples'. The second sheet contains the actual table. Note that the table shows the first stage in which a flowset appears; some flowsets occur in multiple stages (up to 3); this information is included in Table S2 and in the flowset shapefiles (Data S1).

Table S2. The first sheet of this file contains a table of flowsets in each of our reconstructed stages of flow-pattern evolution, and those which are between stages or unassigned to stages. This information is also available in the flowset shapefiles (Data S1). The second sheet of this file contains a table showing the inferred correlations between our stages of ice sheet flow-pattern evolution and regional-scale flow-pattern stages reconstructed over the Kola Peninsula and Russian Lapland by Boyes *et al*. (2023).

Table S3. Comparison between the 'ice flow trace fans' identified by Kleman *et al*. (1997), and the flowsets, reconstructed ice-sheet-scale flow geometries and interpreted flow sequencing in our flow pattern reconstruction. The reader is referred to Kleman *et al*. (1997) for specific definitions of their terminology, such as the definitions of the different 'fan types'. We do not perform a detailed comparison for those Kleman *et al*. (1997) fans which are entirely within the study area of Boyes *et al*. (2023) over the Kola Peninsula and Russian Lapland. The first sheet contains a detailed comparison to each flow trace fan. The second sheet contains summary statistics comparing the correspondence in identified flow patterns, and their broad sequencing, between Kleman *et al*. (1997) and our study.